



**NTNU – Trondheim**  
Norwegian University of  
Science and Technology

# Collision Between Platform Deck and Service Vessel Wheelhouse

**Jan Børge Mork Sætre**

Marine Technology

Submission date: June 2013

Supervisor: Jørgen Amdahl, IMT

Norwegian University of Science and Technology  
Department of Marine Technology





## MASTER THESIS 2013

for

Stud. techn. Jan Børge Sætre

### **Collision Between Platform deck and -Service Vessel Wheelhouse** *Kollisjon mellom plattformdekket og styrhuset på konstruksjonsskip*

Collisions with dedicated vessels or passing vessels are a constant threat to offshore installations. In 2005 collision with a supply vessel initiated a blow-out and subsequent loss of the Mumbai jacket causing 25% reduction of the oil production in India. In the North Sea the collision between the West Venture platform and the supply vessel Far Symphony implied a kinetic energy three times the design energy; very fortunately with no fatalities. The major damage took place in the vessel bow, which was crushed about 3 m.

To keep the risk of collision at a sufficiently low level, current regulations specify that offshore installation to be designed for impacts with ships of given size and speed. At present, the typical accident scenario is impact from a supply vessel with 5000 tons displacement and a speed of 2 m/s. In the NORSOK STANDARD for accidental actions (Appendix A) design curves for various impact scenarios for such supply vessel are given.

The present trend is increased size of supply vessels (5000 tons – 10000 tons) and bulbous bows. The design curves have been developed for non-bulbous bows, and work is carried out to update the NORSOK STANDARD with design curves for bulbous bows of large supply vessels.

A possible scenario is the wheelhouse hitting the platform deck if the ship should pass between the columns of a floating platform. The Far Symphony impact on the West Venture platform was close to realizing this scenario, but luckily the bow hit one of the columns. An impact between the platform columns could mean impact with braces and platform decks, possibly even drill strings or risers. A proper assessment of a complete impact scenario including all relevant structural interaction would be beneficial.

Although not realized yet, it is of considerable interest to know the outcome of wheelhouse hitting the platform deck. It may be expected that it will not be critical for the integrity of the deck, but the wheelhouse may be damaged substantially, with several fatalities and leaving the ship in uncontrolled condition. The purpose of this project is to perform realistic simulations of this scenario.

The work may be carried out in the following steps:

1. Establish a simple calculation model for drift-off for a supply vessel capable of predicting the impact speed. Mean drift motions, as well as first order wave induced motions shall be

- considered. A simple calculation model for the wave induced vertical motion (heave plus pitch) shall also be developed, so as to allow prediction of vertical impact velocity.
2. By means of external impact mechanics estimate the amount of impact energy that must be dissipated as strain energy.
  3. Perform finite element modelling of a representative wheelhouse of a supply vessels for analysis with LS-DYNA. The choice of material/fracture modelling and applied boundary conditions shall be selected and discussed
  4. Establish the realistic structural models necessary to perform between-column impact including topside structures and braces that may be exposed to wheel-house impact. This may be general load-carrying girder, girders supporting living quarters, platform braces and HC piping (risers) located underneath topside structures. The choice of material/fracture modelling and applied boundary conditions shall be selected and discussed
  5. Perform horizontal collision analysis and vertical (wave-induced motion) impact analysis of the wheelhouse against the exposed structures modelled in pt. 2. Force deformation and energy dissipation curves for the wheelhouse and the deck/HC pipes shall be established. Determine the damage level for various impact velocities and discuss the likely consequences with respect to maintaining control of the ship after the accident.
  6. To the extent possible assess the effect of repeated vertical impacts.
  7. Conclusions and recommendation for further work

Literature studies of specific topics relevant to the thesis work may be included.

The work scope may prove to be larger than initially anticipated. Subject to approval from the supervisor, topics may be deleted from the list above or reduced in extent.

In the thesis the candidate shall present his personal contribution to the resolution of problems within the scope of the thesis work.

Theories and conclusions should be based on mathematical derivations and/or logic reasoning identifying the various steps in the deduction.

The candidate should utilise the existing possibilities for obtaining relevant literature.

The thesis should be organised in a rational manner to give a clear exposition of results, assessments, and conclusions. The text should be brief and to the point, with a clear language. Telegraphic language should be avoided.

The thesis shall contain the following elements: A text defining the scope, preface, list of contents, summary, main body of thesis, conclusions with recommendations for further work, list of symbols and acronyms, references and (optional) appendices. All figures, tables and equations shall be numerated.

The supervisor may require that the candidate, in an early stage of the work, presents a written plan for the completion of the work. The plan should include a budget for the use of computer and laboratory resources which will be charged to the department. Overruns shall be reported to the supervisor.



The original contribution of the candidate and material taken from other sources shall be clearly defined. Work from other sources shall be properly referenced using an acknowledged referencing system.

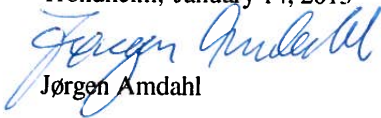
The report shall be submitted in two copies:

- Signed by the candidate
- The text defining the scope included
- In bound volume(s)
- Drawings and/or computer prints which cannot be bound should be organised in a separate folder.

Supervisor: Prof. Jørgen Amdahl  
PhD-student Martin Storheim

Deadline: June 10, 2013

Trondheim, January 14, 2013



Jørgen Amdahl



# Summary

Collisions between ships and offshore structures are rarely occurring events, but pose a constant threat to the safety at sea. Observed trends in recent years has show that the size of both offshore structures and servicing vessels is increasing, making it possible for an offshore structure deck or module to pass above the bow and hit the superstructure and bridge of the vessel. An accident like this could have severe consequences.

The superstructure of ships is typically considerably less stiffened than the submerged part of the hull, making the resistance to deformation equally small. Passenger cabins are typically placed in the forward part of the superstructure of ships, and an impact to this part could be a direct cause of fatalities.

A secondary effect, if the bridge should be partly or completely destroyed, would be the reduced ability to control the ship. If the vessel was get stuck underneath the platform, it could lead to considerable secondary damage to both the offshore- and ship structure, as well as damage to e.g. a production riser connected to the platform.

The external mechanics of collisions may be analyzed by utilizing the principle of conservation of energy and momentum. A moving vessels kinetic energy is dissipated by absorption of strain energy in both the struck and striking structure, as well as viscous damping by the surrounding sea, and transfer of momentum to kinetic translational and rotational energy.

The internal mechanics on the other hand are hard to determine accurately without detailed and time consuming finite element analyses.

Principles behind non-linear finite element analysis is presented, as well as different available solution techniques and their benefits and disadvantages.

In this thesis, collision scenarios for a large offshore service ship superstructure are treated by non-linear finite element analysis. The ship is set to collide with

a simplified Ultra Deep-Water semi-submersible drilling rig, and an aluminium living quarter of a jacket platform.

A detailed model of the superstructure of a 13 600 metric ton offshore service vessel is modeled. In addition, the hull of the ship is modeled as rigid in order to more easily apply global mass properties, as well as restoring forces and moments.

Two offshore structure models are created. The semi-submersible is modeled with representative stiffening and represented as an equivalent box-girder. The living-quarter is modeled in the likeness of that found on the Kvitebjørn jacket. The LQ is modeled as extruded aluminium profiles mounted atop a stiff beam lattice.

Five collision scenarios are successfully tested. All runs utilize prescribed displacement settings.

- Ship vs semi-like rigid plate.
- Ship vs deformable semi.
- Ship vs deformable semi. Bridge impact.
- Ship vs living quarter. Vertical wave motion impact.
- Ship vs living quarter. Horizontal bridge impact.

It was discovered that the wheelhouse has inferior crushing resistance compared to the remaining hull. Great resultant forces are observed in collisions where the semi hits near the forecastle deck due to the large contact area, whereas the upper decks are greatly reduced capacity. In all analyzed load cases, the ship strain energy dominates the energy equilibrium. Results show that strength design can be used as a slightly conservative assumption in most of the analyzed situations.

In Table 1, deformations at various velocities and corresponding kinetic energy levels are extrapolated from the results.

Collision Energy	10	50	100	[MJ]
Velocity	1.1	2.5	3.5	[m/s]
Rigid Plate	0.8	3.2	5.2	[m]
Deformable	1.3	2.4	4.7	[m]
Survival draft	4.0	11.2	-	[m]
Vertical impact	1.8	-	-	[m]
Horizontal impact	4.7	12.7	-	[m]

Table 1: Expected ship deformations vs. kinetic energies.



# Sammen drag

Kollisjoner mellom skip og offshoreinstallasjoner er sjeldne hendelser, men er en stor bidragsyter til risikonivået til sjøs. Observerte trender over de siste årene viser at størrelsen på både offshoreinstallasjoner og skip øker, slik at et sammenstøt mellom en dekksmul og styrhus er mer og mer mulig. En slik ulykke kan få alvorlige konsekvenser.

Overbygget til skip er vanligvis betydelig mindre avstivet enn den nedsenkede delen av skipsskroget, slik at deformasjonsstyrken er tilsvarende redusert. I tillegg er ofte passasjerkabiner plassert i den forreste delen av overbygget. Et sammenstøt i dette området kan være den direkte årsaken til dødsfall.

En sekundær effekt av et ødeleggende sammenstøt mot broen kan være den reduserte evnen til å kontrollere fartøyet. Dersom skipet skulle sette seg fast under offshoreinstallasjonen kan det lede til betydelig skade på både skip og plattformen, samt skade f.eks. eventuelle produksjonsrisere tilkoblet plattformen.

En kollisjons eksterne mekanikk kan analyseres ved å benytte prinsippet om bevaring av energi og bevegelsesmengde. Et fartøys kinetiske energi blir spredd ved absorpsjon av tøyingsenergi i begge fartøyene, samt ved viskøs demping av det omkringliggende vannet, og overføring av bevegelsesmengde til kinetisk translasjons- og rotasjonsenergi.

Den interne mekanikken er derimot vanskeligere å anslå nøyaktig uten å gjennomføre detaljert og tidkrevende elementanalyse. Gjeldende prinsipper bak ulineær elementanalyse blir presentert, samt forskjellige løsningsmetoder og deres fordeler og ulemper.

I denne diplomoppgaven blir kollisjonsscenarioer for et stort offshorefartøys overbygg analysert ved hjelp av ulineær elementmetode. Skipet kolliderer med modeller av en ultra dypvanns halvt nedsenkbar borerigg, samt et boligkvarter til en jacket-plattform i aluminium.

En detaljert modell av styrhuset til et 13 600 tons offshore servicefartøy er laget. Skroget til skipet ble modellert som stivt for å lettere påføre globale masseegenskaper, så vel som gjenopprettende krefter og momenter.

To offshoreinstallasjoner er også modellert. En halvt nedsenkbar borerigg ble modellert som en ekvivalent box-bjelke med realistiske detaljer. Boligkvarteret er tatt inspirert av det som finnes på Kvitebjørn jacketen, og er modellert som ekstruderte aluminiumsprofiler som hviler på en stiv bjelkerist.

Fem kollisjonsscenarioer er testet. Alle analyser benytter foreskrevet forskyvning.

- Skip mot stiv plate.
- Skip mot deformerbar platform.
- Skip mot deformerbar platform. Støt mot broen.
- Skip mot boligkvarter. Vertikalt bølgeindusert støt.
- Skip mot boligkvarter. Horisontalt støt mot broen.

Det ble oppdaget at overbygget har underlegen knusningsmotstand i forhold til resten av skroget. Det ble også observert store resultantkrefter idet den nedsenkbare platformen treffer nær bakken på skipet på grunn av de store kontaktfatene som er involvert i kollisjonen. Analysene nær det øverste dekket viser derimot liten styrke. I alle de analyserte tilfellene ble det observert at skipets tøyingsenergi dominerer energibalansen. Resultatene viser at styrkedesign kan benyttes som en svakt konservativ antagelse i de fleste analyserte tilfeller.

I tabell 2 vises deformasjoner ved forskjellige hastighet, samt NORSOK-kravet, ekstrapolert fra resultatene.

Kollisjonsenergi	10	50	100	[MJ]
Hastighet	1.1	2.5	3.5	[m/s]
Stiv plate	0.8	3.2	5.2	[m]
Deformerbar semi	1.3	2.4	4.7	[m]
Overlevelsedyppgang	4.0	11.2	-	[m]
Vertikalt støt	1.8	-	-	[m]
Horisontalt støt	4.7	12.7	-	[m]

Table 2: Forventede deformasjoner vs kinetisk energi.

# Preface

This master thesis is the result of work performed during the spring semester of 2013 by stud. techn. Jan Børge Sætre at the Norwegian University of Science and Technology (NTNU) for the degree of Master of Science in Marine Technology. The work presented in this thesis is a continuation of the project thesis performed during the fall semester of 2012.

The scope of the master thesis is divided into several parts. The first part is dedicated to presenting the motivation for doing this thesis. Earlier accidents are investigated to help develop proper boundary conditions for the analyses. Further on, basic principles behind non-linear finite element methods are briefly presented before weight is put on the development of the FE-models and boundary conditions. The final part is dedicated to presenting results from the various load cases, and finally discussion of the implications the results have yielded.

Due to the relevant project thesis I already had a basic understanding of finite element modeling and analysis, but the increased level of detail of the master thesis demanded even more knowledge of analysis settings, as well as a keen eye for detail when studying structural drawings.

The task proved to be greater than first anticipated, but upon completion I realize that I am left with solid knowledge about NLFEA and collision analyses. The experience will no doubt be of great value in a professional career.

During the execution of the finite element analysis and writing of the project thesis I frequently had need to discuss problems and receive guidance. The academic staff and fellow students here at the Marine Technology Centre are fortunately extremely knowledgeable, and have provided me with valuable input for the master thesis. In particular I would like to thank the following:

- Professor Jørgen Amdahl - for supervising the thesis and providing valuable guidance and supplying motivation.

- Ph.D. Candidate Martin Storheim - for sharing his vast knowledge about FEA, and for always being available for constructive conversations.

Trondheim, June 3<sup>rd</sup> - 2013



Jan Børge Sætre

# Contents

Nomenclature	xiii
<b>1 Introduction</b>	<b>3</b>
<b>2 Motivation For Analysis</b>	<b>5</b>
2.1 General	5
2.2 Previous Ship Collisions	6
2.2.1 Far Symphony / West Venture - March 7 <sup>th</sup> 2004	6
2.2.2 Ocean Carrier / Ekofisk 2/4-P bridge - June 2 <sup>nd</sup> 2005	6
2.2.3 Big Orange XVIII / Ekofisk 2/4-W - June 8 <sup>th</sup> 2009	8
2.3 Motivation for analysis	9
2.3.1 General	9
2.3.2 Collision Scenarios	12
<b>3 Motion Analysis</b>	<b>13</b>
3.1 General	13
3.2 Short Term Motion Statistics	13
3.2.1 The Response Amplitude Operator	13
3.2.2 Wave spectrum	15
3.2.3 Response spectrum	16
3.2.4 Short term probability distribution	17
3.3 Finding the motion of the ship superstructure	18
<b>4 Simplified Calculation Methods</b>	<b>23</b>
4.1 General Design Principles	23
4.2 Collision Mechanics	25
4.2.1 Finding the external collision energy	25
4.2.2 Dissipation of internal strain energy	27
4.3 Simple Calculation Models	28

<b>5</b>	<b>The Non-Linear Finite Element Method</b>	<b>31</b>
5.1	General . . . . .	31
5.1.1	Geometric Non-linearity . . . . .	32
5.1.2	Material Nonlinearity . . . . .	35
5.1.3	Boundary condition non-linearity . . . . .	37
5.2	Solution Methods . . . . .	37
5.2.1	Static Solution Methods . . . . .	38
5.2.2	Dynamic Solution Methods . . . . .	41
5.3	Non-linear analysis in LS-DYNA . . . . .	44
5.3.1	Time integration . . . . .	44
5.3.2	Critical time step . . . . .	45
5.3.3	Subcycling (Mixed time integration) . . . . .	46
5.3.4	Material models . . . . .	47
5.3.5	Finite element formulations . . . . .	53
<b>6</b>	<b>Finite element modeling</b>	<b>55</b>
6.1	Software . . . . .	55
6.1.1	MSC Patran . . . . .	55
6.1.2	LS-DYNA . . . . .	56
6.2	Reference structures . . . . .	56
6.2.1	Large offshore vessel . . . . .	56
6.2.2	Semi-submersible rig . . . . .	58
6.2.3	Fixed platform living quarter . . . . .	58
6.3	Ship Model . . . . .	59
6.3.1	Geometry modeling . . . . .	60
6.3.2	Simplifications . . . . .	60
6.3.3	Meshing . . . . .	63
6.3.4	Material . . . . .	67
6.4	Semi-submersible Deck Model . . . . .	68
6.4.1	Geometry Modeling . . . . .	68
6.4.2	Meshing . . . . .	68
6.4.3	Material . . . . .	70
6.5	Living quarter model . . . . .	70
6.5.1	Geometry Modeling . . . . .	71
6.5.2	Modeling Simplifications . . . . .	71
6.5.3	Meshing . . . . .	71
6.5.4	Material . . . . .	71
6.6	Collision Setup . . . . .	72
6.6.1	Ship restoring forces . . . . .	72
6.6.2	Boundary conditions . . . . .	73
6.6.3	Collision velocity . . . . .	75

6.6.4	Contact . . . . .	76
<b>7</b>	<b>Finite element results</b>	<b>79</b>
7.1	General analysis settings . . . . .	79
7.2	Results - Collision with semi submersible. . . . .	80
7.2.1	Constant velocity, rigid plate . . . . .	81
7.2.2	Constant velocity, deformable semi . . . . .	85
7.2.3	Initial velocity, deformable semi . . . . .	87
7.2.4	Survival draught . . . . .	93
7.3	Results - Collision with Living Quarter. . . . .	94
7.3.1	Vertical Impact . . . . .	98
7.3.2	Horizontal Impact . . . . .	100
7.4	Validity of boundary conditions . . . . .	106
7.4.1	Ship . . . . .	106
7.4.2	Semi-submersible . . . . .	108
7.4.3	Living quarter . . . . .	110
7.5	Comparison of results . . . . .	112
7.5.1	Pressure-area relationships . . . . .	112
7.5.2	Semi-submersible collisions . . . . .	113
7.5.3	Living quarter collision . . . . .	115
<b>8</b>	<b>Conclusion</b>	<b>117</b>
<b>9</b>	<b>Further work</b>	<b>121</b>
<b>A</b>	<b>Cutplanes</b>	<b>I</b>
A.1	Cutplanes analysis 1 - Ship vs rigid plate . . . . .	I
A.2	Cutplanes analysis 2 - Ship vs deformable semi, fixed . . . . .	III
A.3	Cutplanes analysis 4 - Ship vs deformable semi, survival draft . . . . .	V
A.4	Cutplanes analysis 5 - Ship vs LQ, vertical . . . . .	VII
A.5	Cutplanes analysis 6 - Ship vs LQ, horizontal . . . . .	IX
<b>B</b>	<b>Living Quarter <math>\sigma - \varepsilon</math> contours.</b>	<b>XI</b>
<b>C</b>	<b>Motion characteristics for reference ship</b>	<b>XV</b>
C.1	Response amplitude operators . . . . .	XV
C.2	Phase angles . . . . .	XVII





# List of Figures

2.1	The semi submersible drilling rig "West Venture" after collision. . . . .	7
2.2	The bow of the offshore supply vessel "Far Symphony" after collision. . . . .	7
2.3	Ekofisk 2/4-W platform after impact. . . . .	8
2.4	The bow of the Big Orange XVIII after collision. . . . .	9
3.1	The frame of reference used for floating bodies. [Faltinsen, 1990] . . . . .	14
3.2	The JONSWAP wave spectrum . . . . .	17
3.3	Combined vertical RAO . . . . .	19
3.4	Ship response spectrum . . . . .	19
3.5	Heave probability contours heading $0^\circ$ . . . . .	20
3.6	Heave probability contours heading $45^\circ$ . . . . .	21
3.7	Heave probability contours heading $90^\circ$ . . . . .	21
4.1	Relative strength . . . . .	24
4.2	Force-displacement curve. . . . .	27
5.1	Two-bar arch . . . . .	33
5.2	Deformation and equilibrium for large displacements. . . . .	33
5.3	Snap-through . . . . .	34
5.4	Non-linear stress-strain relationship . . . . .	35
5.5	Isotropic and kinematic hardening rules. . . . .	36
5.6	Original Euler-Cauchy and Improved Euler-Cauchy. . . . .	39
5.7	Original Newton-Raphson with continuously updated $\mathbf{K}_T$ . . . . .	40
5.8	Geometric interpretation of an arc length method. . . . .	41
5.9	LS-DYNA time integration loop . . . . .	45
5.10	Stress-strain curve aluminium alloys. . . . .	50
5.11	Simplified illustration of the critical strain generation procedure . . . . .	52
5.12	Belytschko-Lin-Tsay shell element . . . . .	53
5.13	Hughes-Liu beam element . . . . .	54

6.1	The RLWI vessel Island Wellserver. . . . .	57
6.2	Schematic of the model vessel. The part modeled in detail is dis- tinctively marked. . . . .	57
6.3	A semi-submersible drilling rig. . . . .	58
6.4	The Kvitebjørn platform with eccentric living quarter. . . . .	59
6.5	Ship column dimensions . . . . .	61
6.6	Full wheelhouse model . . . . .	61
6.7	Half wheelhouse model . . . . .	62
6.8	HP-Profile . . . . .	63
6.9	Ship superstructure stiffener layout . . . . .	64
6.10	IsoMesh . . . . .	65
6.11	Paver mesh . . . . .	66
6.12	Longitudinal stiffener mesh . . . . .	66
6.13	Ship girder mesh . . . . .	66
6.14	Geometry of the modeled semi submersible deck. . . . .	69
6.15	Geometry of the modeled Living Quarter. . . . .	70
6.16	Figurative depiction of the applied boundary conditions. . . . .	74
7.1	Analysis 1: Force-deformation curve . . . . .	82
7.2	Analysis 1: Energy-deformation relationship. . . . .	83
7.3	Analysis 1: Time lapse. . . . .	84
7.4	Analysis 2: Force-deformation curves . . . . .	86
7.5	Analysis 2: Energy-deformation curves . . . . .	86
7.6	Analysis 2: Analysis set-up . . . . .	87
7.7	Analysis 2: Time-lapse . . . . .	88
7.8	Analysis 2: Total energy history . . . . .	89
7.9	Analysis 2: Damage to semi-submersible after impact. . . . .	89
7.10	Analysis 2: Semi-submersible deformation contours . . . . .	90
7.11	Analysis 4: Time-lapse . . . . .	95
7.12	Analysis 4: Semi-submersible deformation at analysis end. Fringe levels in meters. Maximum value: 0.27 meter. . . . .	96
7.13	Analysis 4: Force-deformation curves. . . . .	96
7.14	Analysis 4: Energy-deformation curves. . . . .	97
7.15	Analysis 4: Total energies throughout the collision. . . . .	97
7.16	Analysis 5: Initial configuration. . . . .	99
7.17	Analysis 5: The vessel's vertical displacement, velocity, and accel- eration. . . . .	99
7.18	Analysis 5: Set-up for analysis of vertical living quarter collision. .	100
7.19	Analysis 5: Vertical LQ impact. . . . .	101
7.20	Analysis 5: Force-deformation curve. . . . .	102
7.21	Analysis 5: Energy-deformation curve. . . . .	102

7.22	Analysis 6: Positioning of the ship prior to analysis. . . . .	103
7.23	Analysis 6: Time-lapse . . . . .	104
7.24	Force-deformation curve, analysis 6. . . . .	105
7.25	Energy-deformation curve, analysis 6. . . . .	105
7.26	Comparison of restoring forces vs vertical impact force. . . . .	107
7.27	Calculated semi-submersible response. . . . .	110
7.28	Pressure-area relationship based on low wheelhouse impact. . . . .	112
7.29	Pressure-area relationship based on high wheelhouse impact. . . . .	113
7.30	Comparison of the resultant contact force found in analysis 1 & 2. . . . .	114
7.31	Comparison of the computed energies found in analysis 1 & 2. . . . .	114
7.32	Comparison of the resultant force found in analysis 4 & 6. . . . .	116
7.33	Comparison of the total computed energies found in analysis 4 & 6. . . . .	116
A.1	Cutplanes for analysis 1 - Ship vs rigid plate. . . . .	II
A.2	Cutplanes for analysis 2 - Ship vs deformable semi. . . . .	IV
A.3	Cutplanes for analysis 4 - Ship vs semi in survival draft. . . . .	VI
A.4	Cutplanes for analysis 5 - Vertical LQ impact. . . . .	VIII
A.5	Cutplanes for analysis 6 - Horizontal LQ impact. . . . .	X
B.1	Von Mises stress contours LQ, vertical collision. . . . .	XI
B.2	Plastic strain contours LQ, vertical collision . . . . .	XII
B.3	Von Mises stress contours LQ, horizontal collision. . . . .	XII
B.4	Plastic strain contours LQ 5% level, horizontal collision . . . . .	XIII
B.5	Plastic strain contours LQ 10% level, horizontal collision . . . . .	XIII
B.6	Plastic strain contours LQ 20% level, horizontal collision . . . . .	XIV
B.7	Plastic strain contours LQ 50% level, horizontal collision . . . . .	XIV
C.1	RAO Heave center of gravity. . . . .	XV
C.2	RAO Pitch center of gravity. . . . .	XVI
C.3	Heave RAO at wheelhouse top. . . . .	XVI
C.4	Phase angles heave center of gravity. . . . .	XVII
C.5	Phase angles pitch center of gravity. . . . .	XVIII



# List of Tables

1	Expected ship deformations vs. kinetic energies. . . . .	ii
2	Forventede deformasjoner vs kinetisk energi. . . . .	iv
5.1	Material properties for aluminium. . . . .	49
5.2	Power law parameters for aluminium alloys used in analysis. . . . .	50
5.3	Material properties of steel. . . . .	52
6.1	Main principals for the Island Wellserver, UT-767 CD design. . . . .	56
6.2	Principal dimensions of the semi-submersible box girder. . . . .	69
6.3	Principal dimensions of the Living Quarter model. . . . .	71
6.4	The distribution of aluminium alloys throughout the Living Quarter model. . . . .	72
7.1	Material properties for materials used in analyses. . . . .	79
7.2	Analysis setup for semi-submersible collisions. . . . .	80
7.3	Mass properties for the ship. . . . .	90
7.4	Analysis setup for living quarter collisions. . . . .	98
8.1	Expected deformations vs. kinetic energies for various velocities. . . . .	118



# Nomenclature

$\bar{\varepsilon}^p$	Effective logarithmic plastic strain
$\Delta t$	Time step
$\mu$	Friction coefficient
$\nu$	Poisson ratio
$\rho$	Density of material
$\sigma_p$	Proportionality limit
$\varepsilon_{yp}$	Elastic yield strain
$E_t$	Tangent modulus
$f_{0.2}$	Aluminium elastic limit stress
$f_t$	Aluminium stress at rupture
$H'$	Plastic tangent modulus
$L_s$	Characteristic element length
$L_{pp}$	Length between perpendiculars
$L_{wl}$	Length in water line
$M_P$	Plastic bending moment
$M_P$	Plastic bending moment
$t_s$	Skin thickness
$t_w$	Web thickness
$W_P$	Plastic section modulus
<b>C</b>	Damping matrix

<b>F</b>	Force vector
<b>F</b>	Stress divergence vector
<b>H</b>	Hourglass resistance
<b>I</b>	Impulse vector
<b>K</b>	Stiffness matrix
<b>K<sub>T</sub></b>	Tangential stiffness matrix
<b>M</b>	Mass matrix
<b>P</b>	External and internal body force matrix
<b>p</b>	Momentum vector
<b>r</b>	Displacement vector
<b>v</b>	Velocity vector
<b>x</b>	Geometry vector
<b>ï</b>	Acceleration vector
<b>ï</b>	Velocity vector
<b>R<sup>ext</sup></b>	External force vector
ALS	Accidental Limit State
B	Bulk modulus
BLT	Belytscko-Lin-Tsay shell element
c	Speed of sound in material
CAE	Computer Aided Engineering
DAF	Dynamic Amplification Factor
dof	Degree-of-freedom
DP	Dynamic Positioning
FEA	Finite Element Analysis
G	Shear modulus
GBS	Gravity Based Structure
h	Mesh width
HL	Hughes-Liu shell element



k	Strength coefficient
LQ	Living Quarter
MSL	Mean Sea Level
NCS	Norwegian Continental Shelf
NLFEA	Non-Linear Finite Element Analysis
p	Contact Pressure
RAO	Response Amplitude Operator, Transfer Function
RLWI	Riserless Well Intervention
RTCL	Rice-Tracey-Cockcroft-Latham fracture criterion
ULS	Ultimate Limit State



# Chapter 1

## Introduction

Collisions with dedicated- or passing vessels are a constant threat to offshore installations. Offshore structures typically have several vessels working in the immediate vicinity, or are themselves located close to major shipping lanes. To keep the risk of collision at a sufficiently low level, current regulations specify that offshore installations are to be designed for impacts with ships of a given size and speed. A typical impact scenario can be a 5000 tons displacement supply vessel colliding at 2 m/s.

In 2004, the supply vessel *Far Symphony* collided with the drilling platform *West Venture*. The implied kinetic energy was more than three times the design energy. Fortunately, the vessel hit one of the platform's columns with its bow, and only material damage occurred. However, from closer inspection of photos taken after the collision, it is evident that the ship's superstructure would have hit the platform's deck girder had the course been laid a few meters further starboard. This would likely have resulted in large structural damages to the ship, possibly also fatalities among the ship's crew.

A wheelhouse or superstructure collision will most likely have significantly greater structural consequences than a corresponding bow or stern collision. While a hull breach is not critical this far above the waterline, the wheelhouse scantlings are typically inferior to other load bearing parts of the hull, and will thus not have the same resistance to deformation. As the superstructure of ships is commonly reserved for recreational areas, crew's cabins, and the bridge itself, there is significant risk of fatalities should the collision be a fact.

A secondary effect to a direct impact to the bridge in particular would be the

total loss of, or at least reduced ability to control the vessel. If the ship is stuck in underneath the topside, and in heavy weather, the possibility of damaging the production risers, drill string, and even the topside itself is a significant risk that may lead to a catastrophic environmental and material disaster.

Simplified methods for analyzing the average resistance and damage of axial crushing of stiffened bow structures currently exist, but it is uncertain whether these are suitable for analyzing wheelhouse impacts. The most reliable method existing today is doing a complete non-linear finite element analysis (NLFEA). NLFEA is not preferred in a practical point of view, as it is labour intensive and computationally demanding. The approach is not straightforward, but can yield very good results if executed correctly.

Deformation of both structures is typically considered as separate events, where one object is considered deformable, while the other is rigid. Collision between ship and offshore structure is typically more complicated than that. Interactions between the two bodies complicate calculations considerably, as contact area is determined by the deformation of both objects. This may in some cases render the simplified deformation curves invalid.

In this master thesis, methods of analyzing the external and internal mechanics of collisions are presented. External mechanics are the rigid body motions and deformations of the objects involved in a collision, while internal mechanics involve the behaviour of material and internal structures: strains, collapse mechanisms, and deformation of the involved members.

Principles behind NLFEA are briefly presented, but ultimately the focus is on developing a NLFEA model of a ship striking an offshore structure with its superstructure. The goal is to investigate the result of such a collision, both for the striking vessel, as well as for the offshore structure.

Force-deformation-, and energy-deformation curves are created in order to be able to estimate the implications of a possible collision between an offshore vessel wheelhouse and a floating structure at various velocities. In addition, some statistical calculations are done in order to examine the possibility of such a collision happening during normal operating conditions.

Due to the workload being larger than first expected, some points were dropped from the master thesis assignment after having conferred with the advisor.

**Point 1** Computations of drift-off motions and heave velocities are omitted.

**Point 4** Collision against HC-risers have not been considered.

## Chapter 2

# Motivation For Analysis

### 2.1 General

Ship collision are rare events, and usually are of such a nature that there are only material damages. On the Norwegian Continental Shelf (NCS), 115 collisions have been reported in the period 1982-2010. Since 2001, 26 collisions have been reported. While there have been no casualties or personal injury, the economic consequences have been significant [Kvitrud, 2011].

In offshore shipping, most collisions occur while ships are operating near offshore structures while using dynamic positioning (DP). The ships' power supply or DP can in rare events fail, which may in turn lead to drift-off towards the offshore structure should the weather conditions be unfavourable.

Other times, sheer negligence may be the cause of the collision. In such cases, the ship's autopilot might be activated while the bridge personnel are distracted or otherwise engaged. The velocity in these collisions might typically be significantly higher than in drift-off situations, and the possibility for disaster equally so.

Trends indicate that offshore vessels trafficking the Norwegian Continental Shelf are only increasing in size, such that a collision today is even more severe than one happening in the 1980s. The introduction of the bulbous bow to more modern ships, as well as more unconventional wave piercing bows has also resulted in a higher damage potential due to the ramming and cutting nature of the bow.

In the following, the possibility and boundary conditions of a collision with the superstructure of the vessel will be examined and evaluated.

## 2.2 Previous Ship Collisions

### 2.2.1 Far Symphony / West Venture - March 7<sup>th</sup> 2004

In 2004, the offshore supply vessel Far Symphony lost control of navigation, and collided with the semi submersible rig West Alpha.

The supply ship was routinely navigating towards the rig with autopilot engaged. The commanding officer failed to disengage the autopilot in time, and collided bow first into one of the columns of the drilling rig. The ship sustained extensive damages to the bow (indentation of 2.5 - 3.0 m). The rig suffered minor damages. Both vessels were able to navigate safely after the incident, and no personnel were injured. The speed at the time of collision was recorded to be 7.4 knots (3.8 m/s), and a kinetic energy of 39 MJ [Munch-Soegaard and Pettersen, 2004].

After investigating the indentation left by the ship, it is evident the outcome could have been catastrophic if the circumstances were different [Petroleumstilsynet, 2004]. Had the ship passed only a few meters toward the starboard side, the bow would have passed underneath the deck of the drilling rig, and the superstructure would have taken most of the impact. Such a collision would possibly lead to casualties aboard the ship, as well as extensive damage aboard the rig, possible also damage to risers and drilling equipment.

### 2.2.2 Ocean Carrier / Ekofisk 2/4-P bridge - June 2<sup>nd</sup> 2005

The Ocean Carrier was moving towards Ekofisk-P in dense fog when it collided. Due to miscommunication between the captain and a mate, no one was controlling the vessel as it entered the 500 meter zone. When it became apparent that the ship was on collision course, it was already too late to avoid the impact [Petroleumstilsynet, 2005].

The Ocean Carrier collided with the bridge connecting the Ekofisk 2/4-P and 2/4-T with an impact velocity of about 3 m/s, and a kinetic energy of over 20 MJ. The Ocean Carrier sustained substantial damage to the bridge area and to the bow [Kvitrud, 2011].



Figure 2.1: The semi submersible drilling rig "West Venture" after collision.



Figure 2.2: The bow of the offshore supply vessel "Far Symphony" after collision.



Figure 2.3: Ekofisk 2/4-W platform after impact.

### 2.2.3 Big Orange XVIII / Ekofisk 2/4-W - June 8<sup>th</sup> 2009

In 2009, the well stimulation vessel Big Orange XVIII collided with the water injection platform Ekofisk 2/4-W. Ekofisk 2/4-W is an unmanned jacket structure located in the southern North Sea at the Ekofisk field.

The ship collided while en route to the Ekofisk 2/4-X platform intending to stimulate a well. During navigation outside the 500 m. safe zone around the platform, the captain activated the autopilot while answering a short telephone call in a nearby room. The autopilot was erroneously never disengaged when the captain returned to station, and the ship continued to follow the pre-set course until it finally crashed with the W-platform. Any attempts to correct the vessel's course were unsuccessful, as the autopilot could not be overridden manually while engaged.

The report made by Petroleumstilsynet [2009] states that the incident led to large structural damages on both the ship and jacket structure. The ship passed near several other jacket and jack-up structures at speeds up to 10 knots (5.2 m/s). In the end, the ships bow was deformed axially about 2 m, and had several antennae and communications device knocked off of its wheelhouse top. The platform suffered severe damages to legs, braces and risers. The collision energy was estimated to be near 70 MJ [Petroleumstilsynet, 2009].





Figure 2.4: The bow of the Big Orange XVIII after collision.

## 2.3 Motivation for analysis

### 2.3.1 General

By examining previous accidents in section 2.2, it is evident that ship-structure collision happen quite frequently in the North Sea, and is a source of great economic consequence for the owners of both ships and offshore structures.

Although few lives have been lost due to ship / structure collisions, it is likely that casualties will occur in the future should a ship strike an offshore installation with its superstructure or wheelhouse. If the current trend of increasing ship size continues, the risk of casualty and total loss may very well also include the struck structure and its crew, as was nearly the case in the Big Orange XVIII / Ekofisk 2/4-W collision, see section 2.2.3.

From the results obtained by studying the ship motion characteristics, particularly those visible in figure 3.5, we see that even at modest sea states where full operability is still expected, the vertical motion at an extreme point may be high. The possibility of vertical impact is absolutely present for large offshore

vessels operating in or near the offshore structures if the environmental conditions should be unfavourable.

Based on the aforementioned arguments, it is desirable to investigate the possible implications of a collision between a ship and an offshore structure where the ships superstructure is the contact surface. The damages to both the wheelhouse and the struck structure should be investigated using realistic boundary conditions. Based on previous incidents, two main scenarios are envisioned to be tested.

### 2.3.1.1 Collision scenario I - Jacket living quarter

A jacket is a bottom-fixed lightweight truss structure supporting a topside which may include petroleum processing facilities, drilling equipment, storage areas, accommodation, etc. .

Even though most jacket designs are inherently similar of both form and function, several different topside designs exist, making some more susceptible and vulnerable to collision than others.

A likely chain of events leading to a collision between an offshore vessel and a suitable platform could be the following:

1. An offshore vessel is en route to serve a well near a platform in the North Sea, cruising at 8 knots.
2. A high wind has been acting near the oil field for quite some time, causing 3-5 meter waves.
3. The ship enters the 500 m safety zone near the platform. The commanding officer neglects to disengage the autopilot. He is alone on the bridge.
4. Due to the heavy current acting at the oil field, the ship has veered a off course, and is headed dangerously close to the western end of the platform.
5. The commanding officer aboard the ship fails to realize that the autopilot is engaged, and is unable to control the ship. The ship is now on collision course with the platform's living quarter.

**The next events can be imagined to play out in the following ways:**

**Outcome 1** The commanding officer realizes that the autopilot is still activated, and quickly disengages it. He reverses the engines and manages to stop the vessel. At this time the vessel is located directly below

the living quarter. A particularly large wave hits the ship, and the resulting heave and pitch motion causes the ship's wheelhouse to collide with the underside of the living quarter.

**Outcome 2** The commanding officer watches the distance to the platform decrease rapidly, and soon realizes that there is nothing he can do to avoid disaster. The platform and ships crew is notified of the impending collision. At the last possible moment the commanding officer evacuates the bridge. While the ship continues onward, a particularly large wave hits the ship, and the resulting heave and pitch motion causes the ship's wheelhouse to collide with the lower part of the living quarter bulkhead.

### 2.3.1.2 Collision scenario II - Semi-submersible rig deck girder

A semi-submersible rig is a floating unit that can be used for a number of applications, most commonly drilling, processing, and well intervention. Most commercially available consist of two or more rectangular pontoons supporting at least four vertical columns which in turn support the topside.

The semi submersibles' air gap is typically less than that of a conventional jacket, as they are more able to ride atop the waves. As was experienced during the West Venture / Far Symphony collision in section 2.2.1, ships have already collided with semi-submersibles at reasonable high velocities.

If one studies photographs taken at the scene (figures 2.1, 2.2), it is evident that had the passed merely a few meters further starboard, the bow of the ship would have steered clear of the column and experienced a direct hit to the superstructure instead.

A likely chain of events for a collision with a semi-submersible could be the following:

1. An offshore vessel is en route to serve a well near a semi-submersible rig in the North Sea, cruising at 8 knots.
2. It is night-time, and the weather is calm at the rig's location. A slight fog reduces visibility.
3. The ship enters the 500 m safety zone around the vessel. Due to currents in the area, the course is well off, and the ship is heading directly towards the rig. The crew aboard the bridge neglect to disengage the autopilot while performing routine check lists.

4. The crew discover that they are heading directly towards the semi submersible, and try to correct the course. They do not realize that the autopilot is engaged.
5. In a last attempt to avoid collision, the crew tries to reverse the azimuth-thrusters and demand full speed. It is not possible to manually control the thrusters' heading while the autopilot is engaged, resulting in a further acceleration of the ship.
6. The crew ultimately discover their error, disengaged the autopilot and reverses the thrusters. It is, however, too late to avoid a collision, and the bridge crew is forced to evacuate the wheelhouse.
7. The ship continues directly between two columns, parallel to the rigs pontoons. The superstructure hits the topside at high speed.

### 2.3.2 Collision Scenarios

Based on the aforementioned chain of events, the following cases will be investigated further in the thesis:

- Collision with a semi-submersible, where the semi is in normal operating draft. The ship will hit near its forecastle deck. Several boundary conditions should be tested in order to investigate the effect of any simplifications.
- Collision with a semi submersible, where the semi is in survival draft. This will cause the ship's bridge to hit the semi, while the remaining superstructure will steer clear.
- Collision with a living quarter, where the ships bridge collides vertically with the underside of the LQ.
- Collision with a living quarter, where the ships bridge collides horizontally with the LQ. This scenario is similar to a collision with a semi in survival draft, but the contact area is smaller.

In addition, simple ship motion considerations should be made in order to estimate the possibility of a vertical impact of a certain magnitude given a sea state. This will be the focus of Chapter 3.

# Chapter 3

## Motion Analysis

### 3.1 General

One particular result of the increased size concerns the vertical motion of extreme points of the ship, such as the wheelhouse. The combined heave and pitch motion while the ship encounters waves met in normal operating conditions can be high enough to impact a topside which normally would have sufficient air gap. Structures at particular risk are e.g. jacket and gravity based structures with very eccentric modules or living quarters.

### 3.2 Short Term Motion Statistics

#### 3.2.1 The Response Amplitude Operator

For a harmonically oscillating system it is common to express the response characteristic by the response amplitude operator (RAO). This is the mechanical transfer function of the rigid body motions of the system, i.e. the response amplitude per unit wave amplitude. The RAO is usually defined separately for each degree of freedom for the center of gravity of a ship, but may be defined for an arbitrary point on the ship. By using the RAO it is straightforward to calculate the first order response of a vessel for a given wave. For an arbitrary translation

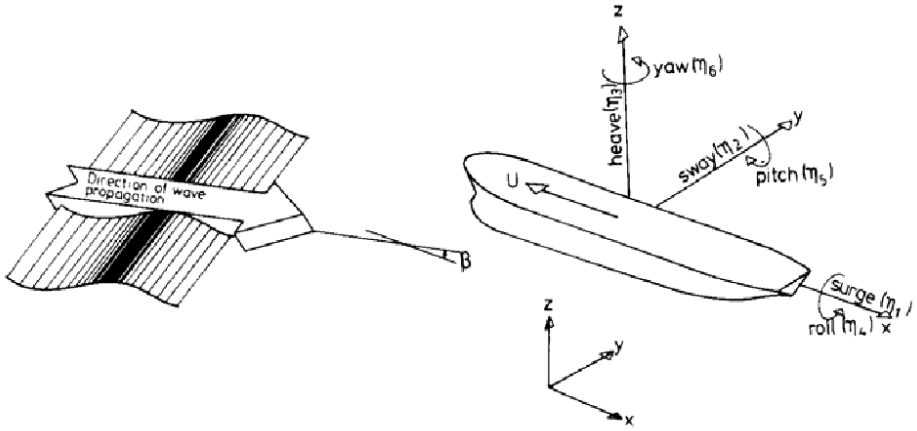


Figure 3.1: The frame of reference used for floating bodies. [Faltinsen, 1990]

degree of freedom, the RAO is defined as:

$$H_{\eta\zeta}(\omega) = \frac{|\eta|}{\zeta_a} \quad (3.1)$$

This means that for an arbitrary incoming wave component it is straightforward to calculate the response for any degree of freedom as long as the RAO is provided.  $H_{\eta\zeta}(\omega)$  is the mechanical transfer function,  $\eta$  is the applicable response, and  $\zeta_a$  is the wave amplitude.

In the case of a ship wheelhouse collision, one is interested in the motions of the most extreme point on the wheelhouse top, meaning that rigid body translations must be combined with rotations. In addition, damping forces caused by the viscosity of the water will cause a phase shift of the motion. In this thesis, the motion will be simplified to a 2D-combined heave and pitch motion, but the procedure can be easily transferred to include the full 6 degrees of freedom.

The motion at an arbitrary point  $p$  can be written as

$$\mathbf{s} = \eta_1 \mathbf{i} + \eta_2 \mathbf{j} + \eta_3 \mathbf{k} + \boldsymbol{\omega} \times \mathbf{r} \quad (3.2)$$

$$\boldsymbol{\omega} = \eta_4 \mathbf{i} + \eta_5 \mathbf{j} + \eta_6 \mathbf{k} \quad (3.3)$$

$$\mathbf{r} = x\mathbf{i} + y\mathbf{j} + z\mathbf{k} \quad (3.4)$$

where  $\mathbf{i}, \mathbf{j}, \mathbf{k}$  are unit vectors along the x,y, and z axis respectively.

This results in the following:

$$\mathbf{s} = (\eta_1 + z\eta_5 - y\eta_6)\mathbf{i} + (\eta_2 - z\eta_4 + x\eta_6)\mathbf{j} + (\eta_3 + y\eta_4 - x\eta_5)\mathbf{k} \quad (3.5)$$

For this application, we are merely interested in the vertical component along the  $\mathbf{k}$  -vector. We assume uncoupled motion and that only the heave and pitch components are significant.

The heave motion at point  $p$  can then be expressed as:

$$\eta_p = \eta_3 - x\eta_5 \quad (3.6)$$

The heave and pitch components can be described by the real parts of their respective complex transfer functions.

$$\eta_3 = \Re \left( \eta_{3a} e^{i(\omega t + \theta_3)} \right) = \Re \left( H_{\eta_3\zeta}(\omega) \zeta_a e^{i(\omega t + \theta_3)} \right) \quad (3.7)$$

$$\eta_5 = \Re \left( \eta_{5a} e^{i(\omega t + \theta_5)} \right) = \Re \left( k(\omega) H_{\eta_5\zeta}(\omega) \zeta_a e^{i(\omega t + \theta_5)} \right) \quad (3.8)$$

Such that the RAO for the vertical motion at point  $p$  can be described by the following expression.

$$H_{\eta_p\zeta} = \frac{\eta_p}{\zeta_a} = \Re \left( H_{\eta_3\zeta}(\omega) e^{i\theta_3} - kx(\omega) H_{\eta_5\zeta}(\omega) e^{i\theta_5} \right) \quad (3.9)$$

Where  $\eta$  are the respective motion amplitudes,  $k(\omega)$  is the wave number, and  $\theta(\omega)$  are the phase angles of the respective motion amplitudes.

### 3.2.2 Wave spectrum

In practice, linear wave theory is used to describe motion of the sea, and to provide statistical estimates of critical values of significant wave height and spectral peak period. It is common to assume that the sea is a stationary *narrow-banded* stochastic process, where the instantaneous surface elevation is Gaussian distributed, and that the wave crests are Rayleigh distributed [Myrhaug, 2005]. In

reality, the wave elevation is quite broad-banded, but assuming narrow bandedness allows for simplifications without introducing very significant errors in this particular context.

Further on, it is assumed that a sea state may be described by a linear superposition of  $n$  wave components, each with a unique period and random phase angle, independently and identically distributed.

The total energy contained in all the wave components can be described by a *wave spectrum*,  $S_{\zeta\zeta}(\omega)$ , and will contain all necessary information concerning the statistical properties of the surface elevation.

In this thesis the Joint North Sea Wave Observation Project (JONSWAP) will be used, as it describes well the not-fully developed sea states most often found in the north sea. The JONSWAP spectrum can be described by the following equation:

$$S_{\zeta\zeta}(\omega) = \frac{5}{32} H_s^2 T_p \left( \frac{\omega}{\omega_p} \right)^5 \exp \left( -\frac{5}{4} \frac{\omega_p}{\omega} \right) (1 - 0.287 \ln \gamma) \gamma \exp \left( -\frac{\left( \frac{\omega}{\omega_p} - 1 \right)^2}{2\sigma^2} \right) \quad (3.10)$$

$$\sigma = \begin{cases} 0.07 & \omega \leq \omega_p \\ 0.0p & \omega > \omega_p \end{cases}$$

$$\gamma = 3.3$$

A wave spectrum for an arbitrary sea state is shown in figure 3.2.

### 3.2.3 Response spectrum

Similarly to the way the wave spectrum includes the total energy content of all wave components of the sea state, the response spectrum contains a complete description of the statistical properties of the response of the vessel in a particular sea state.

The response spectrum for a particular sea state is computed by squaring the RAO and multiplying by the wave spectrum over all wave frequencies.

$$S_{\eta\eta}(\omega) = H_{\eta\zeta}(\omega)^2 S_{\zeta\zeta}(\omega) \quad (3.11)$$



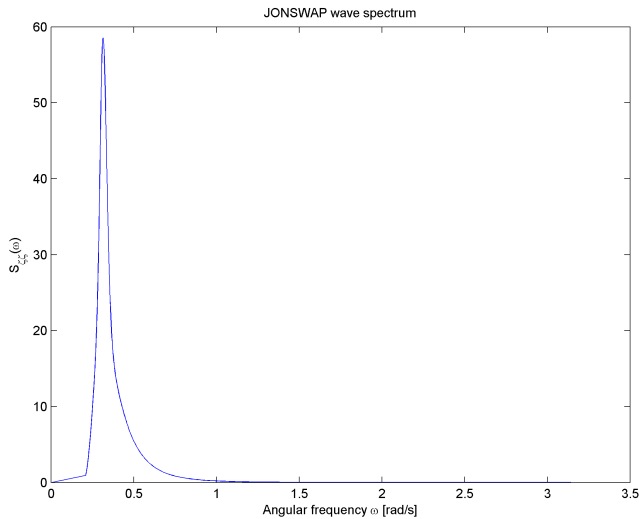


Figure 3.2: The JONSWAP wave spectrum

Statistical properties can be extracted from the spectrum by calculating the spectral moments. The most useful moment used in response analysis is the  $0^{th}$  moment,  $m_0$ , which is the variance of the response spectrum.

$$m_n = \int_0^{\infty} \omega^n S_{\eta\eta}(\omega) d\omega \quad (3.12)$$

$$m_0 = \int_0^{\infty} S_{\eta\eta}(\omega) d\omega = \sigma^2 \quad (3.13)$$

### 3.2.4 Short term probability distribution

For a narrow banded stochastic process, the observed peaks will be Rayleigh distributed. Thus, the wave crest peaks will be Rayleigh distributed. Further on, it can be shown that the response of a mechanical system excited by such a process will also be Rayleigh distributed [Myrhaug, 2005].

The Rayleigh probability density function (PDF) is given by eq. 3.14.

$$f(x, \sigma) = \frac{x}{\sigma^2} \exp\left(\frac{-x^2}{2\sigma^2}\right) \quad (3.14)$$

The Rayleigh cumulative density function (CDF) is given by eq. 3.15.

$$F(x, \sigma) = 1 - \exp\left(\frac{-x^2}{2\sigma^2}\right) \quad (3.15)$$

Where  $\sigma^2$  is the variance of the process, and can be obtained by calculating the  $0^{th}$ -moment of a narrow banded process' spectrum.

### 3.3 Finding the motion of the ship superstructure

In order to calculate the motion characteristics of a particular vessel, RAOs and phase angles for heave and pitch motion of a suitable reference vessel was provided by MARINTEK. The RAOs are provided for headings  $0^\circ$ ,  $45^\circ$ , and  $90^\circ$ .

An extreme point on the wheelhouse top was selected as most critical, with coordinates of  $[x = -53.2 \text{ m}, z = 21.4 \text{ m}]$  from the center of gravity. The RAOs were combined as shown in eq. 3.9 in order to find the RAO for vertical motion in the particular point of interest, as shown in figure 3.3.

By multiplying the wave spectrum by the square of the response amplitude operator, the response spectrum for the particular sea state is obtained. The response spectrum for a sea state with spectral peak period near resonance is presented in figure 3.4. From the response spectrum, various statistical information is obtained by utilizing the fact that response peaks are Rayleigh distributed.

From the corresponding CDF it is possible to calculate the possibility of exceeding a certain level, e.g. exceeding a predefined vertical motion. For this particular case, we are interested in the combination of significant wave height and spectral peak period that will cause the vertical motion of an extreme point on the wheelhouse top to exceed a certain level with a certain probability.

This CDF will uniquely describe the probability of exceedance for all combinations of  $H_S$  and  $T_P$ , since all information regarding sea state and motion characteristics is contained within the variance of the response spectrum,  $\sigma^2$ .

For a range of combinations of  $H_S$  and  $T_P$ , the probability of exceeding a vertical motion of, say, 3 m is calculated for three separate vessel headings.

$$P(\eta_p \geq \eta_{p,crit}) = 1 - F(\eta_{p,crit}, \sigma^2) = \exp\left(\frac{-\eta_{p,crit}^2}{2\sigma^2}\right) \quad (3.16)$$

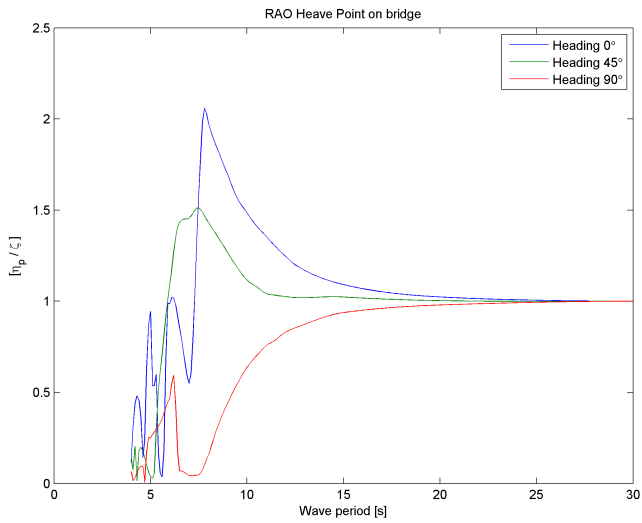


Figure 3.3: The combined vertical response amplitude operator at the wheelhouse top.

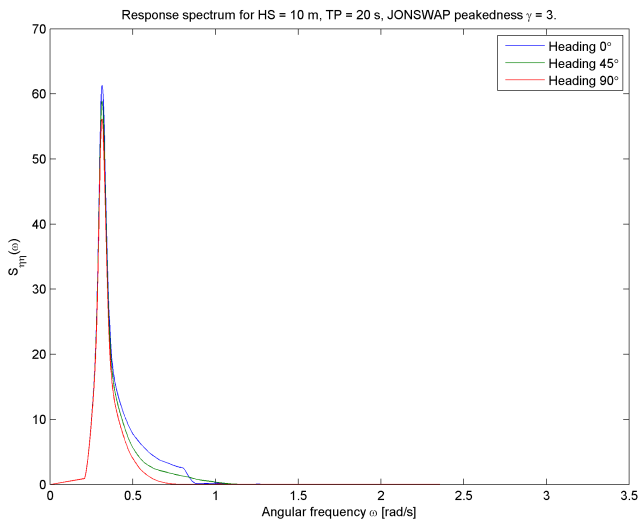


Figure 3.4: The ship's response spectrum for a sea state with peak period near resonance and very high  $H_S$ .

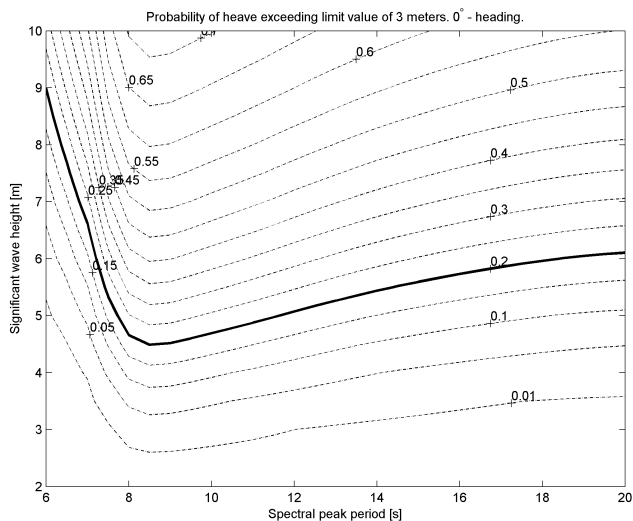


Figure 3.5: The probability of vertical heave motion to exceed a critical value of 3 m, heading  $0^\circ$ .

Where  $\eta_{p,crit}$  is the critical level necessary for contact. The contour plots for the probability of exceeding this level during combinations of sea states is presented in figures 3.5, 3.6, and 3.7 for headings  $0^\circ$ ,  $45^\circ$ , and  $90^\circ$  respectively. The threshold separating sea states with a probability of exceedance higher than 0.2 is marked by a bold curve.

Due to different damping phase angles in heave and pitch, the maximum heave motion may occur at a moment where pitch is not favourable, and thus magnify the vertical motion significantly. From the results, particularly those visible in 3.5 it is evident that there is a relatively high probability that the wheelhouse will have a vertical motion amplitude exceeding 3 m. At sea states where operability is expected, ships will be allowed to remain in close proximity to a platform. During a drift-off situation, a large ship might thus in unfavourable conditions be prone to a vertical impact with an offshore structure.

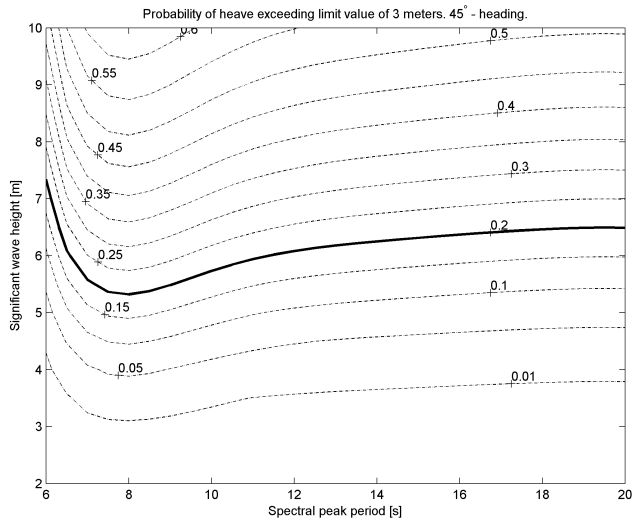


Figure 3.6: The probability of vertical heave motion to exceed a critical value of 3 m, heading  $45^\circ$ .

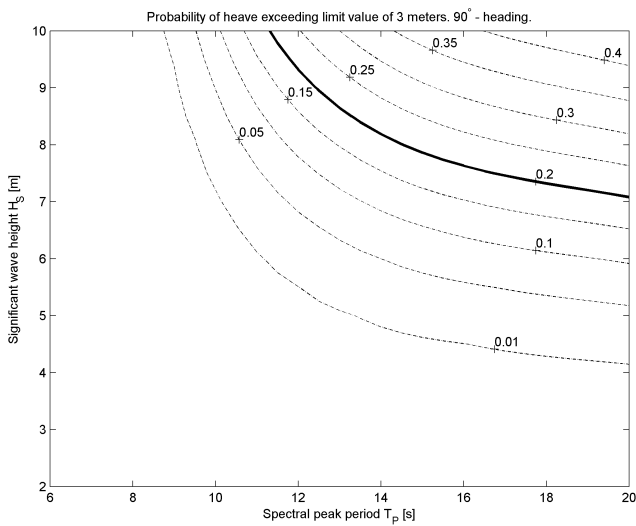


Figure 3.7: The probability of vertical heave motion to exceed a critical value of 3 m, heading  $90^\circ$ .



# Chapter 4

## Simplified Calculation Methods

According to Det Norske Veritas [2012], the structural effects from ship collision may either be determined by nonlinear dynamic finite element analyses, or by energy considerations combined with simplified calculation methods. As the process of doing a full NLFEA analysis is time consuming in both man-hours and CPU-hours, it is often desirable to use simplified methods that still yield good results.

### 4.1 General Design Principles

The collision process is characterized by the kinetic energy of the involved parties. This energy is determined by the individual mass and added mass of the individual object, as well as the striking velocity. During impact, the kinetic energy must be transformed into equivalent energies. A minority will go into increasing the temperature in the material due to friction, and some of it may lead to radiated waves from the hulls. However, the majority of the energy is transformed into strain energy in both the struck and striking objects. This will generally lead to large plastic strains and structural damage to both the striking vessel and the struck installation. The strain energy dissipation is estimated from force-displacement curves. One of the goals of this thesis is to produce such curves for a wheelhouse collision.

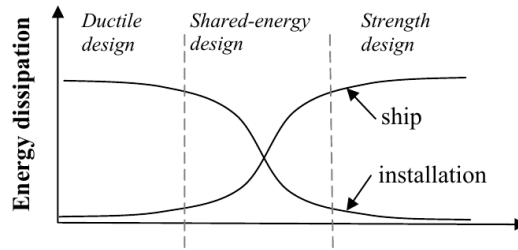


Figure 4.1: Three design principle regimes. Norsk Standard [2012c]

The goal of designing a structure against collision damage is to ensure that the main safety functions of the installation are intact during the accident, and within a certain time period after [Norsk Standard, 2012b]. The main safety functions can be defined as:

- Usability of escapeways
- Integrity of shelter areas
- Global load bearing capacity

There are large inherent uncertainties involved in both determining the nature, as well as the magnitude, of the accidental loads. As the methods of determining it is the designer's responsibility to apply sound engineering judgement and pragmatic evaluations in the design of the structure.

The relative size and strength of the colliding structures will determine the characteristics of the strain energy dissipation. It is common to separate between three separate energy dissipation regimes, where different methods of analyses are applicable.

### **Strength design**

The struck structure is strong enough to withstand the collision force without undergoing large plastic deformations. Most of the strain energy is dissipated in the striking ship.

### **Ductility design**

The struck structure is weak compared to the striking ship, and will not be able to resist the collision forces. Large plastic deformations are expected. The striking vessel will only sustain minor damages.

### **Shared energy design**

The colliding parties have similar structural strength, and will share the



energy that must be absorbed.

To simplify calculations, it is most beneficial to assume either strength- or ductility design. They calculations will yield faster results as one of the vessels may be regarded as rigid, and deformations are thus disregarded. The response of the compliant structure can then be estimated by using the simplified geometry of the assumed rigid structure. Force-displacement diagrams can be used to assess the damage caused by the collision.

Shared energy design collision response are harder to calculate, as the colliding surfaces may change both shape and contact angle. As a result of this, one cannot use the individual force-displacement curves directly, as the contact surfaces will change during the duration of the collision, changing the total force present in the computation. Common for both of these methods are that the integrity of the main safety functions must be confirmed to hold after an accidental action of suitable magnitude.

## 4.2 Collision Mechanics

The mechanics of ship-structure collision may be divided into two parts:

- External collision mechanics deal with the energy released by the impact load impulse, and is released as strain energy. We may express the external strain energy as  $E_{Strain} = \beta \times E_{Kinetic}$   $\beta < 1$ .
- Internal collision mechanics related to the energy dissipated by the crushing of the ship and structure during the collision.

The energy involved in the collision can be derived from energy and momentum considerations. Depending on the type of installation, one can assume the participants to be either compliant, meaning that they are both free to move, or fixed. The installation can be assumed compliant if the duration of the impact is short compared to the fundamental eigenperiod. If the duration is significantly longer, then it may be assumed fixed. The cases run in this master thesis have for ease of computation been modeled as fixed. According to NORSOK N-004, structures like semi-submersibles are normally modeled as compliant, so the modeled system will be too stiff.

### 4.2.1 Finding the external collision energy

For the general problem, these set of equations may be set up to determine the external collision mechanics. For ease of reading, the hydrodynamic added mass in surge for the ship and installation is included in the respective total mass, such that e.g.  $m'_s = m_s + a_s$ .

Conservation of momentum:

$$m'_s v_s + m'_i v_i = (m'_s + m'_i) v_t \quad (4.1)$$

$$v_t = \frac{m'_s v_s + m'_i v_i}{m'_s + m'_i} \quad (4.2)$$

Conservation of energy:

$$E_{tot} = E_S = E_s + E_i = \frac{1}{2} m'_s v_s^2 + \frac{1}{2} m'_i v_i^2 - \frac{1}{2} (m'_s + m'_i) v_t^2 \quad (4.3)$$

$$E_S = \frac{1}{2} \left[ m'_s v_s^2 + m'_i v_i^2 - (m'_s + m'_i) \left( \frac{m'_s v_s + m'_i v_i}{m'_s + m'_i} \right)^2 \right] \quad (4.4)$$

Depending on whether the hit structure is compliant (velocity  $\neq 0$ ) or fixed (velocity = 0), the following relationship are valid when we insert  $v_t$ :

Compliant structure:

$$E_S = \frac{1}{2} m'_s v_s^2 \frac{\left(1 - \frac{v_i}{v_s}\right)^2}{1 + \frac{m'_s}{m'_i}} \quad (4.5)$$

Fixed structure:

$$E_S = \frac{1}{2} m'_s v_s^2 \quad (4.6)$$

The following symbols have been used.

$m'_s$  The mass and added mass of the ship.

$m'_i$  The mass and added mass of the installation.

$v_s$  Velocity of the ship.

$v_i$  Velocity of the installation.

$v_t$  The combined velocity of the ship and installation.

$E_{tot}$  Total kinetic energy.

$E_s$  Kinetic energy of the ship.

$E_i$  Kinetic energy of the installation.

$E_S$  Total strain energy to be dissipated.

## 4.2.2 Dissipation of internal strain energy

As mentioned earlier, the external collision mechanics determine the total strain energy from conservation of energy and momentum. The internal collision mechanics determine how the energy is distributed between the two structures, and may be represented by a force-displacement diagram (c.f. figure 4.2), where the dissipated strain energy is the area under the curves. Here shown as an integral:

$$E_{Strain} = \int_0^{\delta_{platform}} P(\delta_{platform})d\delta_{platform} + \int_0^{\delta_{ship}} P(\delta_{ship})d\delta_{ship} \quad (4.7)$$

The problem at hand lies in calculating  $P(\delta_{platform})$  and  $P(\delta_{ship})$  because the curves will depend on the relative strengths of the structures, c.f. figure 4.1. Historically, the deformation force has been calculated either analytically or semi-empirically with more or less accuracy. These methods may still be applicable in order to assess resistance to deformation in an early design phase, but as more powerful computers and software have been developed in modern days, it is possible to do detailed NLFEA with relatively small penalty to computation time.

## 4.3 Simple Calculation Models

Over the years several simplified methods have been developed in order to easily assess the damages done by ship collision. One of the earliest was Minorsky, who in 1959 published a semi-empirical approach based on investigations of a number of actual ship collisions reported to the U.S. Coast Guard [Minorsky, 1959]. Later

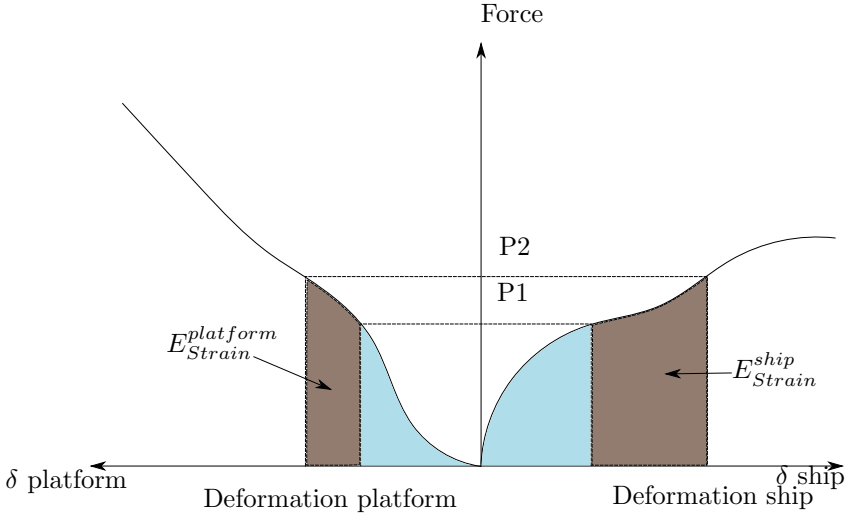


Figure 4.2: Illustrative force-displacement diagram for different force levels.

attempts introduced more advanced and analytical methods by subdividing the ship structure into subcomponents.

Various simplified methods and the theory behind them were discussed in the master thesis, and a short summary is presented here.

In a benchmark study published by Yamada and Pedersen [2008], several simplified analysis methods are compared to experimental data in order to check their applicability in regard to the crushing of bulbous bows. Large-scale models of bulbous bows were subjected to axial crushing. It was concluded that the method by Yang and Caldwell gave the best predictions of the crushing force, while methods by Amdahl, Wang and Ohtsubo, Paik and Pedersen, and Endo and Yamada also gave fairly good results. Most of the methods over-predicted the crushing force estimates for very stiff bows, while less closely stiffened structures had their crushing strength under-predicted. Overall, the mean crushing force and energy absorption was under-predicted by most of the methods.

Gerard's method and Minorsky's method was not benchmarked, most likely due to their empirical nature.

All the simplified methods have originally been developed for ship bow impacts, and assume either that the relative strength of the colliding parties is equal, or that the colliding structure is very stiff. It is therefore uncertain whether any of

these methods are applicable for a wheelhouse impact analysis.

Minorsky's method uses reference volumes of the damaged hull section, and assumes that the structures are strengthened correspondingly. As it draws its empirical constants from observations of various bow impacts, the deviation is likely to be large and non conservative. The wheelhouse is significantly weaker than any hull part, and thus has a much larger "damaged volume". It is not likely that Minorsky's method will perform well in this context.

Amdahl's method assumes that the ship frames be rigid enough such that a so called "accordeon-effect" will take place between the frames, meaning that the areas between the frames will buckle alternately. A wheelhouse does typically not contain the same type of frames, and will most likely experience vertical collapse of the decks as the vertical resistance is diminished. It is therefore uncertain whether Amdahl's method will work well under these conditions.

Application of the methods is not in the work scope of this thesis.



# Chapter 5

## The Non-Linear Finite Element Method

### 5.1 General

Basic structural analysis, and finite element analysis in general, is based on three main principles:

**Equilibrium** Internal- and reaction forces must be balanced. Expressed by stresses.

**Kinematic compatibility** Equality in motion. Expressed by strains.

**Stress-strain relationship** Stresses can be expressed by strains, and vice versa.

In linear analysis, it is assumed that the displacements are proportional to the applied force, that displacements are small, and that the material is linear perfect elastic. With this in mind, equilibrium can be established with regard to the initial position. This also implies that the strains are linear functions of the displacements,  $\varepsilon_x = \frac{\partial u}{\partial x}$ . For the stress strain relationship we can use Hooke's law.

However, when the task at hand deal with calculating ultimate load capacity of structures that may buckle, collapse, or fracture, the assumptions regarding linear analysis are no longer valid, and must needs be modified. Actions and action effects may change as a structure deforms, or the material stresses exceed

the yield stress. Some non-linearities that may be experienced in the analysis of a marine structure:

**Geometric non-linearity** Displacements are large, and may need an updated reference frame.

**Material non-linearity** The material may have a strain-dependent Young's modulus after a certain stress or strain threshold.

**Boundary condition non-linearity** The boundary conditions may change as the analysis progresses, e.g. contact between two bodies.

**Stress-strain relationship non-linearity** If the problem is material non-linear, the stress-strain relationship may be dependent on both stress- and strain level, as well as time.

Non-linear stress analysis may be useful in several applications. Traditionally, non-linear analysis has been limited to small and simple cases. This is due to the computationally exhaustive nature of the analysis. The dawn of inexpensive yet powerful computers now make this of secondary importance. However, modeling and setup of a proper non-linear analysis is still demanding in terms of the complexity of problems, as well as understanding what lies behind the computations. Any novice may set up an advanced analysis, yet still receive results that are unreliable. The old adage is doubly true when it comes to advanced non-linear analysis: "Bad input = bad output".

### 5.1.1 Geometric Non-linearity

In linear analysis it is assumed that displacements are small, such that the loads are carried in the same way throughout the load history. In geometric non-linear problems, the structure may deform in such a way that the load is carried by a completely different mode, or that the response has been magnified due to second order geometric effects, e.g. secondary bending moment in buckling problems. For a colliding ship with a high degree of deformation, the geometric non-linearities have a big impact on the capacity of the structure. Initially, the stiffened plates in e.g. the wheelhouse will carry loads by bending. However, after some amount of deformation, a mechanism will appear as the cross section enter into the plastic range. The bending capacity is then spent, but the stiffened plate will still have significant reserve load carrying capacity due to the now dominating membrane action effect.

Another example of non-linear geometric effects is the so-called "snap-through", where the action effects will suddenly change dramatically due to the structures



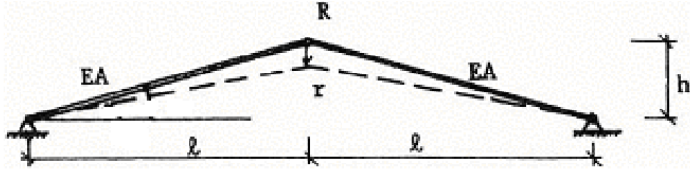


Figure 5.1: A two-beamed arch. Courtesy of Moan [2003]

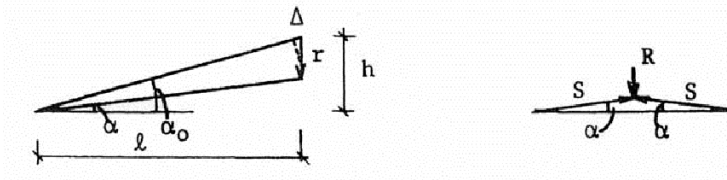


Figure 5.2: Deformation and equilibrium for large displacements.

inability to maintain equilibrium in the current configuration. If we assume our example is a simple two-beamed arch with a concentrated vertical force in the center, the resulting force,  $S$ , will increase proportionally to the deflection angle  $\alpha_0$  caused by the force  $R$ .

As the force is applied, the beams shorten by an amount  $\Delta$ .

$$\Delta = \frac{l}{\cos \alpha_0} - \frac{l}{\cos \alpha} \quad (5.1)$$

And the strain is thus given by then following (positive in compression).

$$\varepsilon = \frac{\Delta l}{l_0} = \frac{\Delta}{l / \cos \alpha_0} = 1 - \frac{\cos \alpha_0}{\cos \alpha} \quad (5.2)$$

Equilibrium for the deformed truss is then:

$$R = 2S \sin \alpha = 2EA\varepsilon \sin \alpha = 2EA \sin \alpha \left( 1 - \frac{\cos \alpha_0}{\cos \alpha} \right) \quad (5.3)$$

By introducing

$$\sin \alpha = \frac{h - r}{\sqrt{l^2 + (h - r)^2}}, \cos \alpha = \frac{l}{\sqrt{l^2 + (h - r)^2}}, \cos \alpha_0 = \frac{l}{\sqrt{l^2 + h^2}} \quad (5.4)$$

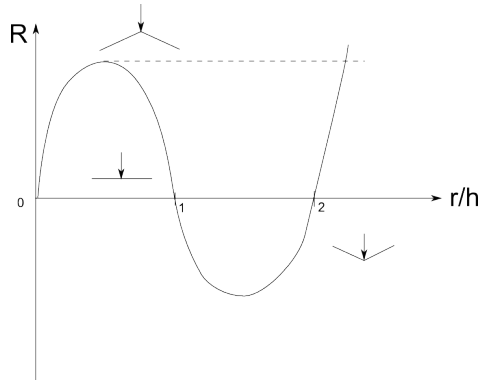


Figure 5.3: Possible equilibrium conditions. Adapted from [Moan, 2003, p.12.8]

We may write eq. 5.3 as the following:

$$R = \frac{2EA}{l} \left( \frac{h}{r} - 1 \right) \left( \frac{l}{\sqrt{l^2 + (h-r)^2}} - \frac{l}{\sqrt{l^2 + h^2}} \right) r \quad (5.5)$$

We see that  $R$  can now be set up as a function of the stiffness,  $R = K(r)r$ , and is now a non-linear function of the displacement  $r$ . This is a good example of material non-linearity. As the deflection increases, the balancing forces must increase dramatically until the angle  $\alpha$  is zero, and has no vertical component. The load will then "snap-through", and the restoring forces must needs change sign to maintain equilibrium, see fig. 5.3.

As can be seen in figure 5.3, there are several solutions, or equilibrium positions for given  $R$ . In general it is not possible to determine the deflection  $r$  for a given external force  $R$  analytically. Several solution methods exist, however, and are described in section 5.2.

In order to solve the non-linear problem, it is convenient to express the equilibrium on differential form, such that the tangent stiffness  $K_I$  can be formulated.

$$dR = \frac{d}{dr} K(r)r dr = K_I dr \implies K_I(r) = \frac{d}{dr} K(r)r \quad (5.6)$$

This way of formulation means that it is possible to solve the structural problem using incremental or iterative methods.

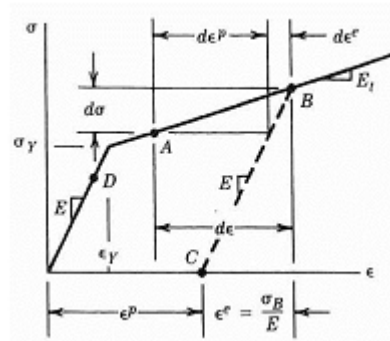


Figure 5.4: Non-linear stress-strain relationship. [Moan, 2003, p.12.37]

## 5.1.2 Material Nonlinearity

In most applications where one wants to determine the ultimate strength of a structure, the material will transcend the linear elastic area, and end up with permanent plastic deformation due to the extreme stresses in the material. A linear elastic material will have a constant relationship between stresses and strains, regardless of the actual strain in the material. A non-linear material on the other hand, have stresses  $\sigma$  and strains  $\varepsilon$  related by a strain-dependent matrix. The problem that then arises is that the equilibrium equations must be solved by material properties depending on strains. The strains, however, are not known in advance, and will lead to computational difficulties.

In FEA analysis, material non-linear behaviour is treated by three rules:

**Flow Rule** The relationship between stresses and strains,

**Hardening Rule** Describes how the materials harden, and at what rate.

**Yield Criterion** Describes when the material starts to yield due to stress.

### 5.1.2.1 Yield Criterion

The yield criterion states that yielding occurs when  $|\sigma|$  reaches  $\sigma_Y$ , in practice the tensile yield strength of the material. In order to continue the yield process, the subsequent stress  $\sigma$  may need to be higher than  $\sigma_Y$  if  $E_t > 0$ . This phenomenon is called strain hardening.

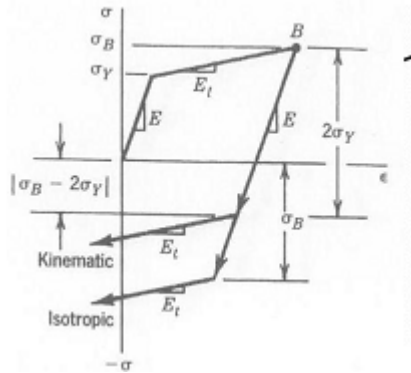


Figure 5.5: Isotropic and kinematic hardening rules. [Moan, 2003, p.12.37]

### 5.1.2.2 Hardening Rule

The hardening rule describes how the yield criterion changes by the history of plastic flow. Material hardening is usually described to either isotropic or kinematic rules.

If a material has been loaded in tension to a point  $B > \sigma_Y$  (figure 5.5), and then consequently unloaded, the strain will follow a linear path with slope parallel to the Young's modulus. Continued loading in the same direction will now cause a linear response until  $\sigma > \sigma_B$ , whereas it earlier was elasto-plastic.

The isotropic hardening rule tells us that a consequent load in compression will have a linear response until the stress again reaches  $-\sigma_B$ . This is a simple rule, however it is not what has been observed experimentally.

Kinematic hardening describes the behaviour that has been observed in laboratories by most common metals. It appears that a metals have an elastic range of  $2 \times \sigma_Y$ , meaning that a material loaded plastically in tension to a level  $\sigma_B$ , will in compression yield at  $\sigma_B - 2\sigma_Y$ .

### 5.1.2.3 Flow Rule

A linear material works in such a way that the stresses are always proportional to the strains, as well as assuming that Young's modulus is constant. In the real world most engineering materials will reach a *proportionality limit*,  $\sigma_p$ , and will start to display elasto-plastic behaviour, where the Young's modulus may

change, leading to a changed strain rate.

One may assume that a strain increment can be superpositioned as an elastic and a plastic contribution, given that the stress level has exceeded the yield stress  $\sigma_Y$ , such that  $d\varepsilon = d\varepsilon^e + d\varepsilon^p$ . The corresponding stress increment  $d\sigma$  can thus be written in the following ways:

$$d\sigma = E d\varepsilon^e = E(d\varepsilon - d\varepsilon^p), d\sigma = E_t d\varepsilon, d\sigma = h' d\varepsilon^p \quad (5.7)$$

$$H' = \frac{\partial \sigma}{\partial \varepsilon^p} \quad (5.8)$$

$$E_t = E \left( 1 - \frac{E}{E + H'} \right) \quad (5.9)$$

Where  $E_t$  is the tangent modulus and  $H'$  is called the plastic tangent modulus. On this form, the expression for  $E_t$  is similar to the general expression for multi axial states of stress.  $E_t$  is in general not constant.

### 5.1.3 Boundary condition non-linearity

In collision-type analyses, the boundary conditions will change continuously as different parts of the structure come into contact with each other, or with themselves. The force-displacement relationship between the colliding parties is then no longer linear. Boundary condition non-linearity can for instance also be attributed to soil stiffness in offshore structures installation.

## 5.2 Solution Methods

As mentioned earlier it is not straightforward to solve non-linear problems as the solution is not necessarily unique, as is the case in linear analysis. Several methods exist that may be applied in order to solve the problem. These methods are either of static nature, and thus solvable by incremental or iterative procedures, or they are dynamic, and may be solved by implicit or explicit methods. They may be based on load control or displacement control. Some of mentioned models that can be applied when the R-r relationship is monotonously increasing are described in the following sections.

### 5.2.1 Static Solution Methods

For static solution methods it is necessary to satisfy two equilibrium conditions, namely the incremental equilibrium (eq. 5.10) and global equilibrium (eq. 5.11).

$$\mathbf{K}(\mathbf{r})\Delta\mathbf{r} = \mathbf{R}^{ext} - \mathbf{R}^{int} \quad (5.10)$$

$\mathbf{K}$  is the stiffness matrix,  $\mathbf{r}$  is the displacement vector, and  $\mathbf{R}^{int}$  and  $\mathbf{R}^{ext}$  are the internal and external load vectors respectively.

$$\mathbf{R}^{ext} = \mathbf{R}^{int} = \sum_i^n \mathbf{a}_i^T \mathbf{S}_i \quad (5.11)$$

Where  $\mathbf{a}_i$  is the topology matrix,  $\mathbf{S}_i$  is the internal element force vector.

#### 5.2.1.1 Load Incremental Methods

A common solution method is the Euler-Cauchy method, which stepwise increases the applied external load  $\mathbf{R}$ , and then calculates the corresponding response  $\mathbf{r}$ . For each load step, the displacements are calculated, followed by updating the system stiffness matrix  $\mathbf{K}_I$  and material properties based on current geometry and stress condition. Then a new load step is applied, and the process is repeated. This method only solves eq. 5.10 is satisfied, and will therefore not ensure that the structure is in global equilibrium. This may yield poor results if the load step  $\Delta R$  is large. The Euler-Cauchy method is a first order method, and is derived from a Taylor series representation of the response. The omission of terms of higher than  $2^{nd}$  order causes a truncation error in each step, proportional to  $O(h^2)$ . The number of steps is proportional to  $1/h$ , hence making the global error proportional to  $h^2(1/h) = h^1$ .

This method is crude, and seldom used in practice without modification. One simple modification is to correct the solution by demanding global equilibrium in each step. After the  $m^{th}$  step, the total load is  $\mathbf{R}_m$  and the calculated displacement is  $\mathbf{r}_m$ . We use this to find an expression for the residual force  $\mathbf{R}_m$ .

$$\mathbf{R}_r = \sum_i (\mathbf{a}_i)^T \mathbf{S}_i(\mathbf{r}_m) - \mathbf{R}_m = \mathbf{R}^{int}(\mathbf{r}_m) - \mathbf{R}_m \quad (5.12)$$

We account for this residual force by adding them to the next load increment, such that the global equilibrium is maintained for the current step. The additional effort involved in computing the residual force means that it is not optimal to go beyond a two-step method [Moan, 2003, p. 12.52]

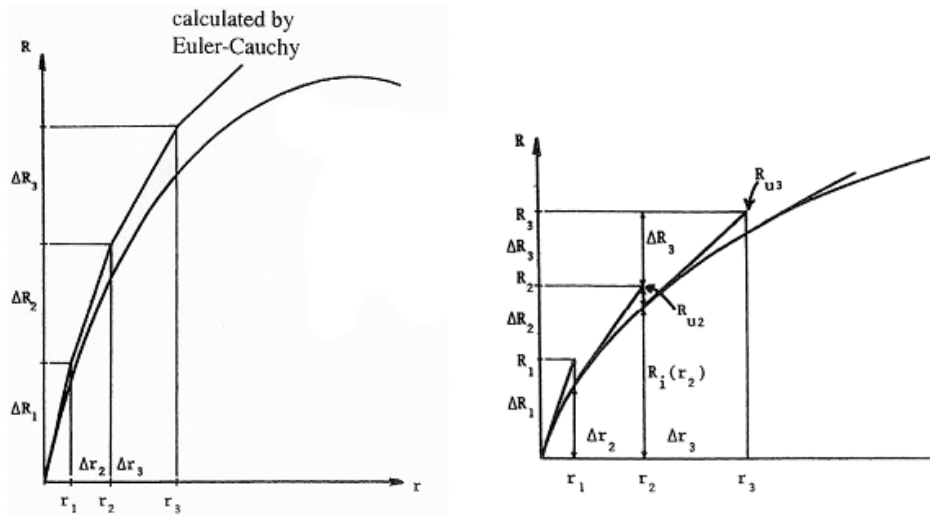


Figure 5.6: Original Euler-Cauchy and Improved Euler-Cauchy.

### 5.2.1.2 Iterative Methods

According to Moan [2003], the most used iterative method for solving non-linear structural problems is the Newton-Raphson method. The algorithm to solve  $r$  for the problem  $K(r) = 0$  is:

$$r_{m+1} = r_m - \frac{K(r_m)}{K'(r_m)} \quad (5.13)$$

$$\frac{K(r_m)}{\tan \theta} = \frac{K(r_m)}{K'(r_m)} \quad (5.14)$$

The method starts with an initial load increment value. The response is then approximated by a the tangential stiffness , and the deformation intercept to the tangent line is calculated. Global equilibrium is verified, and this leads to a correction in the external force, and thus a new iteration is made. The incremental stiffness matrix  $\mathbf{K}_I$  is updated after each iteration, until the displacement has converged for the given external force. The updating of the stiffness matrix is time consuming, and thus not optimal if the system is large.

The method may be modified in such a way that the stiffness matrix may or may not be updated between each time step. This may be more computationally

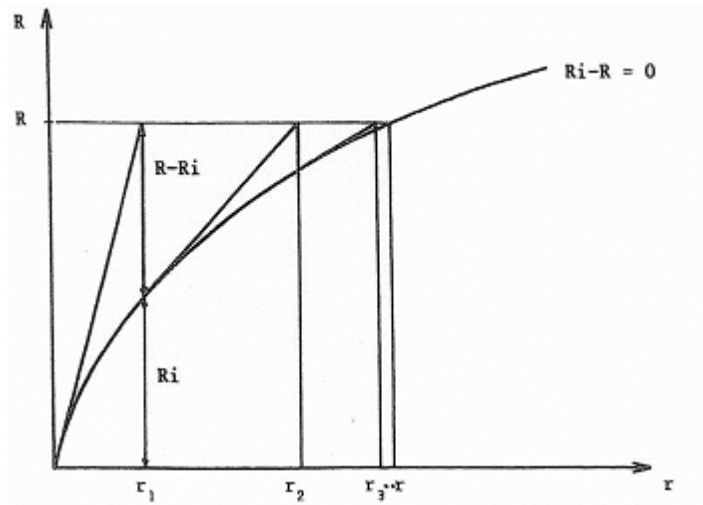


Figure 5.7: Original Newton-Raphson with continuously updated  $\mathbf{K}_I$ .

efficient in the long run. A beneficial method is to update the incremental stiffness matrix less frequently, such that the computational efforts are only slightly lessened, while convergence is increased. The modified Newton-Raphson method updates the stiffness matrix only the first iteration. It may therefore need more iterations to converge, but is less computationally demanding.

Incremental and iterative methods may be combined in order to achieve a more effective solution method. Commonly a load increment is introduced, and then the corresponding deformation is iterated from there.

### 5.2.1.3 Arc Length Methods

If the structure has a monotonously increasing stiffness characteristic, the methods are quite reliable, and will provide a solution. If the structure suddenly collapses or buckles locally, the tangential stiffness will at some point be zero, making the solution singular. This is for instance the case for the two-beam example shown earlier in section 5.1.1. In such a case, a displacement control method may be preferred. In such a method, incremental displacements are made instead, which in turn generate internal stresses and strains contributing to nodal forces and moments. This leads to better control of the deformation history of the structure, and is often preferred as the tangential stiffness is better conditioned,



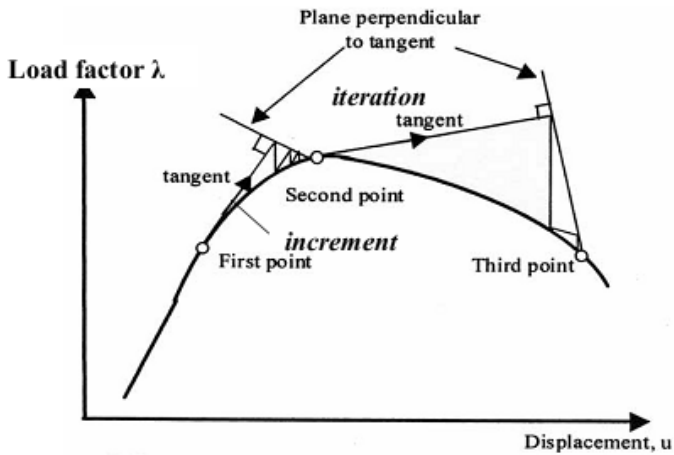


Figure 5.8: Geometric interpretation of an arc length method.

giving faster convergence of the solution. One will also avoid having a singular tangential stiffness at local peak resistances (buckling).

Because of this it is necessary to look elsewhere for a solution method that will be able to yield results for post-collapse response. In general, an incremental displacement method may be successful, but it is generally necessary to utilize so-called arc length methods, as proposed by Wempner (1971) and Riks (1972). Arc length methods in general find a single equilibrium path in space defined by the nodal displacements  $\mathbf{r}$  and a loading parameter  $\lambda$ . The methods are so-called predictor-corrector method, meaning they require the use of both increments and iteration. The increment size is defined as a length along the solution arc rather than being fixed to one of the axes.

### 5.2.2 Dynamic Solution Methods

A collision can be characterized by:

- Rapid increasing load.
- Short duration.
- Large deformations.
- Large changes in inertia and kinetic energy.

- Contact forces and varying boundary conditions.

For such an event it is necessary to include dynamic effects that are not accounted for in a normal static non-linear analysis. In order to capture all these effects, the dynamic equation of motion (eq. 5.15) must be solved in the time-domain.

$$\mathbf{M}\ddot{\mathbf{r}}(t) + \mathbf{C}\dot{\mathbf{r}}(t) + \mathbf{K}\mathbf{r}(t) = \mathbf{R}(t) \quad (5.15)$$

Where  $\mathbf{M}$  is the mass matrix,  $\mathbf{C}$  is the damping matrix, and  $\mathbf{K}$  is the stiffness matrix. The solution is typically found using a finite difference method and applying direct integration techniques stepwise. Either implicit or explicit methods may be used, depending on the nature of the problem.

In explicit time integration, eq. 5.15 is satisfied at time =  $t$ , such that displacements, velocities, and accelerations for time =  $t + \Delta t$  can be found based on the response history. The solution is obtained without needing to solve any systems of equations, and are thus quite computationally cheap. Explicit methods are only conditionally stable, though, and may need a time step size that is much smaller than that needed to obtain sufficient accuracy. The time step size is determined by the smallest element length. The method is therefore time consuming, and best suited for transient analyses of very short duration, such as collision.

$$\mathbf{r}(t + \Delta t) = f(\mathbf{r}(t), \dot{\mathbf{r}}(t), \ddot{\mathbf{r}}(t), \mathbf{r}(t - \Delta t), \dot{\mathbf{r}}(t - \Delta t), \ddot{\mathbf{r}}(t - \Delta t), \dots) \quad (5.16)$$

An implicit method requires that a system of equations be solved for each time step, because it is also dependent of velocities and accelerations at time =  $t + \Delta t$  in order to calculate displacements. This leads to a more computationally demanding solution. Many implicit methods are unconditionally stable, meaning that the time step can be relatively large without risking non-converging solution. The time step length is dictated only by need for accuracy [Baig and Bathe, 2005].

$$\mathbf{r}(t + \Delta t) = f(\mathbf{r}(t), \dot{\mathbf{r}}(t), \ddot{\mathbf{r}}(t), \mathbf{r}(t + \Delta t), \dot{\mathbf{r}}(t + \Delta t), \ddot{\mathbf{r}}(t + \Delta t), \dots) \quad (5.17)$$

In practice, the differences between an explicit method and an implicit method boils down to stability and computational time requirements, and must be evaluated on a case to case basis. Implicit methods are computationally more heavy than explicit methods, but does not require short time steps in order to converge. Explicit methods, on the other hand, are computationally cheap, but require very small time steps in order to converge.

As the number of elements in a model increases, the computational time will increase differently between the two. For explicit analysis, the computation time

increases proportional to the number of elements, while for an implicit analysis, the computational time will increase proportional to the square of the number of elements [Kreyzig, 2006]. Regarding the need for memory capacity, it is for explicit methods not necessary to store the global stiffness matrix  $\mathbf{K}$ , as the internal force vector can be found by summation of element contributions.

An analysis can be categorized as either a *wave propagation problem*, or a *structural dynamic problem*.

**Wave propagation problem** Characterized by a an rapid load, blast explosion or collision. High frequency modes are present may be excited. Small time step necessary in order to get accurate results. Explicit method is beneficial.

**Structural dynamics problem** Response dominated by lower modes due to slower load application and rise time. An implicit method is preferred.

### 5.2.2.1 Explicit solution method

As the nature of the analyses conducted in this thesis are collision analyses, an explicit solver is utilized. A good example of such a method is the central differences method. This is based on Taylor's expansion of  $\mathbf{r}_{n-1}$  and  $\mathbf{r}_{n+1}$ . The central differences method consists of two steps:

$$\mathbf{r}_{n+1} = \mathbf{r}_n + \Delta t \dot{\mathbf{r}}_n + \frac{\Delta t^2}{2} \ddot{\mathbf{r}}_n + \frac{\Delta t^3}{6} \dddot{\mathbf{r}}_n + \dots \quad (5.18)$$

$$\mathbf{r}_{n-1} = \mathbf{r}_n - \Delta t \dot{\mathbf{r}}_n + \frac{\Delta t^2}{2} \ddot{\mathbf{r}}_n - \frac{\Delta t^3}{6} \dddot{\mathbf{r}}_n + \dots \quad (5.19)$$

By subtracting eq. 5.19 from eq. 5.18, we end up with eq. 5.20. Adding eq. 5.19 to eq. 5.18, yield eq. 5.21. Terms of  $O(\Delta t^3)$  and higher are omitted.

$$\dot{\mathbf{r}}_n = \frac{1}{2\Delta t} (\mathbf{r}_{n+1} - \mathbf{r}_{n-1}) \quad (5.20)$$

$$\ddot{\mathbf{r}}_n = \frac{1}{\Delta t^2} (\mathbf{r}_{n+1} - 2\mathbf{r}_n + \mathbf{r}_{n-1}) \quad (5.21)$$

Substituted into the dynamic equation of motion, we end up with the following expression:

$$\left[ \frac{\mathbf{M}}{\Delta t^2} + \frac{\mathbf{C}}{2\Delta t} \right] \mathbf{r}_{n+1} = \mathbf{R}^{\text{ext}}_n - \mathbf{K}_n \mathbf{r}_n + \frac{\mathbf{M} \mathbf{r}_n}{\Delta t^2} - \left[ \frac{\mathbf{M}}{\Delta t^2} - \frac{\mathbf{C}}{2\Delta t} \right] \mathbf{r}_{n-1} \quad (5.22)$$

As the time step used in explicit analysis is typically of  $O(10^{-6})$ , omitting terms of  $O(\Delta t^3)$  should in practice yield sufficient accuracy for all but the highest modes.

## 5.3 Non-linear analysis in LS-DYNA

In the following, theory excerpted from the LS-DYNA theory manual is presented [Hallquist, 2006].

### 5.3.1 Time integration

LS-DYNA utilizes a modified central difference method in order to explicitly solve the equation of motion. The equation of motion is made semi-discrete (eq. 5.23), and central difference time integration is applied, here shown for step number  $n$ .

$$\mathbf{M}\ddot{\mathbf{r}}_n = \mathbf{P}_n - \mathbf{F}_n + \mathbf{H}_n \quad (5.23)$$

Where  $\mathbf{M}$  is the diagonal mass matrix,  $\mathbf{P}$  accounts for internal and external body force loads,  $\mathbf{F}$  is the stress divergence vector, and  $\mathbf{H}$  is the hourglass resistance. To advance to time  $t_{n+1}$ , the central differences time integration is applied.

$$\ddot{\mathbf{r}}_n = \mathbf{M}^{-1} (\mathbf{P}_n - \mathbf{F}_n + \mathbf{H}_n) \quad (5.24)$$

$$\dot{\mathbf{r}}_{n+\frac{1}{2}} = \dot{\mathbf{r}}_{n-\frac{1}{2}} + \ddot{\mathbf{r}}_n \Delta t \quad (5.25)$$

$$\mathbf{r}_{n+\frac{1}{2}} = \mathbf{r}_n + \dot{\mathbf{r}}_{n+\frac{1}{2}} \Delta t_{n+\frac{1}{2}} \quad (5.26)$$

$$\Delta t_{n+\frac{1}{2}} = \frac{\Delta t_n + \Delta t_{n+1}}{2} \quad (5.27)$$

After this the geometry,  $\mathbf{x}$ , is updated by adding the displacement vector  $\mathbf{r}$ .

$$\mathbf{x}_{n+1} = \mathbf{x}_n + \mathbf{r}_{n+1} \quad (5.28)$$

The analysis procedures are looped in the following way (figure 5.9), and displays the step-by-step nature of the explicit method in LS-DYNA.

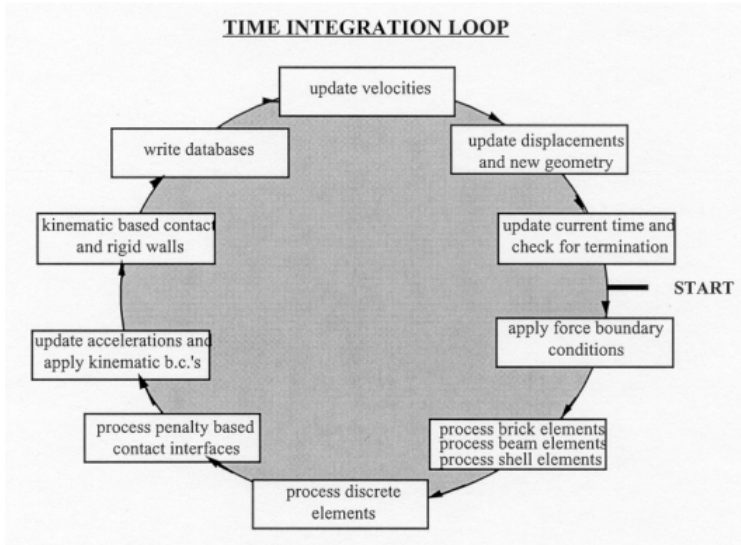


Figure 5.9: LS-DYNA time integration loop, as presented in the theory manual [Hallquist, 2006].

### 5.3.2 Critical time step

As mentioned in section 5.2.2, the critical time step in an explicit method is governed by the size of the smallest element in the model. In order for the method to be stable, the time step must be smaller than the time it takes for a pressure wave to pass through the element. A violation of this criteria would mean that pressure waves could pass through the element undetected, leading to inaccuracies at best, or an unstable solution. For contact analyses, the time step must also be adequately low in order to maintain numerical stability of the solution.

During the solution, the critical time step of all elements are cycled through, and the time step is determined from the lowest critical time step. This is again scaled by some safety factor  $a$ , typically 0.9 or less in order to ensure that the critical time step criterion is not violated.

In the model created for this thesis, shell elements are used almost exclusively. The critical time step for quadratic shell elements is governed by the speed of sound in the element,  $c$ , as well as the *characteristic length*,  $L_s$ , [Hallquist,

2006].

$$\Delta t = \frac{L_s}{c} \quad (5.29)$$

$$c = \sqrt{\frac{E}{\rho(1-\nu^2)}} \quad (5.30)$$

For determining the *characteristic length*, three options are available.

- Characteristic length based on the four lengths of the element sides. This is the default value used in LS-DYNA.
- Characteristic length based on a the longest of the element diagonals. This is a conservative method which may yield very low time steps where elements are highly distorted.
- Characteristic length based on bar wave speed, when very small triangular elements are present. Typically yield larger time steps, and is non-conservative.

In this analysis the default option is chosen. The characteristic element length is then calculated from equation 5.31.

$$L_s = \frac{(1 + \beta) A_s}{\max(L_1, L_2, L_3, (1 - \beta) L_4)} \quad (5.31)$$

$\beta = 0$  for quadrilateral shell elements, and  $\beta = 1$  for triangular shell elements.  $A_s$  is the area of the element, and  $L_i$  are the individual element lengths.

### 5.3.3 Subcycling (Mixed time integration)

After the critical time step has been found, LS-DYNA applies a method called subcycling, or mixed time integration, in order to increase the efficiency of the solution. The elements are sorted into groups and assigned time steps of integer multiples of the critical time step. This ensures that the smallest time step is only applied for the smallest elements, while the larger elements are updated at the multiples of the time steps. The response in between the larger elements time steps is linearly interpolated. For crash type analyses, it is typical that the mesh is quite uniform in size. In that case, subcycling will not be beneficial, and may yield a net increase in computational effort, decreasing the efficiency of the solution. For subcycling to have a significant effect, the ratio between the major and minor time step should be large, and the number of minor time steps should be small. In such cases the computational gain could be as much 50% as the ratio of major and minor time steps increase.

### 5.3.4 Material models

In order to analyse the collision in LS-DYNA, three material models have been applied. The impacted semi-submersible platform was modeled as both completely rigid and deformable, whereas the ship wheelhouse was analysed using a modified elastoplastic power law material with a RTCL fracture criterion. The living quarter was modeled using the same elastoplastic power law material, but without a fracture criterion.

#### 5.3.4.1 Rigid Material

The rigid body material is a convenient way of modeling geometry that is not expected to deform in any significant way. In this thesis, the hull of the ship is modeled as a rigid body.

Elements which are rigid are bypassed in the element processing, and has no allocated memory for storage of history variables. This makes the material very computationally efficient. Young's modulus, Poisson ratio, and density is defined in order to have the contact forces and sliding parameters behave correctly.

The material properties of the rigid body material is set equal to that of steel.

#### 5.3.4.2 Aluminium

For modeling the aluminium used in the living quarter, Dahl [2012] successfully applied an elastoplastic material with isotropic power law hardening rule. The same material law will be utilized in this thesis. In *LS-DYNA*, this is achieved by utilizing the \*MAT\_POWER\_LAW\_PLASTICITY material card.

The power law obeys the following equation:

$$\sigma = K \varepsilon^n = L (\varepsilon^{yp} + \bar{\varepsilon}^p) \quad (5.32)$$

Where K is the strength coefficient,  $\varepsilon_{yp}$  is the elastic strain to yield,  $\bar{\varepsilon}^p$  is the effective logarithmic plastic strain, and n is a hardening exponent.

The elastic yield strain is given as:

$$\varepsilon_{yp} = \left( \frac{E}{K} \right)^{\frac{1}{n-1}} \quad (5.33)$$

The material strain rate is also accounted for using a Cowper and Symonds models which scales the yield stress with the following factor. C and p are strain

parameters, and  $\dot{\epsilon}$  is the strain rate.

$$1 + \left( \frac{\dot{\epsilon}}{C} \right)^{\frac{1}{p}} \quad (5.34)$$

This model does not include a fracture criterion, and it is therefore necessary to carefully control the strain levels of the finished analyses in order to establish if the critical strain limit has been breached.

Aluminium is a lightweight metal, about one third the density of conventional steel. The Young's modulus is also about one third that of steel, while its thermal expansion coefficient is about twice that of steel. The elastic limit of aluminium is commonly reached at a strain level of 0.2%. The stress corresponding to this strain level is commonly referred to as  $f_{0.2}$ , and has the same meaning as the yield stress in steel [Mazzolani, 1995]. Unlike steel, aluminium develops strain hardening immediately after the onset of yield.

The ultimate strength of aluminium is commonly referred to as  $f_t$ . This level corresponds to the stress level where the strain is no longer uniformly distributed, but is concentrated locally, commonly known as necking.

Pure aluminium exhibit poor mechanical properties: it is very ductile and has a low strength. Other materials are therefore commonly added to the metal in order to create alloys which may have desirable properties for different applications.

Unlike steel, aluminium generally does not react positively to welding, and will frequently have reduced capacity in the heat affected zone (HAZ) near a weld. As a rule of thumb, 25 mm is commonly used to describe the width of the HAZ. Amdahl and Stornes [2001] say that the general trend for aluminium alloys is that the higher strength of the alloy, the larger is the strength loss in the HAZ and the smaller is the hardening.

The reduction in strength of the HAZ may influence the energy dissipation negatively. As the material yields at a (sometimes much) lower stress level, the surrounding material may not even be activated. The strains may therefore be localized to a narrow HAZ.

The aluminium alloys used in the construction of the living quarter are of the 5000- and 6000-series. The 5000-series primarily have magnesium (Mg) added to allow for increased strength, yet still retain a high degree of ductility. Corrosion resistance is excellent, and the alloy is well suited for welding, as the strength is not drastically reduced in the HAZ. The 6000-series contains mainly silicon (Si) and magnesium additives which, after heat treatment, yields increased tensile



strength. The alloys of this series are well suited for extrusion, and have excellent corrosive properties, making them suitable for use offshore without any form of protective coating. These alloys will however display some negative influence from welding.

Steel is an isotropic material, meaning that it has uniaxial material properties. This is a property that aluminium does not share. Depending on the additives used, the alloy will display varying degrees of anisotropy.

In the conducted analyses, some simplifications regarding the material have been made in order to reduce the work load to a manageable size.

**Heat Affected Zone** The negative effects related to welding are neglected in the analyses, simply due to the immensely increased work load related to this. In many areas the structural components are heat treated, which aids in reducing the negative effect in the HAZ. In Amdahl and Stornes [2001], laboratory tests are done to investigate the negative effects of welding in 5083 alloy aluminium. The effect on yield stress was found to be moderate, whereas the ultimate strength was not affected significantly after heat treatment. The consequence of this will be that the results are non-conservative: the model is likely to be stiffer than what is actually true.

**Anisotropy** Mechanical properties in these analyses are said to be equal in all load directions. This is not generally true for aluminium, but Amdahl and Stornes [2001] investigated the anisotropic properties of 5083 alloy aluminium, both heat treated and non-heat treated, and found a fairly small effect. The modeled material is therefore used as if it was be isotropic. The consequence of this simplification will also cause the results to be slightly non-conservative: the material will yield at the given stress, or at a lower level, depending on the orientation of the material.

<b>Density</b>	$\rho$	2700	[kg / m <sup>3</sup> ]
<b>Young's Modulus</b>	<b>E</b>	70000	[MPa]
<b>Poisson's Ratio</b>	$\nu$	0.3	[-]
<b>Shear Modulus</b>	<b>G</b>	26923	[MPa]
<b>Bulk Modulus</b>	<b>B</b>	58333	[MPa]

Table 5.1: Material properties for aluminium.

Material data for the aluminium used is supplied by Leirivk Module Technology [2003]. Three different alloys are used.

Alloy	Strength Parameter K [MPa]	Hardening Exponent n [-]	Yield Limit $f_{0.2}$ [MPa]	Ultimate Strength $f_t$ [MPa]	Elongation at rupture $\epsilon_t$ [-]
<b>6082-T6</b>	350	0.05	260	310	0.1
<b>5383-H116</b>	370	0.08	220	305	0.1
<b>5083</b>	410	0.2	125	275	0.15

Table 5.2: Power law parameters for aluminium alloys used in analysis.

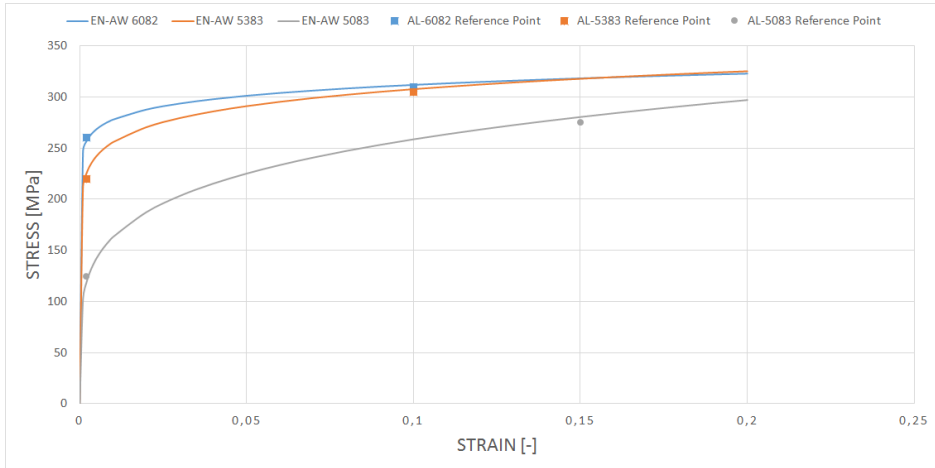


Figure 5.10: The stress-strain curves of aluminium alloys resulting from the power law parameters.

Material curves are created by solving eq. 5.32. Data points marking the elastic limit  $f_{0.2}$  and elongation at rupture  $\epsilon_t$  are marked, and the power law parameters K and n are determined by curve-fitting.

### 5.3.4.3 Steel

The modeling of steel is based on the same elastoplastic isotropic power law hardening as section 5.3.4.2, but it has been modified by Alsos [2008] to also include an RTCL fracture criterion. An element that exceeds a given stress/strain level is deleted, thus simulating a fracture. The purpose of adding a fracture model to the analyses is to more accurately determine the resistance against collision. Once fracture occurs, resistance towards further damage may drop

dramatically. This may in turn also accelerate the hull rupture process, further compromising the structural integrity of the wheelhouse.

Due to the sheer size of ships, it is not practically applicable to use small enough elements to accurately model a propagating crack. This would be too computationally demanding due to the critical time step discussed in section 5.3.2. Global ship and platform structure models are usually modeled with quite a coarse mesh, which will not capture stress and strain hot spots that will appear prior to the initiation of a crack. It was therefore deemed necessary to implement a element size dependent fracture criterion that applies a limit to the maximum allowable equivalent plastic strain in an element.

Moreover, shell elements are especially sensitive to the element discretization at large deformations. The effect is apparent in zones where the strain gradients are especially large, e.g. near crack tip openings, structural intersections, cutouts, necking zones, etc. Due to the shell elements plane stress formulation, they do not have a built in resistance to element thinning, as solid elements do. Shell elements are only restrained by neighbouring elements in terms of in-plane compatibility. This may lead to excessive strain in small elements, whereas large elements cannot capture the hot-spot strains at all.

To be able to capture all relevant effects, Alsos [2008] recommends that the shell size shall be no more than 5-10 times the plate thickness. Failure mechanisms such as local necking typically takes place in narrow bands, often no wider than the plate thickness itself. With a element size 5-10 times the plate thickness, such mechanisms are not detectable. This is taken care of by scaling the failure strain to a lower level in order to simulate the onset of fracture at the correct indentation and internal energy level, the idea being that the total strain energy at fracture should be similar regardless of the mesh size.

In uniaxial tension the scaling law can be expressed as:

$$\varepsilon_{cr} = n + (\varepsilon_n - n) \frac{t}{l_e} \quad (5.35)$$

$n$  is the power law exponent and  $t$  and  $l_e$  are the thickness and length of the shell element, respectively. Alsos notes that expressing the failure strain as a function of element size may be dangerous, as it is not guaranteed that there are large strains locally prior to fracture. For marine structures it is generally accepted make such an assumption.

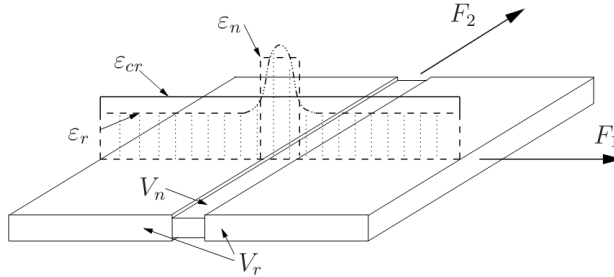


Figure 5.11: Simplified illustration of the procedure to generate the critical strain  $\varepsilon_{cr}$  for an element. The critical strain,  $\varepsilon_{cr}$  is the volume weighted result of an assumed element failure strain distribution.  $\varepsilon_r$  is the average strain outside the necking localization, and  $\varepsilon_n$  is the average strain inside the necking localization [Alsos, 2008].

Density	$\rho$	7 850	[kg / m <sup>3</sup> ]
Young's Modulus	$E$	210 000	[MPa]
Poisson's Ratio	$\nu$	0.3	[-]
Shear Modulus	$G$	80 770	[MPa]
Bulk Modulus	$B$	175 000	[MPa]
Strength Parameter	$K$	850	[MPa]
Hardening coefficient	$n$	0.24	[-]
Yield stress	$\sigma_Y$	275	[MPa]

Table 5.3: Material properties of steel.

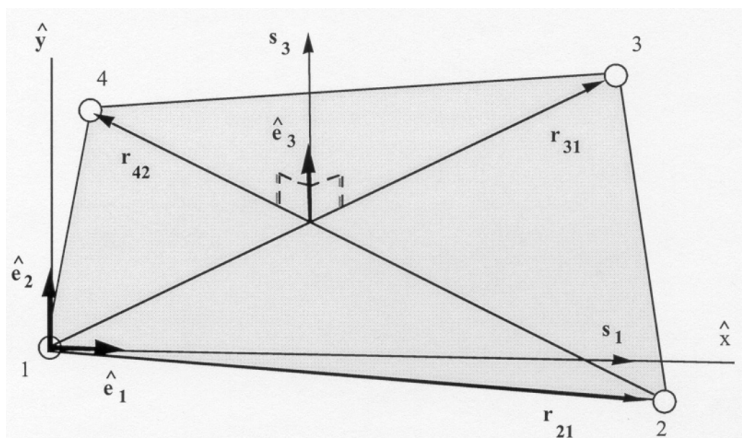


Figure 5.12: Belytschko-Lin-Tsay shell element.

### 5.3.5 Finite element formulations

In the following, brief descriptions of the finite elements used in the analyses is presented. A more complete description of the elements is available in Hallquist [2006].

#### 5.3.5.1 Shell elements

The default shell element used in LS-DYNA is the Hughes-Liu (HL) element, a four-noded quadrilateral element with uniformly reduced integration. In the analyses done in the master thesis however, the Belytschko-Lin-Tsay (BLT) shell element has been used all over. The BLT-element is computationally much more efficient than the HL-element. For shell elements with five through-thickness integration points, the BLT-element requires 725 mathematical operations, while the HL-element requires 4050 operations for the under-integrated element, and 35 350 operations for the selectively integrated element.

The BLT-element is based on a combined co-rotational and velocity-strain configuration. These kinematic properties simplify the mathematics a great deal, which is what makes the element so computationally efficient. A co-rotational formulation separates the strain producing deformations from the rigid body deformations by comparing the current configuration with the reference geometry. The current configuration is a complete description of the spatial location and orientation of each element.

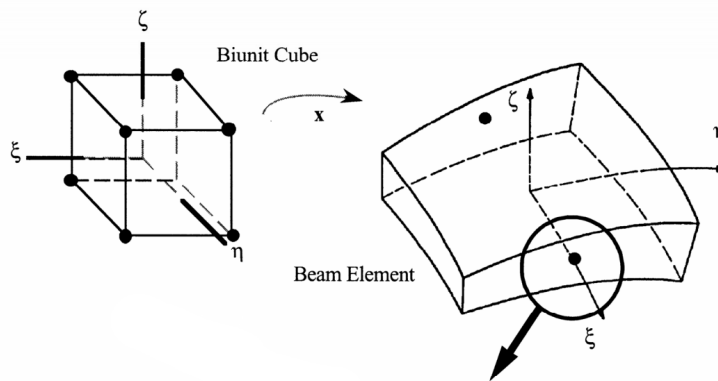


Figure 5.13: Hughes-Liu beam element.

The reference surface of the element is defined by the location of the elements four corner nodes. The complexities of the non-linear mechanics is avoided by including a local coordinate system in each element. The coordinate system deforms along with the element, and is described by the nodal coordinates. The elements normal vector is constructed from the unit vector normal to the main diagonals of the element.

### 5.3.5.2 Beam elements

To model the vertical columns supporting decks of the ship, Hughes-Liu beam elements were used. The HL beam formulation is based on the shell formulation by the same authors, and is simple, therefore also computationally effective. The element is based on a degenerated 8-noded isoparametric solid element.

The element consists of two nodes, each with three translational and three rotational degrees of freedom. The displacements are tracked using a Total Lagrangian formulation, meaning that all displacement refers to a fixed initial position.

# Chapter 6

## Finite element modeling

### 6.1 Software

There are several providers of commercial software available on the market which are all suitable for computer aided engineering . Some software specialize in different areas of application, and are more suited for analysis of solids, static linear analysis, or linear dynamic analysis. For the problem treated in this thesis, software that is able to handle large and complex non-linear problems is necessary. MSC Patran was chosen for the pre-processing, i.e. modeling and meshing. LS-DYNA was used to explicitly solve the problem.

#### 6.1.1 MSC Patran

MSC Patran is produced by MSC Software Corporation, the largest single provider of finite element analysis solutions to the CAE market [MSC Software Corporation, 2012]. It contains a very powerful toolset, with the possibility of defining almost any geometry imaginable. It may in some cases be cumbersome to work with, and is best used in cases where the design is already known: once the geometry is created, it is not practical to edit the model significantly in retrospect.

One of the greatest benefits of this software is that the user has complete control of the way the mesh is applied. For unfavourable geometry it might be impossible for a conventional "auto-mesher" to efficiently mesh the surface, costing the

user additional computational effort. In these cases, the Patran user may manually edit the location of each node and element, which may greatly improve the computational efficiency and accuracy of the solution.

### 6.1.2 LS-DYNA

LS-DYNA is a general purpose finite element program designed to simulate complex real world problems. It is capable of handling highly nonlinear transient dynamic problems. Although originally developed for the automotive industry, it is widely used in both for both marine and aerospace applications [Hallquist, 2006]. LS-DYNA utilizes explicit time integration to solve dynamic problems.

## 6.2 Reference structures

### 6.2.1 Large offshore vessel

In order to perform a realistic simulation of the scenario, a suitable vessel designed for use in the North Sea was used to base the model upon. The vessel is designed by Rolls Royce Marine AS, and built at STX's shipyard in Langsten, Norway in 2008. The Island Wellserver is an advanced Riserless Well Intervention vessel (RLWI). The nature of the ship's missions frequently bring the vessel in close proximity to offshore structures, and it is thus a suitable candidate for collision analyses. The vessels main principals are listed in table 6.1.

<b>UT-767 CD</b>	
<b>Lpp [m]</b>	102.6
<b>Beam [m]</b>	25.0
<b>Depth [m]</b>	11.2
<b>Draught [m]</b>	8.7
<b>Displacement [tons]</b>	13 600

Table 6.1: Main principals for the Island Wellserver, UT-767 CD design.

An estimated hydrodynamic added mass of 20% of the weight displacement is added, as proposed in Faltinsen [1990]. This yields a total mass of about 16 300 tons.





Figure 6.1: The RLWI vessel Island Wellserver.

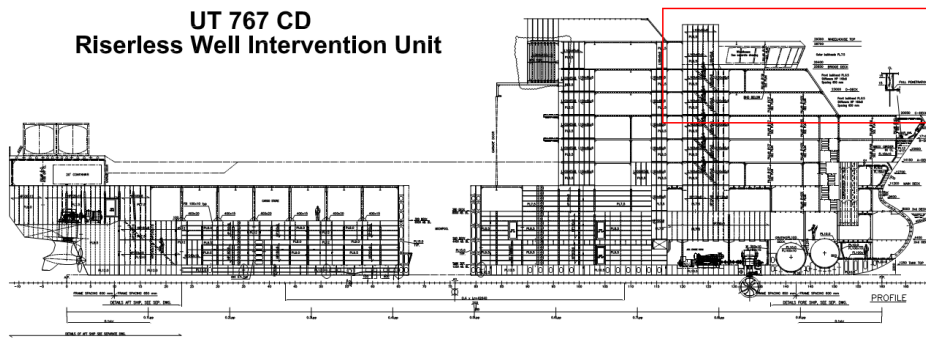


Figure 6.2: Schematic of the model vessel. The part modeled in detail is distinctively marked.



Figure 6.3: A semi-submersible drilling rig.

### 6.2.2 Semi-submersible rig

A semi-submersible rig is a floating offshore vessel capable of propelling itself at sea. They are capable of injecting large amounts of water into onboard ballast tanks, partially submerging the structure. This allows for stability during the vessels operations. Structures of this type are normally moored by anchor chains, or able to stay dynamically positioned by their onboard thrusters.

Semi-submersible rigs typically consist of a topside supported by four or more vertical columns resting atop pontoons that provide buoyancy. Semi-submersible rigs are among the most common moveable offshore structures found on the Norwegian Continental Shelf, and are thus suitable candidates for collision.

A simplified box-girder that might make up the deck of such a structure was created on background of structural drawings, details available in section 6.4.

### 6.2.3 Fixed platform living quarter

A jacket is a bottom-fixed lightweight truss structure supporting a topside which may include petroleum processing facilities, drilling equipment, storage areas, accommodation, etc. .

Even though most jacket designs are inherently similar of both form and function, several different topside designs exist, making some more susceptible and vulnerable to collision than others.

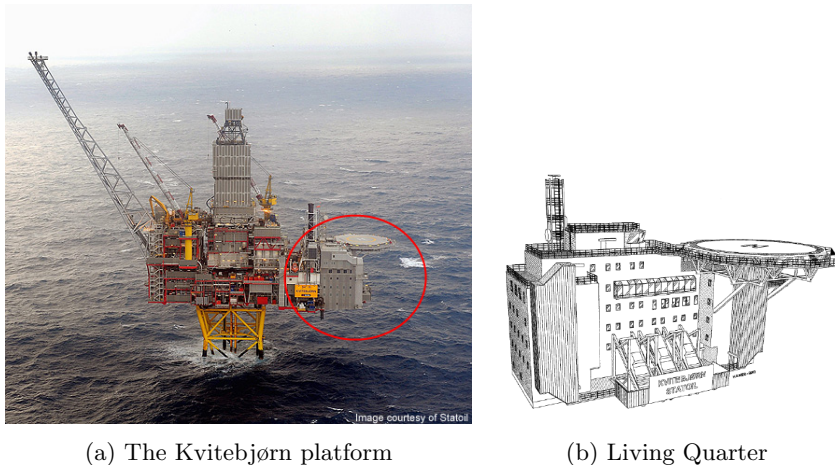


Figure 6.4: The Kvitebjørn platform with eccentric living quarter.

One design that is of particular interest is the Kvitebjørn platform. Kvitebjørn is a gas/condensate field located in the Tampen area in the northern part of the North Sea.

The Kvitebjørn platform has a highly eccentric living quarter (LQ) placed in the western end of the platform. Based on the *stressed skin* principle, it is supported vertically at two locations near the base of the LQ, and restrained from horizontal movement at two locations near the middle of the eastern bulkhead, towards the rest of the topside.

The LQ is constructed out of structural aluminium by Leirvik Sveis, and is made up of extruded aluminium profiles that make it both lightweight and tough. It has an airgap of 24.1 m above mean sea level, meaning that it is well within the range of being struck by closely passing ships influenced by wave induced motion.

### 6.3 Ship Model

The scope of this thesis is to investigate the collision behaviour of a ship's superstructure. It was therefore decided to do detail modeling of the reference ship's superstructure from the C-deck up to the wheelhouse top. A shell of the remaining ship hull and decks was also created for aesthetic purposes, as well as making it easier to define mass properties.

### 6.3.1 Geometry modeling

Creation of the wheelhouse geometry was done on background of the supplied classification society drawings. The ship superstructure was found to be almost completely symmetric. Due to this, minor simplifications were made to the geometry such that only half the model needed be created, and could later be mirrored.

The first part of the modeling was carried out by creating splines that outlined the individual decks. Points were first created marking the major intersections on each deck. Secondly, curves were drawn between points, making an outline of the deck geometry. The surrounding curves were then used to define the surface of the deck.

The positions of the longitudinal HP-stiffeners (bulb profile) were defined by creating several equidistant planes (650 mm) in the ship transverse direction. These planes were used to cut all intersecting decks. This created curves that the stiffeners' web were then extruded from. The same procedure was followed in order to make transverse frames and girders. The transverse frames are modeled as-built by T-girders. The HP-stiffeners have been simplified as flat-bars, as explained in section 6.3.2.

The wheelhouse external walls were likewise created drawing surfaces from deck to deck. The walls were cut by several planes equidistant in the longitudinal direction (650 mm), and HP-stiffeners were likewise extruded from these cuts.

In order to support the ship's decks vertically, cylindrical columns were drawn between the decks and transverse girders. Dimensions of the columns are 114 mm x 8 mm at the upper decks, increasing to 140 mm x 12.5 mm at the lower C-deck.

### 6.3.2 Simplifications

The scope of the detailed modeling was limited to the four decks from C-deck to the wheelhouse top. The detailed model spans from section 152 to station 115, a distance of 21.6 m. The geometry was simplified such that the wheelhouse was symmetric about the center line. In the actual design, only minor details separated the two halves. As the thesis' focus is on superstructure collision only, the helideck seen in figure 6.1 is not included in the model. Most of the vertical force of the helideck is transferred by heavy exterior columns to the C-deck and the ship girder, making it unnecessary to additionally strengthen the superstructure.

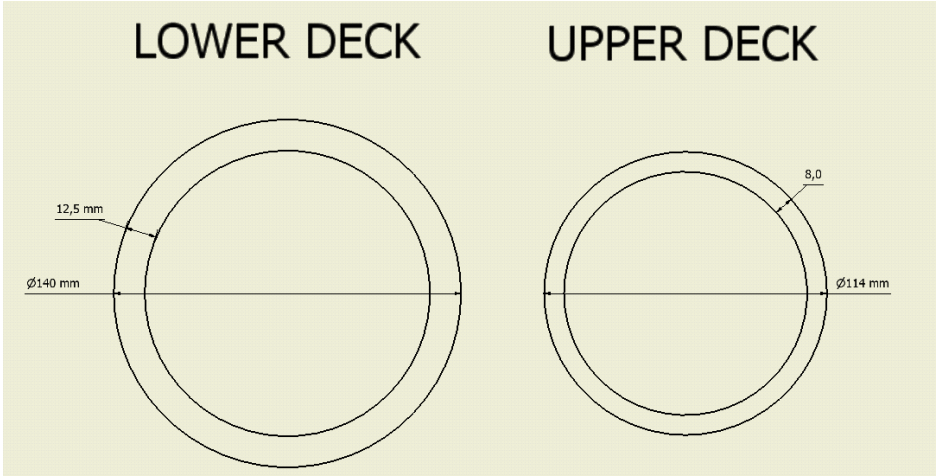


Figure 6.5: Dimensions and shapes of the vertical pillars used in the ship model.

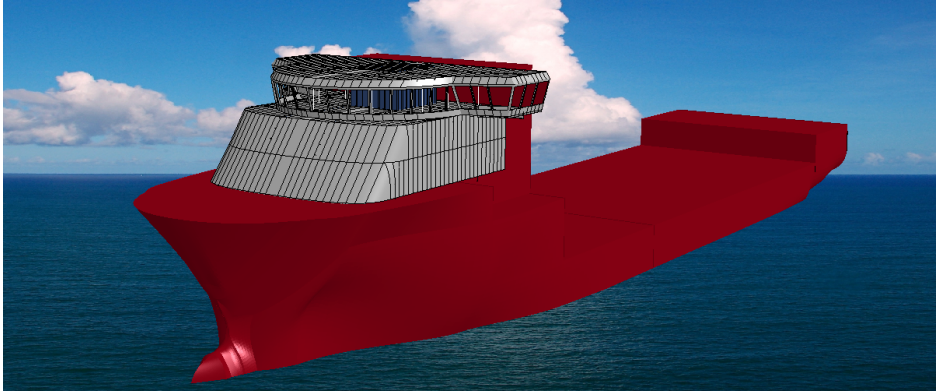


Figure 6.6: The full ship model. Mirrored about the xz-plane.

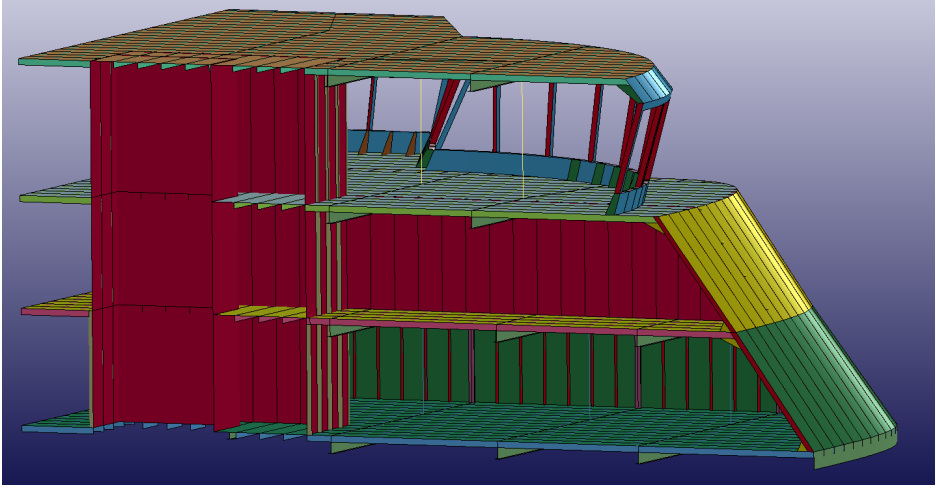


Figure 6.7: The half wheelhouse model with visible stiffeners, frames, and decks.

The stiffener geometry was simplified in an effort to reduce modeling and computational effort. The vessel's stiffeners were originally HP-profile stiffeners. After having conferred with the advisor, the decision was made to simplify the HP-profiles as flatbars with an equivalent thickness such that the plastic section modulus,  $W_P$  of the two would be equal.

The plastic section modulus is used to calculate the full plastic capacity of the cross section before it fails. The plastic section modulus for a cross section together with the yield stress of the material will result in the plastic moment capacity of the cross section,  $M_P$ .

$$M_P = \sigma_Y W_P \quad (6.1)$$

The plastic section modulus is defined as the sum of the areas on each side of the plastic neutral axis multiplied by the distance from the individual centroids to the plastic neutral axis.

$$W_P = A_{Top} y_{Top} + A_{Bottom} y_{Bottom} \quad (6.2)$$

The bulb-profile cross sections are based on NS-EN-10067 [Norsk Standard, 2012a], and have typical dimensions 160mm x 8mm. To calculate the plastic section modulus of the cross section, it is transformed into an equivalent L-profile with flange adjusted as to get a corresponding cross section area and minimum deviation in  $I_{xx}$  and  $I_{yy}$ , second moment of area.

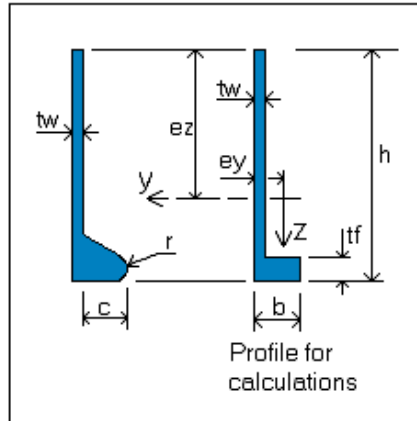


Figure 6.8: HP-profile with equivalent flange L-profile [StruProg, 2012].

Internal bulkheads made of wood and similar materials have not been included in the model due to their assumed negligible contribution to the resistance of the structure. Other details that were omitted are very small brackets, knees, cutouts in the frames, detailed geometry of corners, fatigue cutouts, etc.. This was done in order to reduce the workload of the modeling, and as their detail was judged to be of minor importance related to the crashworthiness of the ship.

The transformations are done in the following way, [StruProg, 2012].

$$b = t_w + c - 0.45r \quad (6.3)$$

$$t_f = \frac{(A_x - ht_w)}{b - t_w} \quad (6.4)$$

Where  $A_x$  is the cross section area of the profile. The modification caused an increase in stiffener thickness from 8 mm to 9.1 mm.

### 6.3.3 Meshing

According to Moan [2003], the mesh should be as regular as possible, and without large distortions in order to yield accurate results. Since most of the geometry is made up of rectangular plates, this has been possible to do without much difficulty. In some select few places it was found to be necessary to include triangular shell elements in order to avoid infinitesimally short element sides.

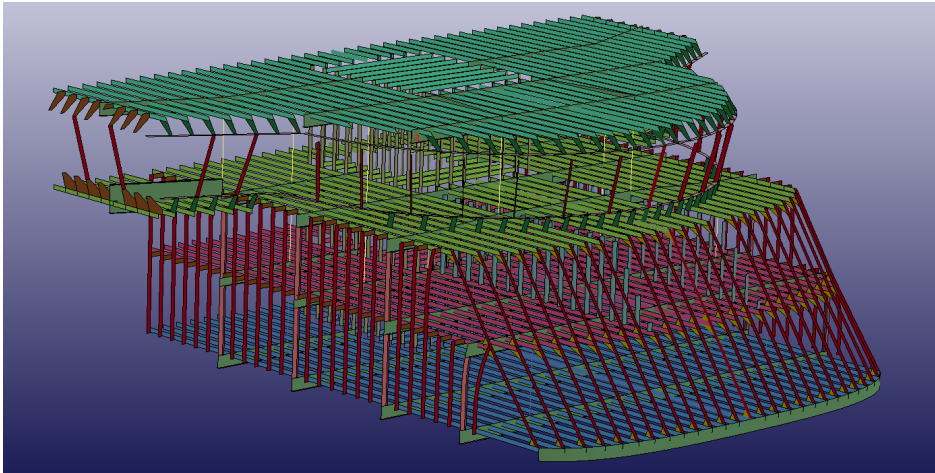


Figure 6.9: The layout of the ships' stiffeners throughout the superstructure.

Moan [2003] says that triangular elements should be used with care, as they are less accurate than quadrilateral shell elements. This advice has been heeded. Meshing the structure is quite tedious, and can be a lengthy process if not done correctly.

The ship's columns are meshed with 2 node Hughes-Liu beam elements. These elements were not compatible with the steel material used, so a linear elastic material with the same mechanical properties as the rest of the ship was utilized. Two distinct cross sections of for the beams were used, both cylindrical.

Patran have included two meshing routines for automatic creation of quadrilateral shell elements.

### 6.3.3.1 IsoMesh

IsoMesh will create equally-spaced nodes along each edge in real space—even for nonuniformly parametrized surfaces. IsoMesh computes the number of elements and node spacing for every selected geometric edge before any individual region is actually meshed. This is done to ensure that the new mesh will match any existing meshes on neighboring regions. IsoMesh requires the surfaces to be parametrized, and to have either three or four sides. Surfaces which have more than four sides must first be decomposed into smaller three- or four-sided surfaces. Trimmed surfaces must also be decomposed into three- or four-sided



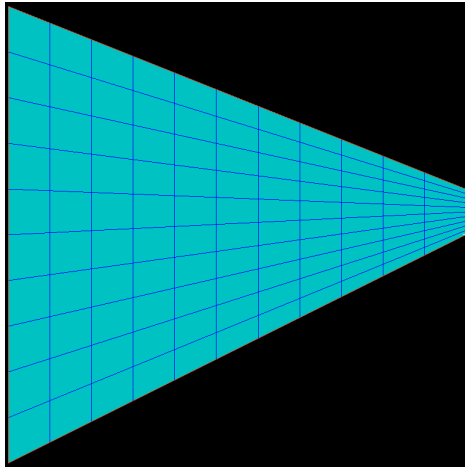


Figure 6.10: A trapezoid surface meshed with IsoMesh. IsoMesh creates very slightly distorted equally spaced nodes along each edge. This is good for surfaces that have equal sides, but can create trouble with surfaces that are as in the figure.

surfaces before meshing with IsoMesh [MSC Software Corporation, 2012]. See figure 6.10.

### 6.3.3.2 Paver

Paver is best suited for trimmed surfaces, including complex surfaces with more than four sides, such as surfaces with holes or cutouts. Paver is also good for surfaces requiring “steep” mesh transitions, such as going from 4 to 20 elements across a surface. Similar to IsoMesh, the paver calculates the node locations in real space, but it does not require the surfaces to be parametrized [MSC Software Corporation, 2012]. See figure 6.11.

During the geometrical modeling it is important to think ahead and plan how it is best to model with regard to the meshing. Geometric entities that have adjoining sides of equal length will automatically have their individual meshes connect, whereas that is not guaranteed if the plate lengths are not equal. Much time and effort can be saved if this is done. The global mesh size is set to 50 mm, which is about seven times the thinnest plate thickness. This will result in global element thickness - plate thickness ratios of 5-10. This was done in order to properly capture the fracture and failure mechanism discussed in section

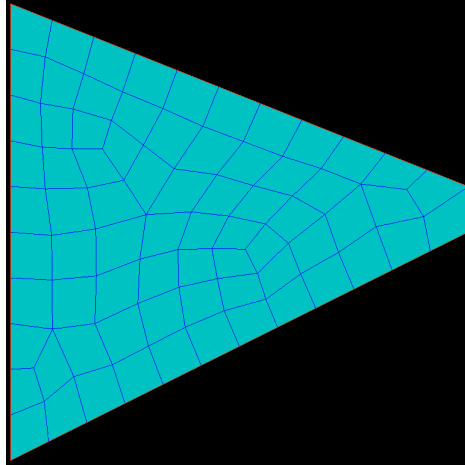


Figure 6.11: A trapezoid surface meshed with Paver. Paver is more lax with regard to distortion of elements, and is more focused on making all elements fairly equal in size. This will in general yield better results for irregular shapes than IsoMesh.

5.3.4.3. The mesh size results in having three elements across the height of the HP-stiffeners, nine elements across the frame web, and four elements across the frame flange.

It is important to be thorough when one applies the mesh to the structure. As discussed in section 5.3.2, the critical time step in an explicit method is governed by the shortest edge of the smallest element. As seen in figures 6.10 and 6.11, there will be a considerable computational penalty if IsoMesh is used for the surface in question.

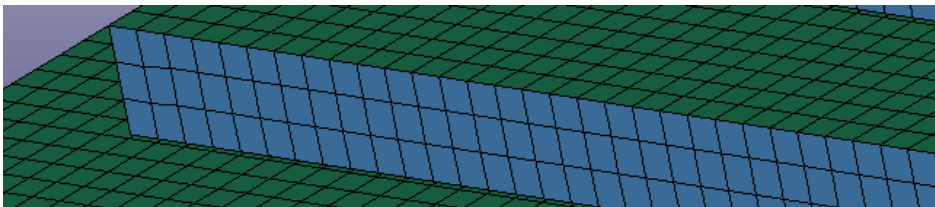


Figure 6.12: Example of how the longitudinal stiffeners are typically meshed. Three elements across the web.

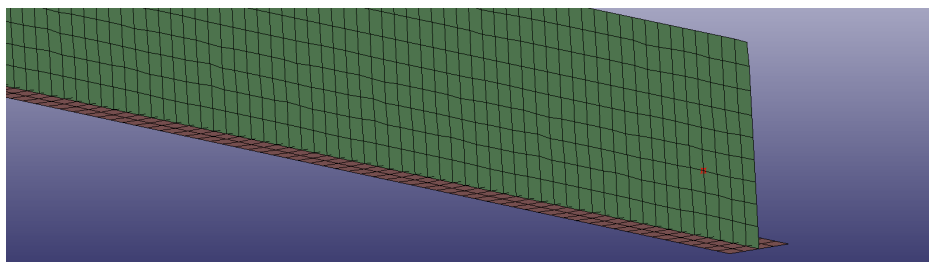


Figure 6.13: Example of how the frame girders and flanges are typically meshed. Four elements across the flange, nine elements across the web.

The critical time step at the analysis beginning was in the vicinity of  $1.3 \times 10^{-6}$ s. This is not an uncommon time step size for meshes of this size, but it could have been reduced considerably if the mesh had been controlled better. For an ideal mesh with all sides equal to 50 mm, the critical time step is  $9.2 \times 10^{-6}$ s. Due to distortion of the mesh, the shortest element length is slightly less than 8 mm.

The full ship model includes in total over 1 270 000 elements, which is quite large, considering that the structures to be collided with contains up to half this number of element. This is, however, necessary size in order to be able to capture the important effects taking place in a collision. Some effort could have been saved by using a coarser mesh in the aft part of the superstructure, but as it was uncertain how large the resistance towards collision would be in the superstructure, it was decided to keep the mesh uniform. The mesh used for the ship's hull is most places 100 times coarser than that used in the wheelhouse.

It is of the utmost importance to make sure that all nodes are connected in order to have reliable results. Patran provides two tools in order to check and rectify this. In order to check if surface edges are connected or not, the tool *verify free edges* was used. It will show a solid line for all edges that are free, and thus are not attached to any adjacent elements.

In order to merge nodes, the *mesh equivalence* was used. This option creates a sphere or box of a user defined radius around every node. Every node that are within this tolerance are merged, thus creating common nodes. If the mesh is properly created, all connecting nodes should be in the exact same space. If not, it is possible to create so-called mesh seeds that will specify exactly where a mesh is supposed to be created. If all else fails, nodes and elements may be manually inserted into the model.

### 6.3.4 Material

The wheelhouse is made of steel, and was modeled with an elastoplastic material with included fracture criterion. The material is called in LS-DYNA by *\*MAT\_USER\_DEFINED*, developed by Alsos [2008]. The ship's hull was modeled as completely rigid using the built-in *\*MAT\_RIGID*. The materials used are described further in section 5.3.4. It was estimated beforehand that a fracture model would be important in order to model the behaviour the the structure correctly. The plate thickness and stiffener scantlings of the superstructure are substantially less than that of the hull, and is typically not designed to withstand a collision at full speed.

## 6.4 Semi-submersible Deck Model

As mentioned in section 2.3, it was decided that a likely scenario for a superstructure impact would be if the ship passed in between two of the columns of a semi submersible. Typical airgap for such a structure is around 13-15 m, which will mean that the deck will go well clear of the bow and thus hit the superstructure. Typically, strength design is assumed for semi-submersible column collisions. The deck girder is in most cases less stiffened than the column, such that strength design cannot be assumed without further investigation of the strength of the deck girder.

### 6.4.1 Geometry Modeling

A structure representative of a semi-submersible deck girder is modeled. The semi is a box girder simple plate structure and lightly stiffened. There are two internal decks. The girder is longitudinally stiffened by HP-profiles (typ. 180 mm x 9 mm), spaced 650 mm apart. Vertical T-frames (typ. 400 mm x 200 mm x 12 mm x 20 mm) are placed equidistantly 2.5 m apart. For every four frames there is a vertical bulkhead, stiffened by HP-beams. Plate thickness is typically 12-14 mm. Due to the repeating structure, use of symmetry and translating surfaces the modeling work went quite efficiently compared to the modeling of the ship.

The HP-profile stiffeners are modeled as equivalent L-profiles according to StruProg [2012], as shown in section 6.3.2. Portholes are not included in the model as they are believed to not have any significant impact on the collision resistance. Further more, cutouts for wires and pipes have not been included.

Length	40	m
Height	9	m
Depth	15	m

Table 6.2: Principal dimensions of the semi-submersible box girder.

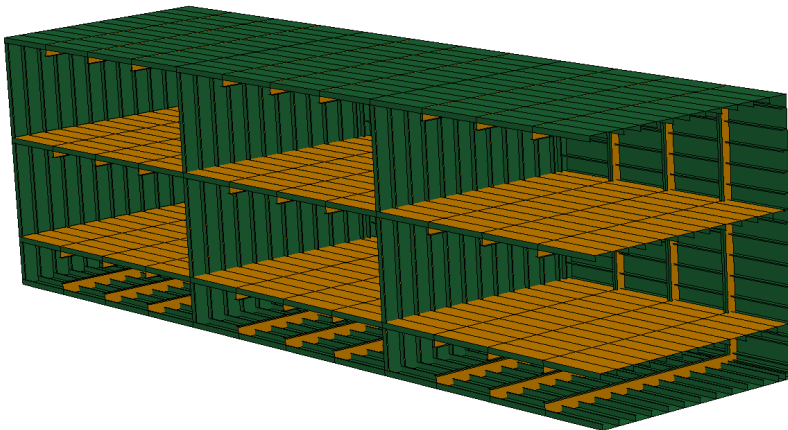


Figure 6.14: Geometry of the modeled semi submersible deck.

### 6.4.2 Meshing

The model was meshed using quadrilateral shell elements and Belytschenko-Lin-Tsay - finite element formulation. IsoMesh and a global mesh size of 50 mm was applied. The mesh is well-behaving due to the simple geometry, and the mesh is thus quite optimal. In total the full semi-submersible contains in excess of 650 000 elements. This high number was reduced by utilizing symmetry boundary conditions, and removing parts of the backside, in effect making the structure immovable.

### 6.4.3 Material

The box girder is modeled with the same steel material with RTCL-fracture criterion included as the ship. Its properties are listed in table 5.3. This will ensure a proper shared energy design behaviour.

## 6.5 Living quarter model

The living quarter is made up of a lattice of aluminium beams supporting the actual living quarter. The LQ is made out of extruded aluminium profiles that are welded together to form a strong, yet lightweight box structure.

### 6.5.1 Geometry Modeling

Due to the collision scenario being collision from underneath and to the lower part, only the first level is modeled with any degree of detail. The remaining decks are modeled as a completely rigid shell. The model was based off of technical drawings found in Leirvik Module Technology [2003].

Curves were drawn across the base-level where the main girders are situated. From these, the main girders were extruded.

Length	41	m
Height	25	m
Depth	15	m
Operating mass	1 550	tons

Table 6.3: Principal dimensions of the Living Quarter model.

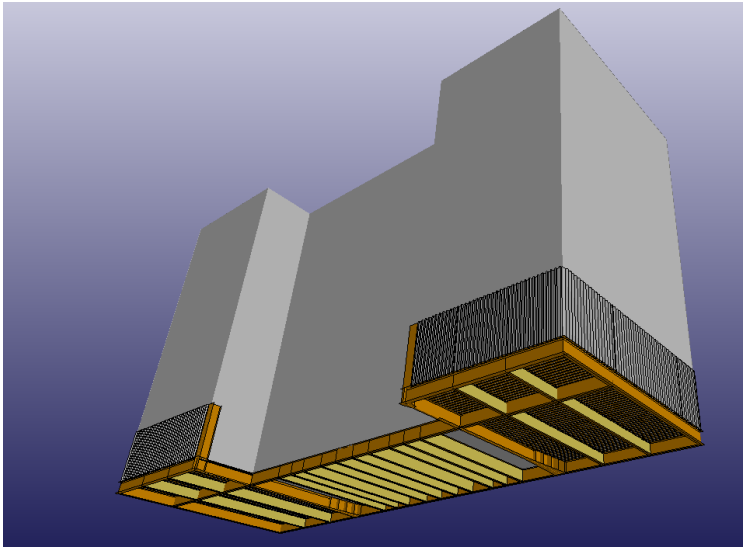


Figure 6.15: Geometry of the modeled Living Quarter.

## 6.5.2 Modeling Simplifications

The Living Quarter exterior wall panels have a number of cutouts to allow for light to enter the cabins. These are not included in the finished model, resulting in a more stiff structure. In addition, internal walls that are not necessary for the structural integrity of the LQ have not been included. Only parts of the first deck has been modeled as deformable, as it was initially assumed that the extent of the applied damage would be local.

## 6.5.3 Meshing

The LQ is meshed with shell elements all over. For the detailed section, a more or less uniform element size of 60 mm has been applied. For the rigid section, a mesh size of 1000 mm is applied.

The model contains just in excess of 250 000 shell elements and 220 000 nodes.

### 6.5.4 Material

The Living Quarter is made almost entirely out of aluminium in order to create a lightweight and robust structure. This is implemented in LS-DYNA by using the

\**POWER\_LAW\_PLASTICITY* card, which is an elastoplastic material with power-law hardening, used successfully by Dahl [2012].

Three different aluminium alloys are used in the model, the properties of which are describe in section 5.3.4.

The distribution of aluminium alloys throughout the model can be found in table 6.4.

Structural element	Alloy	Temper
Extruded profiles	AA 6082	T6
Plates $t \leq 30$ mm	AA 5383	H116
Plates $t \geq 40$ mm	AA 5083	0

Table 6.4: The distribution of aluminium alloys throughout the Living Quarter model.

## 6.6 Collision Setup

In order to be able to run the analysis in LS-DYNA, it is necessary to export keyword-files (file ending \*.key) from Patran. This is done by setting up Patran in LS-DYNA compatibility mode, and then exporting the input files using Patran's *analyze*-menu. The keyword files can then be imported to LS-PrePost, which is a pre- and post processor created by LSTC. Here boundary conditions are applied, and the final analysis input file is written. The input file was then transferred to a powerful computer containing the LS-DYNA code, and the analysis is then run remotely via a terminal window.

### 6.6.1 Ship restoring forces

Due to the various force components that may cause moments in a superstructure collision, restoring coefficients are included in heave and pitch for the ship, in order to simulate the effect of increased / decreased buoyancy of the ship.



It was discovered in the project thesis that the resulting vertical force component could potentially lead to a significant average vertical motion.

This change in displacement will lead to force and/or moment acting in the opposite direction of the motion. The restoring force/moment can be thought of as linear and rotational springs that act upon the center of gravity of the ship.

This is implemented in the following way:

- Two \*DEFINE\_CURVE\_FUNCTION cards are written in order to track the heave and pitch motion of the vessel. This cards enables the user to create load curves with arithmetic expressions as functions of the ships movement.
- Two \*LOAD\_NODE\_POINT cards are created. The cards will apply a vertical force and moment about the transverse axis respectively. The magnitude of these loads are determined by the ships heave, and its pitch angle.

The vertical restoring force is calculated in the following way:

$$F_3 = \rho g A_{wp} \eta_3 \quad (6.5)$$

Where  $A_{wp}$  is the water plane area,  $\eta_3$  is the heave motion. For small heave motions it is a good approximation to assume the water plane area as constant.

A simplified equation for the restoring moment is defined in Faltinsen [1990] as the following, valid for small angles.

$$F_5 = \rho g \overline{GM}_L \nabla \eta_5 \quad (6.6)$$

Where  $\overline{GM}_L$  is the longitudinal metacentric height,  $\nabla$  is the volumetric displacement, and  $\eta_5$  is the pitch angle in radians.

## 6.6.2 Boundary conditions

The boundary conditions reflect a simplification of the real world physics. As it is not practical to model the entire structures with shell elements, simplifications in the form of various boundary conditions is necessary, particularly in order to prevent rigid body motion, cf. figure 6.16.

## Clamped lower exterior bulkheads of ship superstructure

The frames connected to the lowest of the superstructure's decks have been fixed in the vertical translational degree of freedom (dof). This is due to the fact that the remaining ship's hull is modeled by using a completely rigid material, and does not allow for any deflection. The boundary condition itself should be good as long as the lower frames are strong enough to withstand the vertical force caused by the deflected decks. The vertical forces are transferred by columns vertically to the hull girder, as well as by the exterior bulkheads. The fixed edges may lead to an overly stiff structure.

## Symmetry about the xz-plane of the ship

As long as the ship collides head on with the structure, it is valid to utilize symmetry. Only the half model is used instead, decreasing the number of elements in the analysis by 50%. It creates some limitations regarding load cases, but reduces the computational effort considerably.

Symmetry is also utilized for the semi-submersible model, as well as for the living quarter.

## Semi-submersible fixed edges

The semi submersible is assumed to have much greater mass than the colliding ship, and will not have time to react in the short time it takes to complete the collision. All dofs along the rim facing the vertical columns are therefore fixed. In reality, some of the collision energy will go towards displacing the semi-submersible, but as a simplification, it is assumed otherwise.

### 6.6.3 Collision velocity

The ship's collision velocity can be defined in two main ways: Prescribed velocity, or initial velocity. Both have different benefits and drawbacks.

#### Prescribed velocity collision

The ship is set up as moving at a constant velocity along the ship's longitudinal axis. The platform model is raised such that it will hit slightly under the second deck.

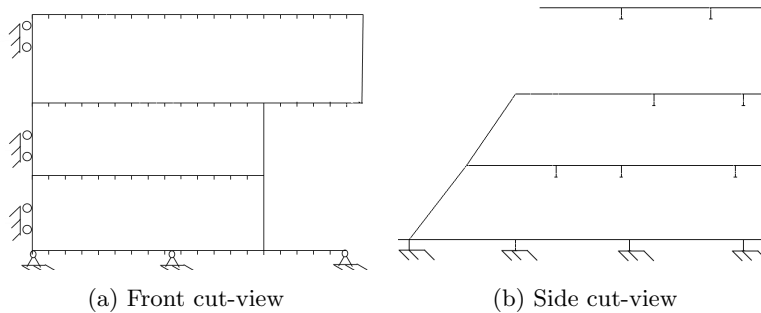


Figure 6.16: Figurative depiction of the applied boundary conditions.

The ship's displacement is defined by creating displacement curves that describe the models position in space as functions of time. By defining a linear displacement curve, the velocity is constant, irrespective of any obstacle that should come in the way.

This will not capture inertia effects and speed loss due to energy dissipation and transfer of momentum, but it is possible to observe the energy that is spent to deform the steel structure of the wheelhouse, and are thus able to create force-displacement and energy-displacement curves that may be analyzed later. In LS-DYNA, velocity is determined in the card `*BOUNDARY_PRESCRIBED_DISPLACEMENT`. In order to avoid dynamic instabilities in the beginning of the analysis, an initial velocity is also assigned using the `*INITIAL_VELOCITY` card, such that there are no sudden accelerations within the model.

This method is useful for interpolating collision results for a variety of collision velocities. It is common to use a relatively high impact velocity, such that the analysis will be completed faster. As the results are only concerned by the energy dissipated by internal strain, it is irrelevant whether the structure collides at 1 m/s or 10 m/s.

The downside to this method is that the prescribed displacement acts as boundary conditions throughout the analysis, such that any resulting vessel motion will be neglected. In collisions where the analyzed body is floating freely, this could possibly lead to an overly conservative response, or even results that are completely wrong.

### Initial velocity collision

In order to account for the mass and inertial properties of the colliding ship, it is necessary to include mass matrix of the ship in the analysis.

In *LS-DYNA*, the *\*PART\_INERTIA* card allows to override the built-in calculated mass properties for rigid bodies, and instead insert more correct terms for the global model. In conducted analyses, the translational mass of the particular vessel was known beforehand. To allow for hydrodynamic added mass in surge, 20% mass was added.

The mass moment of inertia for the particular vessel was not known, but reference radii of gyration for a similar, smaller ship was made available by *MARINTEK*. The radii of gyration was extrapolated to account for the added size of the reference vessel by keeping the  $r_{ii} / L_{pp}$  - ratio constant. The mass moment of inertia was then calculated.

$$I_{ij} = M_{ij}r_i^2 \quad (6.7)$$

$$\mathbf{M} = \begin{bmatrix} M_{11} & 0 & 0 & 0 & 0 & 0 \\ 0 & M_{22} & 0 & 0 & 0 & 0 \\ 0 & 0 & M_{33} & 0 & 0 & 0 \\ 0 & 0 & 0 & I_{44} & 0 & 0 \\ 0 & 0 & 0 & 0 & I_{55} & 0 \\ 0 & 0 & 0 & 0 & 0 & I_{66} \end{bmatrix} \quad (6.8)$$

The cross terms were not included in the mass matrix. This is in general only valid if the body is symmetric about all axes. Such a simplification may lead to error where diagonal movement is concerned. As the analyses deal mostly with collisions along the principal axes, the cross terms were assumed to have little effect on the global motions as a whole. The collision duration is considered to be small related to a typical wave period, such that the error is assumed to be small.

#### 6.6.4 Contact

In order to tell the solver that elements will be in contact with other elements during the analysis, *\*CONTACT*-cards are used. In the conducted analysis, two types of contact checking algorithm is applied:

*\*CONTACT\_SINGLE\_SURFACE* Defines that a structure may bend inwards and come into contact with itself. A friction coefficient  $\mu = 0.3$  is applied to elements in contact (dry steel on steel), according to Gieck and Gieck [2006].

\**CONTACT\_AUTOMATIC\_SURFACE\_TO\_SURFACE* Tells LS-DYNA that the wheelhouse elements and platform topside elements may come in touch with each other. A friction coefficient  $\mu = 0.3$  is applied to elements in contact.

Contact treatment forms an integral part of many large-deformation problems. Accurate modeling of contact interfaces between bodies is crucial to the prediction capability of the finite element simulations. LS-DYNA covers a large number of contact types. Some types are for specific applications, and others are suitable for more general use. Users are faced with numerous choices in modeling contact.

In LS-DYNA, a contact is defined by identifying (via parts, part sets, segment sets, and/or node sets) what locations are to be checked for potential penetration of a slave node through a master segment. A search for penetrations, using any of a number of different algorithms, is made every time step. In the case of a penalty-based contact, when a penetration is found a force proportional to the penetration depth is applied to resist, and ultimately eliminate, the penetration. Unless otherwise stated, the contacts discussed here are penalty-based contacts as opposed to constraint-based contacts. Rigid bodies may be included in any penalty-based contact but in order that contact force is realistically distributed, it is recommended that the mesh defining any rigid body be as fine as that of a deformable body.

Though sometimes it is convenient and effective to define a single contact that will handle any potential contact situation in a model, it is permissible to define any number of contacts in a single model. It is generally recommended that redundant contact, i.e., two or more contacts producing forces due to the same penetration, be avoided by the user as this can lead to numerical instabilities [Hallquist, 2006].

In Sætre [2012], collision analysis between a deformable ship superstructure and a rigid wall was conducted. In this thesis, the analysis was expanded to allow for both bodies to be deformable.



# Chapter 7

## Finite element results

### 7.1 General analysis settings

During the run of this master thesis, several analyses have been completed. The models used have had different analysis settings applied, as well as different materials.

The ship's hull was modeled as completely rigid with mass properties equal to those of the real ship. Where input has been missing, properties for similar ships have been used. The numerical input has been scaled to correct for any difference in size.

The ship's superstructure was modeled using mild steels with an included fracture model. It was estimated beforehand that the wheelhouse structure would not be able to withstand much of the compressive force exerted by the semi-submersible, and that cracks would soon propagate and deteriorate the integrity of the structure.

Material	Density $\rho$ [kg/m <sup>3</sup> ]	E-Modulus E [MPa]	Poisson's ratio $\nu$ [-]	Yield Stress $\sigma_Y$ [MPa]	Strength coeff. k [-]	Hardening expnt n [-]	Shear Modulus G [MPa]	Bulk Modulus B [MPa]
Rigid	7 850	210 000	0.3	[-]	[-]	[-]	[-]	[-]
Steel	7 850	210 000	0.3	275	850	0.24	8 077	17 500
Aluminium	2 700	70 000	0.3	220 - 250	350 - 410	0.05 - 0.2	27 000	58 000

Table 7.1: Material properties for materials used in analyses.

Material properties for the steel material model are taken from Alsos [2008].

For each analysis, a suitable time frame is analyzed, either until a sufficient amount of energy has been absorbed, or the vessel has come to a complete stop. Results are printed every 0.02 seconds, and contain vast amounts of information about deformation magnitudes, pressures, energy absorption, strain levels, etc.. LS-DYNA calculates the critical time step, and also the estimated time the analysis needs in order to complete. Due to the size and amount of deformation present in the model, each analysis in general needed 3-7 full days to finish, running on 6-12 CPU cores.

The most important for collision applications are the force-displacement curves, and the energy-displacement relationships that are integrated from the force-deformation relationship. This information may then be evaluated together with the external mechanics, and can be checked for the classification societies demands. Several cut-planes are also presented in the appendix in order to show visual depiction of the load history.

## 7.2 Results - Collision with semi submersible.

Numerous analyses were run, where four main parameters were changed. They are presented in table 7.2.

Title	V. position [mm]	Velocity [m/s]	Boundary	Impact angle	Rigid/ Deformable
Analysis 1	1500	10	Forced vel.	0°	Rigid
Analysis 2	1500	10	Forced vel.	0°	Deformable
Analysis 3	1500	5	Initial vel.	0°	Deformable
Analysis 4	7750	10	Forced vel.	0°	Deformable

Table 7.2: Analysis setup for semi-submersible collisions.

Vertical position is defined as the distance from the top plating of the forecastle deck and to the bottommost point of the topside. For the three initial collisions, the distance is set as 1.5 m above the deck, such that the topside will strike just below the second deck, (D-deck). In the project thesis it was discovered that this location yielded the highest amount of resistance towards crushing amongst all the tested load cases.

The first analysis is run with the ship colliding with a rigid plate of similar shape as the cross section of a semi-submersible rig deck. This is meant as a control



analysis in order to check the importance of modeling the semi-submersible as deformable.

The second analysis is run with forced velocity, meaning that the kinetic energy transferred to the semi submersible will not in any way reduce the collision velocity. This is done to extract the total dissipated energy that is consumed in deforming the structures a set amount. The applied kinetic energy is proportional to the velocity squared, meaning that the response can be extrapolated for other velocities also. These extracted energies may be used to create collision design curves.

The third analysis has applied an initial velocity that will decrease as the kinetic energy is transformed into strain energy. This mode will allow for a less constrained model, and a more accurate result. The velocity is comparable to that of the Big Orange XVIII incident, see section 2.2.3.

The fourth analysis is run with forced velocity, and it is imagined that the semi is now in survival draught, such that the very top of the bridge only will collide. Prescribed displacement settings are used.

The main objectives of the semi-submersible analyses are:

**Analysis 1:** Establish a control case for a collision with a rigid plate.

**Analysis 2:** Investigate whether the semi-submersible will contribute significantly to the energy dissipation.

**Analysis 3:** Ascertain whether global motions of the ship will change the energy balance for the collision.

**Analysis 4:** Investigate the deformation resistance of the ship's bridge.

### 7.2.1 Constant velocity, rigid plate

In order to gauge the maximum axial crushing strength of the ship's superstructure, it was forced against a rigid plate with roughly the same shape as the actual deformable model. A section of 10.8 m was crushed at a constant velocity of 10 m/s.

Inspection of the deformation history reveals that the superstructure fails initially by bending of the forward facing bulkheads and stiffeners. The curvature of the semi's deck forces the superstructure to flatten, thus supporting columns and bulkheads are forced to deform vertically.

As the lightly stiffened bridge and wheelhouse top impacts the plate the are crushed. The contact area now is of such a magnitude that the friction caused by the sliding surfaces is greater than the strength of the lower exterior bulkheads. This causes the exterior bulkhead between decks C and D to tear. The crack propagates all along the C-deck, and causes the remaining parts of the wheelhouse to be crushed against the rigid plate.

By studying the load history, fig. 7.1, a nearly linear relationship between force and deformation is visible up to about 2.5 m, caused by the increase of contact area. A load peak first appears of just under 35 MN at 2.5 m deformation. At this point, the front facing external bulkhead between decks C and D fractures. The load level drops slightly after this, but then continues to build. The global maximum load level occurs at roughly 5 m deformation. At this point, the wheelhouse top is just about to buckle due to the immense pressure. A horizontal crack is propagating along lower C-deck, thus reducing the crushing capacity of the cross section substantially.

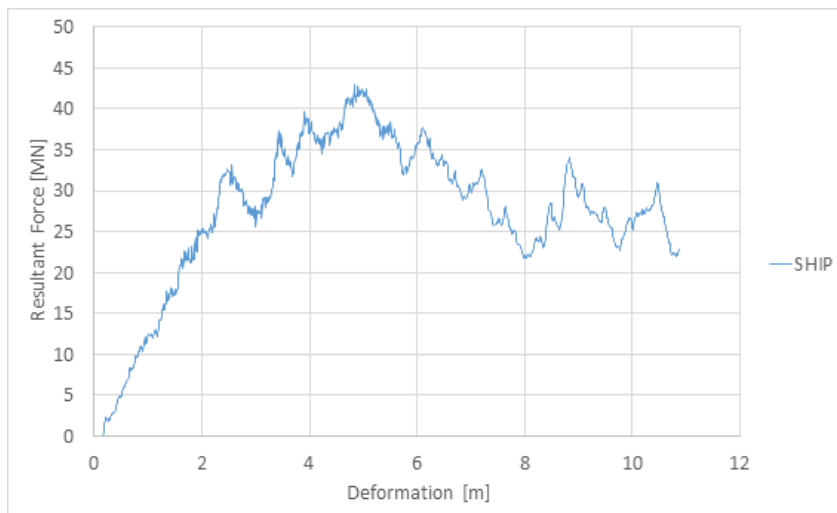


Figure 7.1: Force-deformation curve for analysis 1: Rigid plate collision.

In figure 7.2, the total strain-, friction-, and hourglass energy curves are presented. Strain- and friction energy contributes directly to the energy dissipation, and must be accounted for in the analyses, but the hourglass energy is the product of spurious zero energy modes, which are a byproduct from the finite element formulation, and do not contribute to the dissipated energy.

At the end of the analysis, the strain energy contributes to 83% of the total

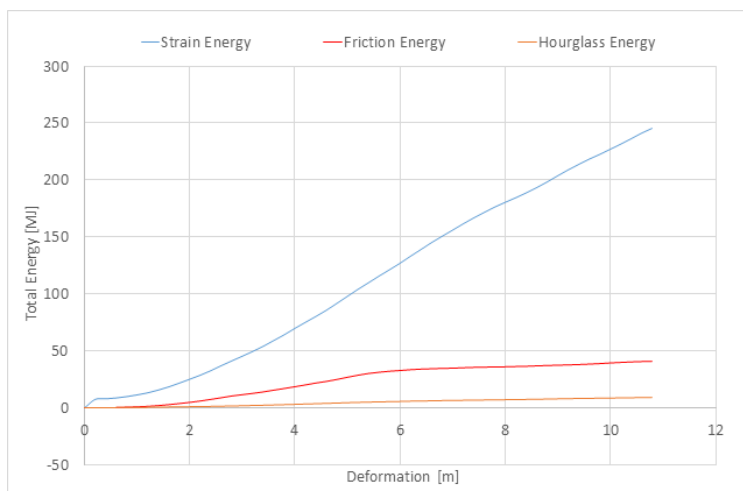
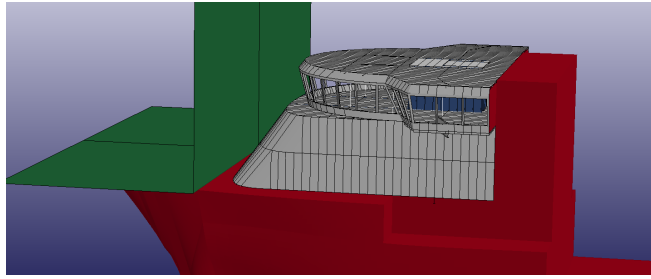


Figure 7.2: Analysis 1: Energy-deformation relationship.

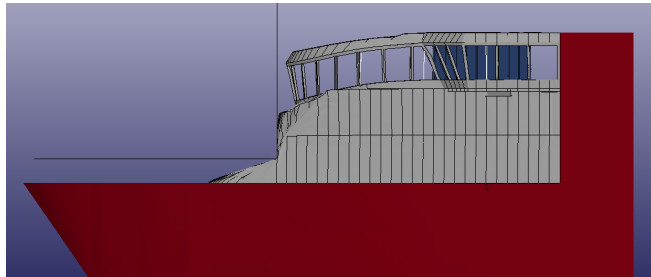
dissipated energy, while the friction energy is 14%, and hourglass energy is 3%. Ideally, the strain energy should dominate the energy balance even more than what is apparent in these results. The high friction energy can be attributed to the great amount of sliding that takes place as the lower part of the superstructure passes underneath the rigid plate. The hourglass energy is  $\leq 5\%$ , which is within acceptable bounds.

It is common in conventional axial crushing analyses to directly integrate the resultant force in order to obtain the internal energy dissipated. This is acceptable when the entire cross section is uniformly crushed. In this case, however, it is clear that less energy is absorbed as the wheelhouse is first bent, then ruptures. Thus, not all the material is activated and able to withstand the deformation. In the following results, only the strain energy curve obtained from adding the individual internal energies will be presented.

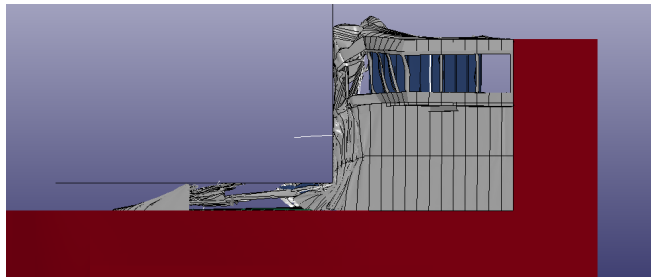
At the end of the analysis, nearly 290 MJ of kinetic energy has been transformed into strain- and friction energy. This is the equivalent of a 16 200 tonne vessel (accounting for added mass), colliding at 6.0 m/s - 11.6 knots, and coming to a full stop.



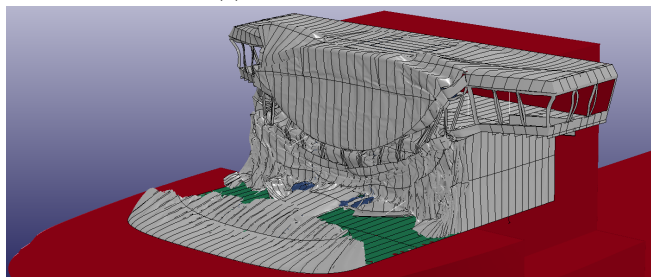
(a) Initial configuration.



(b) Prior to tearing.



(c) End of simulation.



(d) Total deformation at the simulation end.

Figure 7.3: Time-lapse of analysis 1: Wheelhouse vs rigid plate collision.

## 7.2.2 Constant velocity, deformable semi

In this analysis, the rigid plate used in section 7.2.1 was substituted by a model of a representative deck girder of a large semi-submersible rig. This was done in order to establish the energy absorption level of the semi-submersible vs the ship.

The ship and semi are modeled using the same steel material with elastoplastic power law properties and fracture criterion. The vessel is forced head-on towards the semi-submersible at constant velocity of 10 m/s. Only a velocity component along the longitudinal axis is included. The vessel is prevented from motion in any direction but longitudinally.

The deformations are now shared between the two bodies, and will as such deform unequally based on the relative stiffening of the hulls. The force-, and energy-deformation curves may help determine if it is possible to utilize strength design or ductility design when analyzing the impact.

As there is no universal way of creating force-deformation diagrams for impacts where the impactor is also deformable, focus has been on creating curves based on the resultant deformation of a node that is representable for the most extreme deformation on both bodies. For conventional axial bow crushing scenarios, the entire forward part of the ship is equally deformed. In this case, the wheelhouse is not uniformly crushed, as rupture occurs and basically limits the deformation to the part of the wheelhouse that still impacts the plate, while the other half passes underneath the deck and is otherwise unharmed.

The first load peak can be related to the time when the full width of the superstructure is in contact with the semi-submersible rig, and the consequent bending of the bridge top. The force level decreases after this, but reaches another peak as the bridge wings are reached and destroyed. After this point the results become unreliable, as part of the structure that is not modeled correctly starts to deform.

By studying the total energy curves (figure 7.8) we may observe that the total hourglass energy is just over 5% of the total energy, which is acceptable. Hourglass energy is a result of viscous damping or elastic stiffness that is added to the model in order to deal with zero-energy modes that may appear in some FE-formulations. Work done by the hourglass resistance is neglected in the energy equation due to them being orthogonal to the strain calculations. This may however lead to a loss of energy in the system Hallquist [2006]. Hourglass modes are best reduced by creating an efficient mesh, or using selective reduced integration. The sliding interface energy is 13 % of the total energy in the collision,

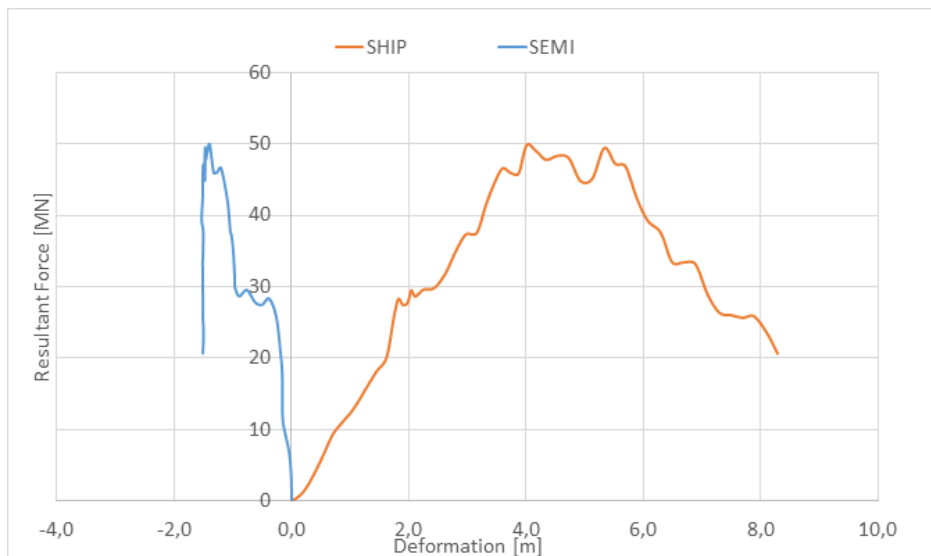


Figure 7.4: Force-deformation relationships for collision 2: Constant velocity, deformable semi.

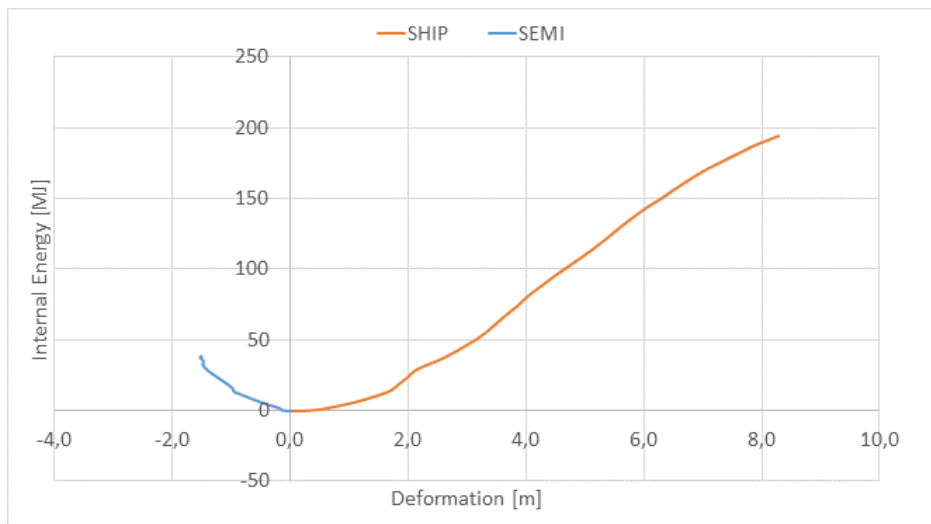


Figure 7.5: Internal energy-deformation relationship for collision 2: Constant velocity, deformable semi.

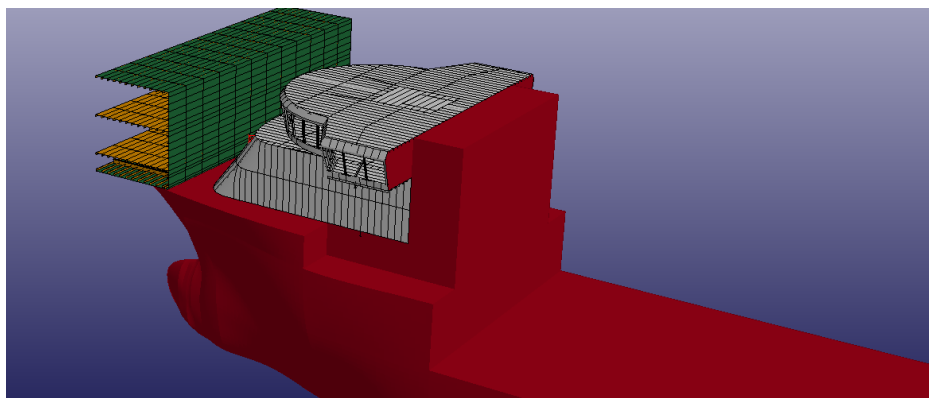


Figure 7.6: Model set-up for analysis 2: Ship vs semi-submersible collision.

which is similar to what was experienced in the rigid plate collision, and also quite high.

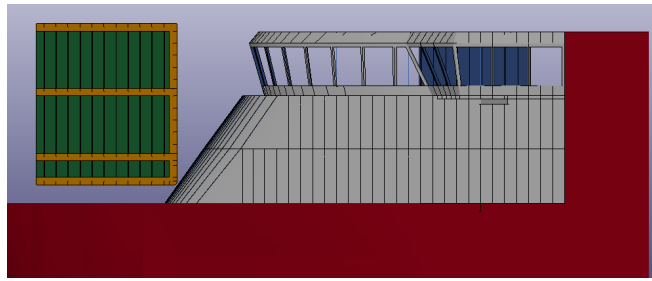
From the semi's perspective, moderate amounts of damage is visible after the impact. The strain energy absorbed by the semi is equal to 12 % of the total energy dissipated during the collision, which is not very much compared to the energy absorbed by the semi.

### 7.2.3 Initial velocity, deformable semi

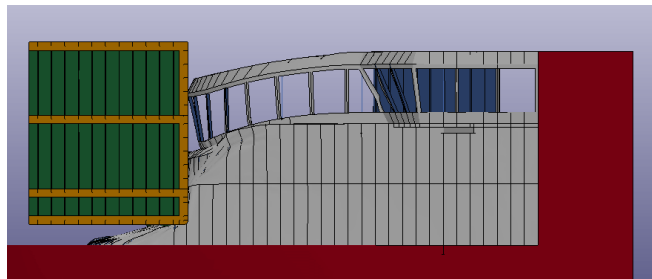
For this analysis, it was of interest to investigate the effect the collision would have on the global motion of the ship, and if so, would the motion cause more severe damage to the ships' superstructure.

The analysis was carried out using an initial velocity of 5 m/s (9.7 knots), corresponding to a total kinetic energy of 202.5 KJ. The ship was left free to heave and pitch as the collision progresses, and would have its velocity decrease as energy is absorbed in the ship and the semi.

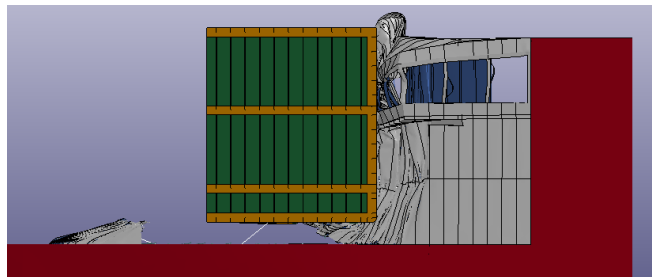
The analysis was ended prematurely after 1.94 seconds due to a significant drop in timestep, grinding the collision to a standstill. This effect was caused by distortion of elements in the fracture zone, cf. section 5.3.2. At this point, the ship's velocity was reduced to 1.3 m/s. However, when the results were presented it was clear that the analysis had been unsuccessful.



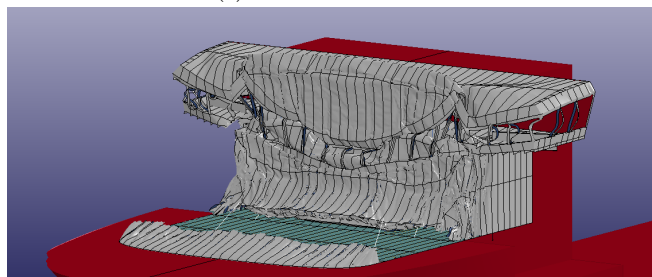
(a) Initial configuration.



(b) Prior to tearing.



(c) End of simulation.



(d) Total deformation at the simulation end.

Figure 7.7: Time-lapse of analysis 2: Wheelhouse vs deformable semi.



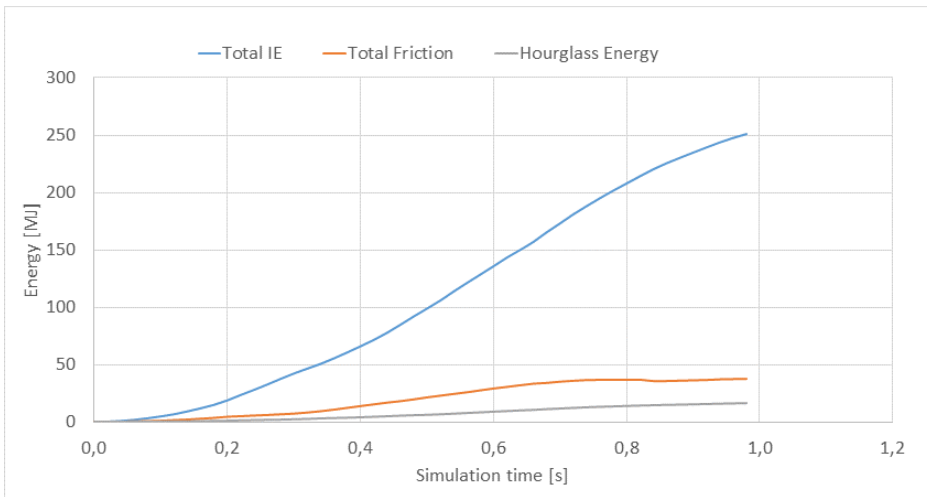


Figure 7.8: Total energy history for analysis 2: Wheelhouse vs deformable semi.

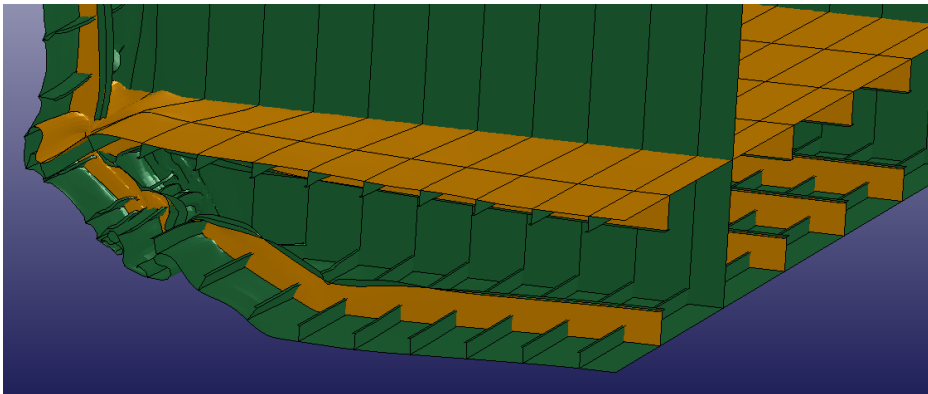


Figure 7.9: Analysis 2: Damage to semi-submersible after impact.

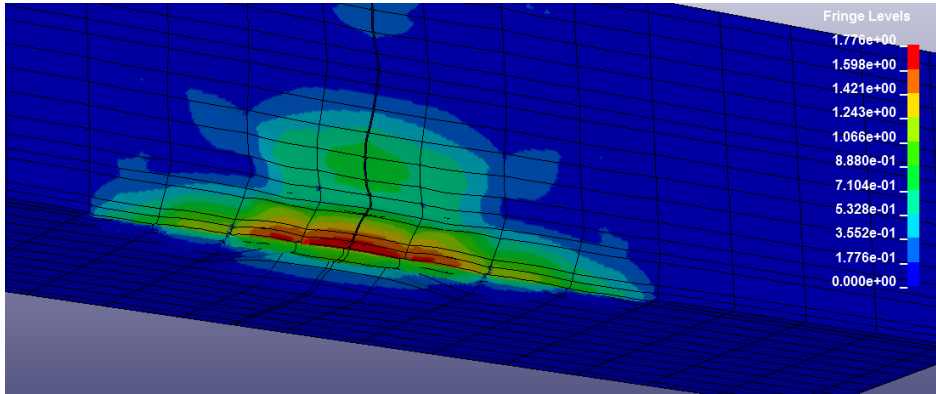


Figure 7.10: Analysis 2: Deformation levels of semi-submersible after impact (fringe levels in meters).

Component	Unit	Value
Mass, incl. Added mass	[kg]	16200.0E3
Radius of gyration, $r_{44}$	[m]	10.0
Radius of gyration, $r_{55}$	[m]	29.0
Radius of gyration, $r_{66}$	[m]	29.0
Mass moment of inertia, $I_{XX}$	[ $kgm^2$ ]	1.6E9
Mass moment of inertia, $I_{YY}$	[ $kgm^2$ ]	13.6E9
Mass moment of inertia, $I_{ZZ}$	[ $kgm^2$ ]	13.6E9
Vertical restoring $C_{33}$	[N/m]	20.0E6
Pitch Restoring $C_{55}$	[Nm/rad]	13.2E9

Table 7.3: Mass properties for the ship.

### 7.2.3.1 Global motion of the ship

When investigating the resulting global motion of the ship at the end of the analysis, it was obvious that the ship was not behaving as expected. Instead of yielding a combined heave-pitch response, the ship experienced a global upwards heave motion, with no pitch component whatsoever.

Due to time constraints, it was not possible to troubleshoot the problem further. The investigation of the effect that global motion has on the resultant force and energy is important, and could be a topic for a master thesis in itself.

A quick estimate of the resulting pitch angle would be to calculate the quasi-static moment equilibrium about the center of gravity. If one assumes that the collision force only acts horizontally, and at a fixed point in space, it is possible to estimate the average collision force.

$$F_5 = C_{55}\eta_5 \quad (7.1)$$

$$F_5 = P_{avg}h \quad (7.2)$$

$$P_{avg} = \frac{1}{\delta_{Ship}} \int_0^{\delta_{Ship}} P(\delta_{Ship})d\delta_{ship} = \frac{E_{internal}}{\delta_{Ship}} \quad (7.3)$$

$$\eta_5 = \frac{F_5}{C_{55}} \quad (7.4)$$

Where  $F_5$  is the total pitch moment,  $\eta_5$  is the pitch angle,  $E_{int}$  is the total internal energy, and  $h$  is the distance from the center of pressure to the center of gravity.  $C_{55}$  is the vessel's restoring in pitch.

Using the results obtained in section 7.2.2, the average resultant force is 23 MN. The distance from the center of pressure to the center of gravity of the ship is 14.5 m. This leads to a total pitching moment of 330 MNm. The vessel would thus reach equilibrium at an upwards pitch of  $1.4^\circ$ . This corresponds to an elevation of the bow of just over 1.4 m (if the ship's submerged shape is assumed box-like). Should the elevation be so high that the bow were to touch the underside of the semi, it is likely that this would limit the rotation considerably.

The impulse delivered by the ship is defined as the integral of force over time, and gives the change of momentum to the system.

$$\mathbf{I} = \int_{t_1}^{t_2} \mathbf{F}(t) dt \quad (7.5)$$

$$\mathbf{F} = \frac{d\mathbf{p}}{dt} \quad (7.6)$$

$$\mathbf{I} = \int_{t_1}^{t_2} \frac{d\mathbf{p}}{dt} dt = m\mathbf{v}_2 - m\mathbf{v}_1 \quad (7.7)$$

For an average contact force of 23 MN, the impulse duration can thus be found by the following expression.

$$\mathbf{F}\Delta t = m\Delta\mathbf{v} \quad (7.8)$$

$$\Delta t = \frac{m(\mathbf{v}_2 - 0)}{\mathbf{F}} \quad (7.9)$$

This leads to an expected impulse duration of 3.5 seconds for the initial velocity collision. This is about half what is found to be the natural periods of the ship in heave and pitch. The undamped, uncoupled eigenperiods are calculated by:

$$T_{3N} = 2\pi\sqrt{\frac{M + A_{33}}{C_{33}}} = 5.7s \quad (7.10)$$

$$T_{5N} = 2\pi\sqrt{\frac{I_{55} + A_{55}}{C_{55}}} = 6.4s \quad (7.11)$$

These are defined as *long impulses* by Larsen [2009], and may typically yield Dynamic Amplification Factors (DAF) of up to twice the static load, depending on the impulse shape. This would first and foremost influence the pitch angle of the ship.

The motion of the center of gravity is constantly measured by the functions defined in *\*DEFINE\_CURVE\_FUNCTION*. The functions, described further in Hallquist [2006], are *DZ(Node1, Node2)* and *AY(Node1, Node2)*. *DZ* monitors the vertical displacement of Node 1 in relation to the local coordinate system of Node 2. *AY* monitors the rotation displacement of Node 1 about the Y-axis of Node 2. When no Node 2 is defined, the global coordinate system is defined. Node 1 is the center of gravity.

The restoring forces are defined such that they apply a force or moment proportional to the displacement of the node, and in the opposite direction of motion. This is in LS-DYNA done through the *\*LOAD\_NODE\_POINT*-card. The idea behind this way to implement the response was that the load function would mimic the response of a linear spring element, and thus circumventing the extra work of the making linear spring elements follow the vessels motions. Instead, the response from the springs would be directly applied to the hull.

A simplified model of the problem was tested successfully using the exact same settings as in the conducted analysis. The model consisted of a rigid hull and an elastic box that collided in a rigid wall. The model uprighted itself nicely when exposed to both vertical forces and a heeling moment. As such, there is no reason to expect that the method will not work according to plan, given that the motion properties are applied correctly.

Unfortunately, a method of directly extracting the load curves from LS-DYNA is not implemented in the available version of the software (LS971 R4). It is therefore not straightforward to extract the load histories of the curves in order to locate the source of the problem. In the newest version, LS971 R7, an option (*\*DATABASE\_OPTION\_CURVOUT*) exist that will directly export the load curves. This could be used in a later stage to troubleshoot the lack of resulting motion.

There is reason to believe that the pitching motion would reduce the friction energy caused by the sliding underneath the semi-submersible deck, as the superstructure would likely not be torn apart to the same degree. This reduction in dissipated energy would most likely thus lead to a greater degree of deformation of the hull. By using prescribed motion analysis, the superstructure *must* follow the hull regardless of its contact status. Due to this, large membrane- and friction forces are bound to occur. In addition, the albeit slight diagonal angle of attack might cause the resultant force to change. As witnessed in section 7.3.1, the vertical crushing resistance of the wheelhouse was found to be low. The implication may be that the resistance towards crushing is even less than what is discovered in the results herein.

#### 7.2.4 Survival draught

For this analysis, it was of interest to investigate the wheelhouse strength in an impact where the semi is de-ballasted to survival draft. This will lead to only the wheelhouse top deck impacting the platform, a section estimated to have only light stiffening due to the great amount of windows, necessary for navigation.

The vessel is positioned such that the wheelhouse top is located 1.5 m above the semi bottom plating. Prescribed displacement is utilized, and the ship is set to move constantly at 10 m/s throughout the analysis. The vessel is prohibited from moving in any other direction but longitudinally.

By studying the load history and force-deformation curves (cf. figure 7.13), we can relate the deformations to the relevant force levels. In the first part of the impact, the force level is steady at 3-4 MN. At 5 m deformation of the ship, a load peak of about 12 MN appears as the wheelhouse top deck visibly buckles. After the buckling, the load level returns to previous values, before steadily rising again up to about 20 MN near the simulation end. This can be related to the crushing of the bridge wings and stairwell.

At the simulation end, the semi does not seem affected by the collision in any significant degree compared to the ship. Only minor local dents are visible in the exterior plating.

By studying the strain energy curves, it is confirmed that the semi-submersible does indeed not absorb any particular amount of energy. At the end of the analysis, the ship has absorbed nearly 20 times more strain energy than the semi.

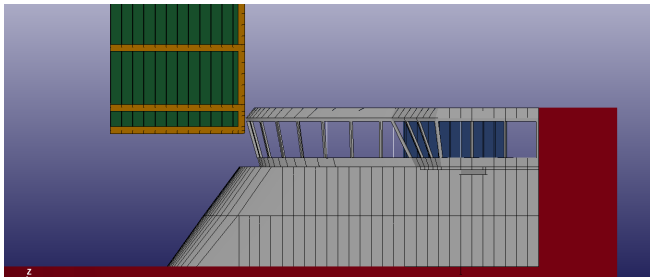
In figure 7.15, the total strain, friction, and hourglass are plotted as functions of the analysis time. Strain energy is shared between the ship and semi, but the friction and hourglass components are "common" to the entire analysis. The two latter components are therefore not straightforward to relate to the motion of one node, so it is easiest to display the curves in the domain they have in common - time.

In comparison to the previous analyses, where friction energy was a big factor in the energy equilibrium, the bridge collision is dominated by strain energy. This is due to the fact that the crushing mode is much more prominent than sliding in this particular case.

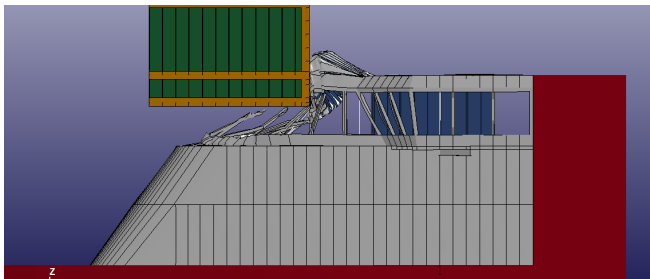
### 7.3 Results - Collision with Living Quarter.

In this section, a collision with a jacket supported platform's living quarter is envisioned. Two main scenarios are analyzed:

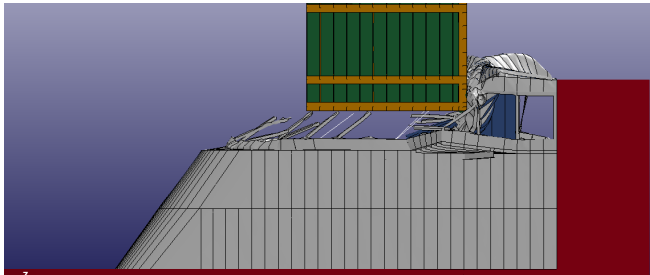
For analysis 5 - vertical impact, the ship is imagined to just have stopped underneath the living quarter. An incoming (long) wave causes the ship to heave with an amplitude of three meters. The process is accelerated in the analysis in order to save computational time, such that the wave period is 4 seconds.



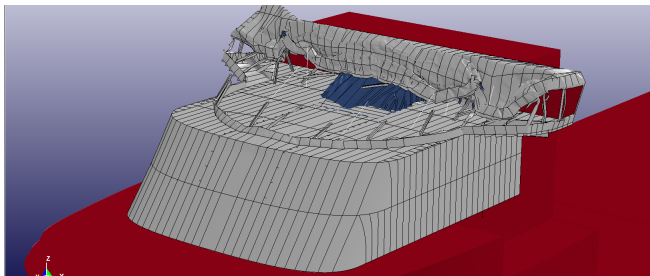
(a) Initial configuration.



(b) Prior to tearing of window frames and buckling of the deck.



(c) End of simulation.



(d) Total deformation at the simulation end.

Figure 7.11: Time-lapse of analysis 4: Wheelhouse vs deformable semi in survival draft.

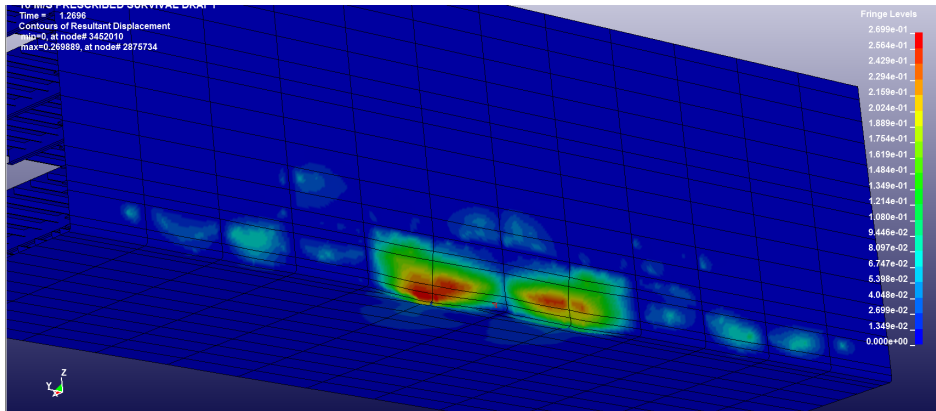


Figure 7.12: Analysis 4: Semi-submersible deformation at analysis end. Fringe levels in meters. Maximum value: 0.27 meter.

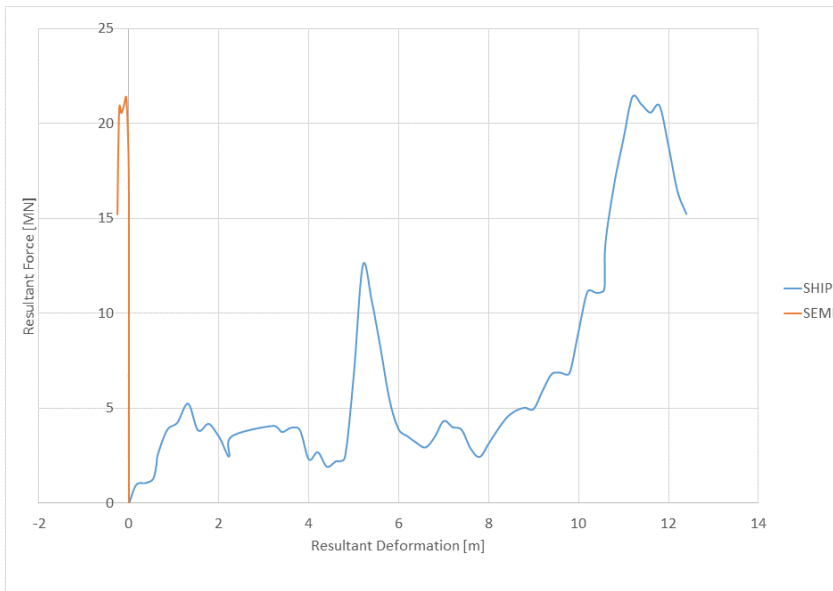


Figure 7.13: Analysis 4: Force-deformation curves.



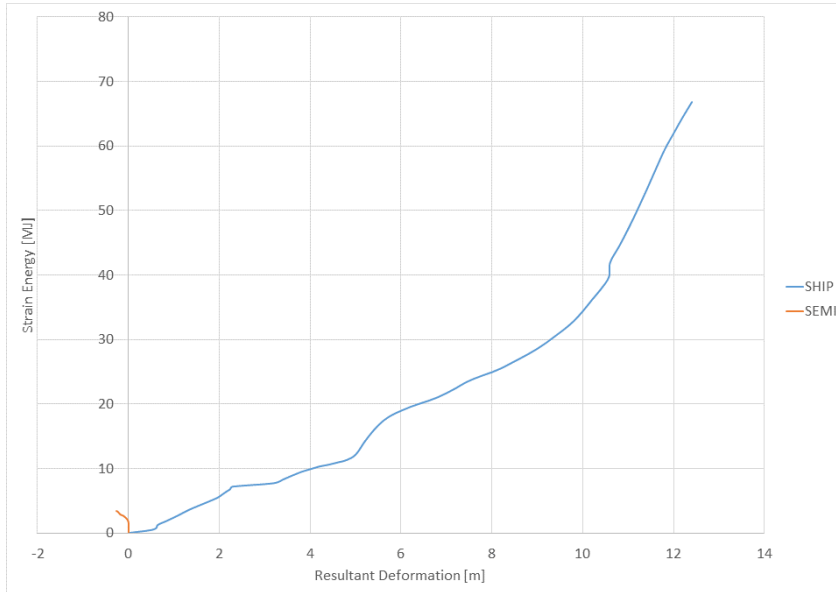


Figure 7.14: Analysis 4: Energy-deformation curves.

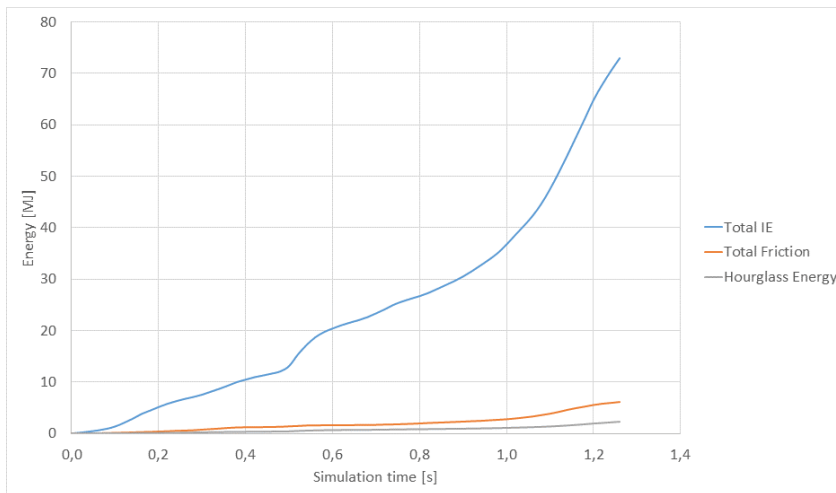


Figure 7.15: Analysis 4: Total energies throughout the collision.

Title	Direction	Velocity [m/s]	Boundary	Impact angle	Rigid / Deformable
Analysis 5	Vertical	Max 4.7	Prescribed	0°	Deformable
Analysis 6	Horizontal	10	Prescribed	0°	Deformable

Table 7.4: Analysis setup for living quarter collisions.

A prescribed displacement is applied to the hull, and the ship is positioned as far inwards as possible towards the remaining part of the platform. This leads to the ship's bridge being positioned with about 25 % of its area underneath the LQ.

For analysis 6 - horizontal impact, the ship is moved towards the lower deck of the LQ. A large wave causes a heave motion that will make the bridge be on collision course with the lower deck. This is a location where the wheelhouse supposedly is weakest.

A prescribed displacement is applied, such that the vessel moved with constant velocity towards the LQ.

### 7.3.1 Vertical Impact

In this impact scenario, the vessel acts as a rigid body, and heaves with a relatively high initial velocity, but decelerates as the wave motion reaches its apex. At a glance, it becomes quite clear that the LQ is much stiffer than the wheelhouse, and causes the wheelhouse to deform without much resistance. This was indeed expected due to the modest vertical stiffening found on the bridge deck, whereas the LQ is supported by a stiff beam lattice.

The initial contact causes moderate bending of the LQ's beam flanges in the area in direct contact with the wheelhouse, see fig. 7.19d. On the bridge, the vertical forces are mainly balanced by the beam columns which transfer the forces through the ship's decks and into the hull girder. The lightly stiffened window frames at the bridge buckle early, and are thus not able to withstand the vertical pressure.

The longitudinally stiffened wheelhouse top is not able to withstand much of the bending moment after the window frames have buckled. The light stiffeners (typ. HP160 mm x 8 mm) are no match to the LQ's heaviest beams (850 mm x 300 mm x 40 mm x 40 mm). It is therefore of no surprise to see the ship's vertical columns buckle before much damage is visible to the LQ. The ship's internal elevator- and

stairway shaft contributes somewhat to the resistance towards deformation, but also this buckle after the first few centimeters of deformation.

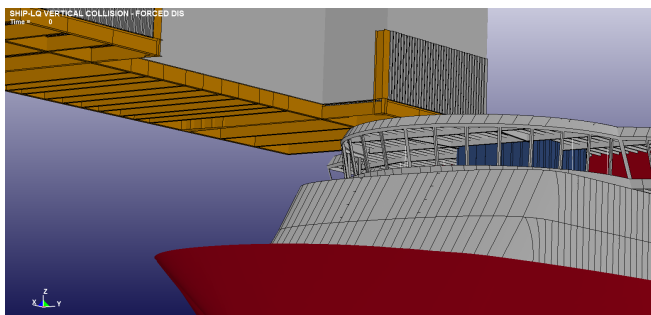


Figure 7.16: Analysis 5: Initial configuration.

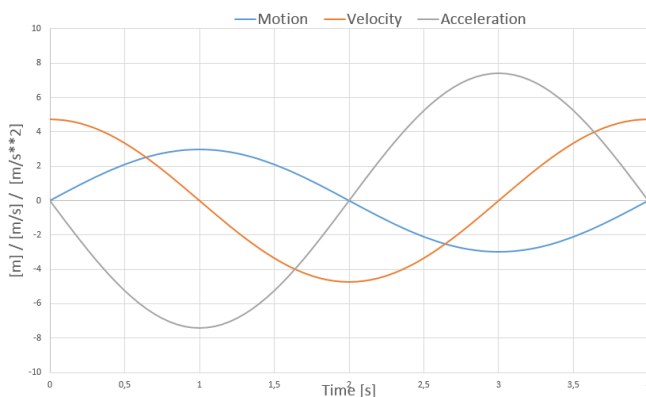


Figure 7.17: Analysis 5: The vessel's vertical displacement, velocity, and acceleration.

The initial observations are supported by examining the force-deformation relationships. A near-constant resultant force is evident with magnitude of about 6.5 MN. Nodes representing the global displacement of the two models are chosen to display the relative deformations and force/energy levels at the various parts of the impact.

By studying figures 7.20 and 7.21, it is easily discernible that the wheelhouse will indeed absorb most of the energy and deformation from the impact. It is also of interest to note that the damage is present at the bridge only, and does not spread significantly to the remaining decks.

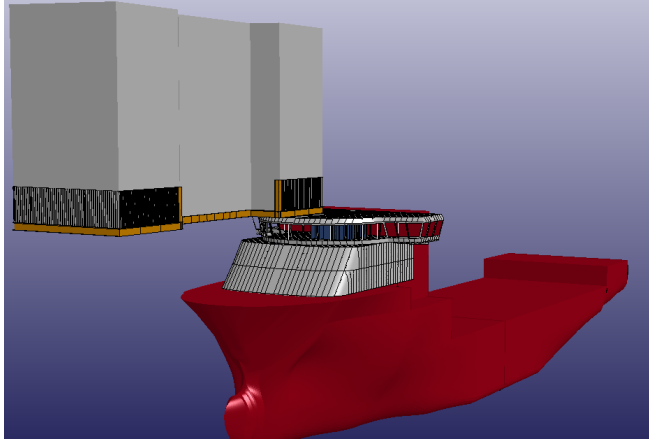


Figure 7.18: Analysis 5: Set-up for analysis of vertical living quarter collision.

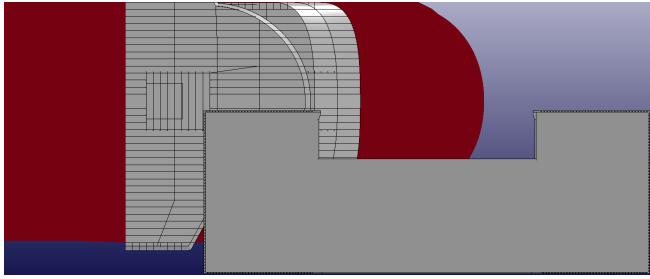
### 7.3.1.1 Repeated vertical impacts

In chapter 3, the motion characteristics of a service vessel were investigated. It was found that there is a degree of probability for significant vertical motion should the conditions be unfavourable for the ship. As discovered in the NLFEA of the corresponding load case, the crushing resistance is inferior in the wheelhouse compared to the LQ. Consequently, it would seem that additional vertical impacts would yield equal or less dissipated energy should a previously untouched area of the bridge impact the LQ. As the motion is powered by the displacement of seawater, the ship's kinetic energy will not be reduced, as might be the case in a horizontal collision. As such, continued vertical impacts pose a significant risk of doing increased damage to the ship.

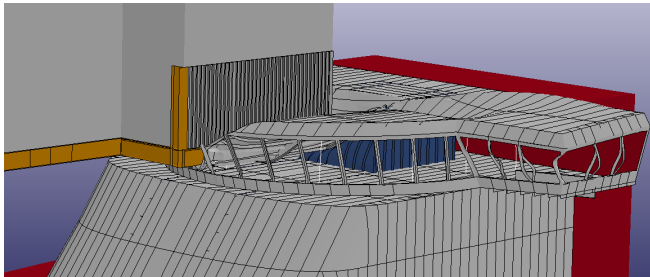
### 7.3.2 Horizontal Impact

It was expected beforehand that an impact directed towards the bridge deck would yield substantially less resistance towards deformation than what was experienced in section 7.2.2. The ship was positioned such that half the bridge would collide with the LQ, and the other half would go clear. Vertically, the lowest part of the LQ is positioned 3 meters below the wheelhouse top, 0.5 meters above the bridge deck. Prescribed displacement is utilized.

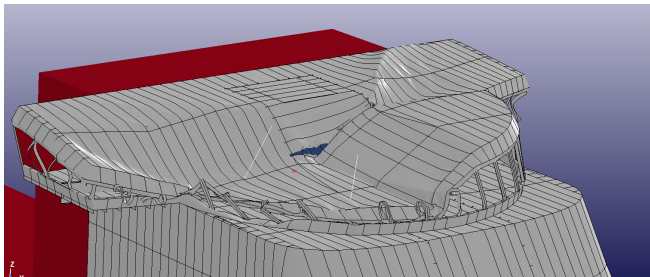
As the event unfolds, it is visible that the LQ exterior bulkheads deforms markedly before the wheelhouse in the initial stages of the collision. As the mode of load



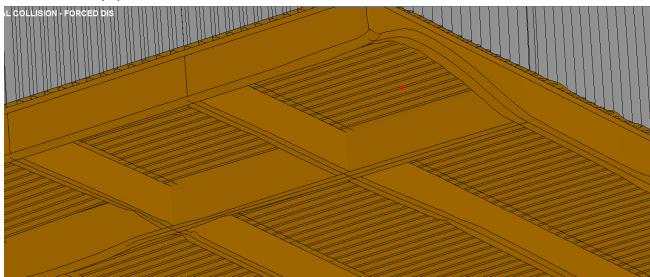
(a) Positioning of the ship prior to collision.



(b) Combined damage level after collision.



(c) Damage level wheelhouse after collision.



(d) Damage level LQ after collision.

Figure 7.19: Analysis 5: Vertical LQ impact.

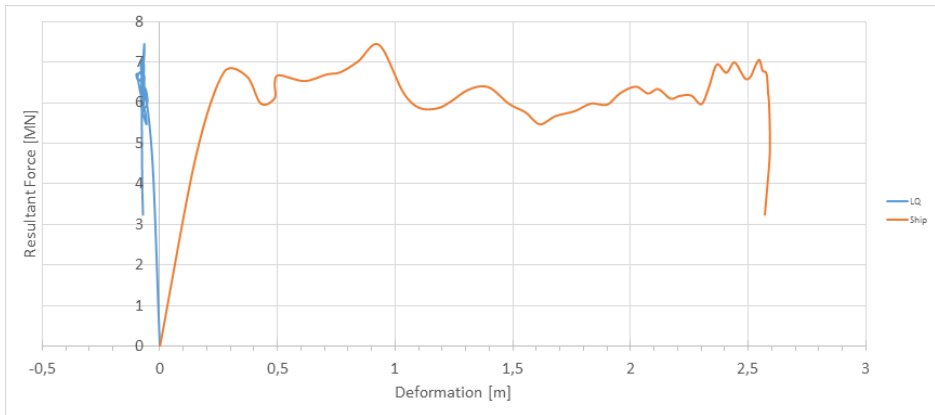


Figure 7.20: Analysis 5: Force-deformation curve.

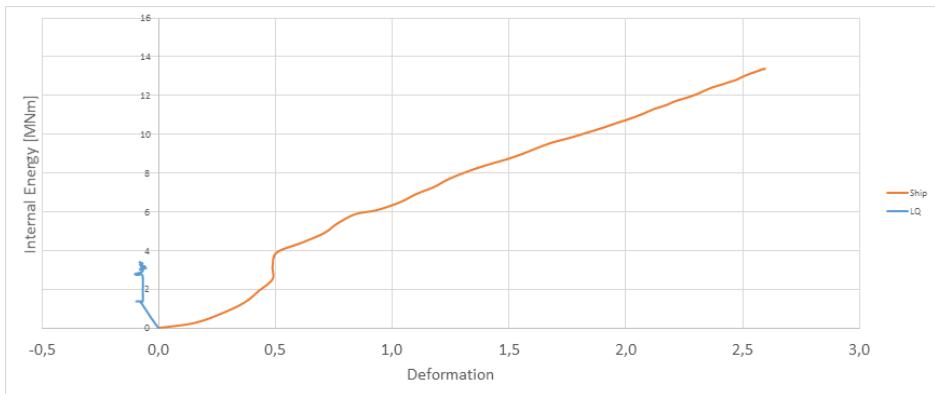


Figure 7.21: Analysis 5: Energy-deformation curve.

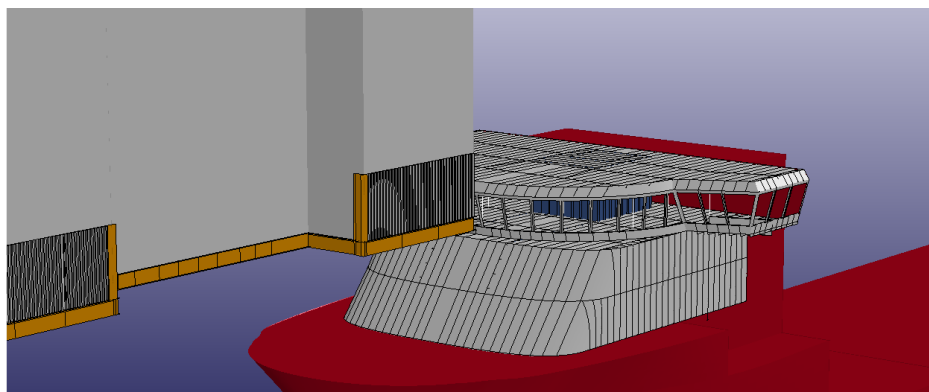


Figure 7.22: Analysis 6: Positioning of the ship prior to analysis.

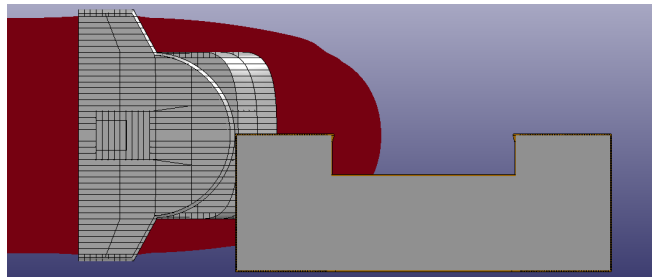
carrying changes from bending to membrane, the deformation is shifted to the wheelhouse.

Even though only half the wheelhouse top is in direct contact with the LQ, the remaining half is held back as the collision transpires. The deck is forced to fold back, causing the window frames to shear off of the deck. For the remaining part of the collision, the wheelhouse top deck buckles alternately. At the time where the bridge wings impacts, their increased stiffness leads also to the bridge deck being folded.

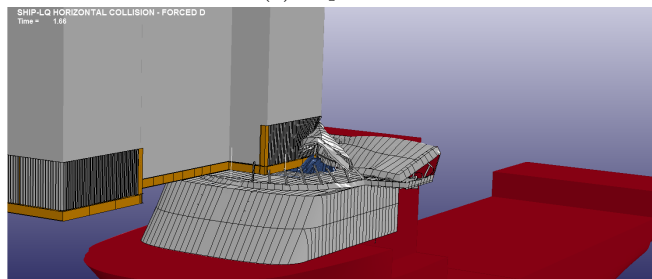
The deformation of the wheelhouse is sampled from the most protruding point of the wheelhouse top, whereas the LQ deformation is traced at the point where the maximum deformation is visible at the end of the simulation. This point is located at the southwest corner of the structure, visible at the center of figure 7.23d. As the deformations are not uniform throughout the cross section, the deformation values are indicative only.

By studying the force-deformation relationship, figure 7.24, it is seen that the resultant force and resistance to deformation varies between 3-5 MN for the better part of the collision. The initial load peak is related to the first and second buckling of the wheelhouse top deck. The resistance drops significantly after this point, similar to what is witnessed in crushing experiments done in laboratories. Between 5-6 m deformation, the resistance continues to build, related to the third buckle of the deck.

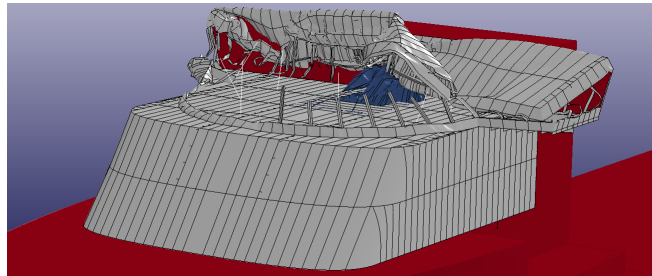
After this point, the resistance increases steadily as the contact area increases, and the main stairwell casing and bridge wings contribute to the energy dissipation.



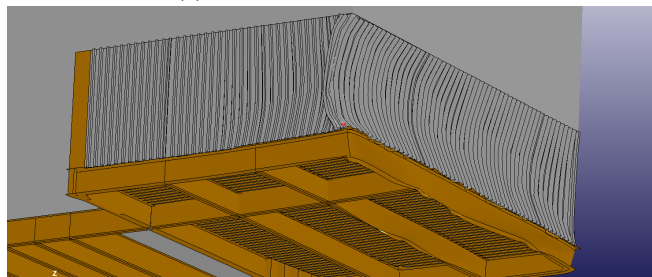
(a) Top view.



(b) Damage level after the collision. 78 MJ energy absorbed.



(c) Damage level wheelhouse.



(d) Damage level LQ.

Figure 7.23: Analysis 6: Time lapse of damage level.



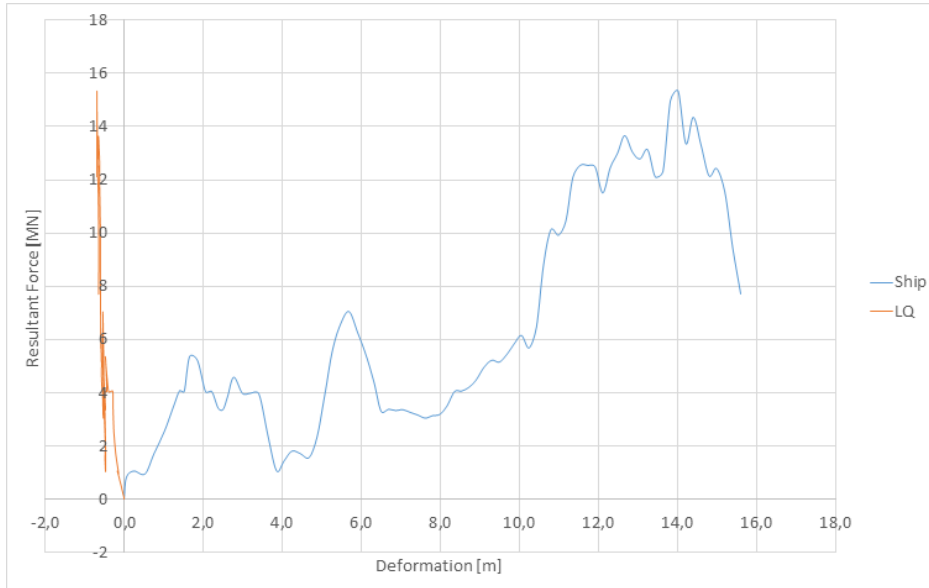


Figure 7.24: Force-deformation curve, analysis 6.

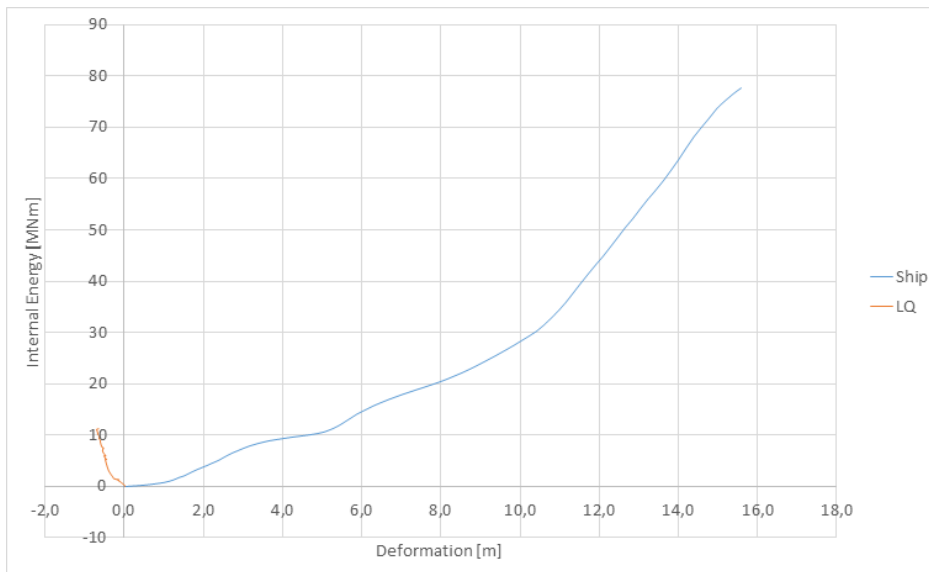


Figure 7.25: Energy-deformation curve, analysis 6.

At the analysis end, 78 MJ strain energy has been absorbed by the wheelhouse. This corresponds to the vessel colliding at 3 m/s (6 knots) and coming to a complete stop.

## 7.4 Validity of boundary conditions

### 7.4.1 Ship

The modeled ship is a well intervention vessel which frequently operates near existing or new oil field. The wheelhouse is modeled according to the supplied drawings with as few simplifications as possible.

The transverse girders supporting the C-deck (lower deck) are prevented from displacing vertically, effectively causing all vertical force components to be absorbed by the wheelhouse. The actual girders are supported by heavy pillars and bulkheads, and will most likely deflect a small amount, depending on the position of the impact. However, the low relative strength of the wheelhouse compared to the rest of the hull suggests that the approximation is of no significant importance.

Related to the global motion of the ship, there are several simplifications that may affect the response significantly. The cross terms are neglected in the global mass matrix, such that the effects of asymmetries of the hull are not included. This may be a significant factor in determining the actual resulting global response.

Further more, as all collision are "head-on" and have no impact angle, the hull is only allowed to move vertically, longitudinally, and in pitch. This is a good approximation for the semi-submersible collisions, which are symmetric. The LQ-impacts have transverse force- and moment components acting, and may introduce some error, even though the wheelhouse's resistance towards deformation is small. For the horizontal LQ impact, the transverse force peaks at the same order of magnitude as the longitudinal force component. The full effect of neglecting this part is not studied further in this thesis.

#### 7.4.1.1 The effect of neglecting vertical waterplane stiffness

The current analysis was conducted with prescribed displacement settings, meaning that the ship's rigid body hull is forced to displace, and the wheelhouse must deform in order to accommodate for the new position. Due to the nature of this particular impact, the vertical force *could* possibly result in some increased draft

of the ship's hull. It has been assumed that because a collision is typically a short event, the ship's global motions will not be affected in a large way due to the great amount of inertia involved. A change in draft could however result in reduced damage to the ship's wheelhouse if the change was large enough.

In order to assess this, some assumptions regarding the ship's shape and main particulars must be made. A common water plane area coefficient for vessels of this type is 0.79 [IHS, 2013]. The water plane area coefficient is given as:

$$C_{wl} = \frac{A_{wl}}{L_{pp} \times B} \quad (7.12)$$

Where  $A_{wl}$  is the total waterplane area and  $L_{pp}$  is the length between perpendiculars.

This leads to a total estimated waterplane area of about 2000 m<sup>2</sup>. By comparing the vertical restoring force due to change in buoyancy and the vertical force caused by the impact, a quasi-static force equilibrium may be established.

Figure 7.26 clearly displays that the waterplane stiffness is in fact slightly smaller than the resistance of the wheelhouse top for the initial centimeters of the impact. For a quasi-static load case, where the load was applied slowly, it is likely that the displacement would be more or less equally divided between an increase of draft and deformation of the wheelhouse for the first 30 cm. After this, the waterplane stiffness would dominate the equilibrium, forcing the wheelhouse top to deform.

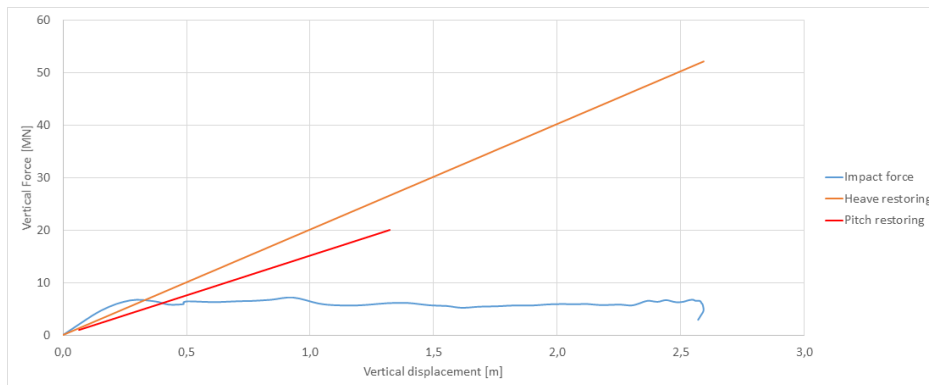


Figure 7.26: Analysis 5: Comparison between the restoring  $C_{33}$  and  $C_{55}$  vs vertical impact force.

The results thus indicate that the omission of the vertical restoring force will not introduce any significant error as long as the deformation is large.

An effect that could prove important, however, is the resulting pitch motion that might arise from such a vertical force. As the point of impact is far removed from the ship's rotational center, a large moment will be created. As described in section 7.2.3, more particularly equation 7.2.3.1, the static vertical displacement due to the vertical force can be estimated if the displacement are small. By assuming that the vessel pitches about the center of gravity, an indication of the vertical displacement is learned.

The distance from the center of impact to the center of gravity is about 34 m. This will result in a (static) displacement between 0.4 - 0.5 m using the results obtained in the analysis, assuming only the uncoupled restoring coefficient in pitch is applied, and that the ship acts as a rigid body. This could prove a significant reduction in draft, and may indeed influence the wheelhouse deformation positively.

As an impact scenario is inherently a short lived event, the draft increase would, however, most likely be limited by the inertia carried by the vessel. The full extent the moment would have on the global motion is not explored further in this thesis, but could prove to be an interesting topic to explore further in a later project.

#### 7.4.2 Semi-submersible

The modeled semi-submersible is imagined to be of the Ultra Deep-Water drilling rig. Such a vessel has a large displacement, and is therefore modeled to be fixed in space along the edges and the rear. A typical UDW drilling rig displaces between 50 000 - 60 000 metric tons (Eirik Raude, West Capricorn). When one in addition allows for 20 % added mass, the mass that must be moved approaches in excess of 70 000 metric tons. In comparison, the ship displaces about 13 500 tons, meaning that the rig is between 3.5 - 4.5 times heavier than the ship. Even though not valid in this context, utilization of conservation of momentum and assuming a perfectly inelastic collision will yield the following relationship, good for estimating the resulting velocity.

$$m_{\text{ship}}v_{\text{ship}} = (m_{\text{ship}} + m_{\text{rig}})v_{\text{rig}} \quad (7.13)$$

$$m_{\text{rig}} = \alpha m_{\text{ship}} \quad (7.14)$$

$$m_{\text{ship}}v_{\text{ship}} = m_{\text{ship}}(1 + \alpha)v_{\text{rig}} \quad (7.15)$$

$$v_{\text{rig}} = \frac{v_{\text{ship}}}{1 + \alpha} \quad (7.16)$$

Where  $m$  is the mass of the body,  $v$  is the velocity, and  $\alpha$  is the mass-ratio of the two bodies. For a ship colliding at 5 m/s with a body 4.5 times it's own mass, the resulting velocity would be 0.9 m/s. This does however demand that no energy is lost during the event, which is by no means the case in a marine collision. Hydrodynamic damping, friction, anchor chains' restoring, etc. play large roles in maintaining the energy balance, and will most certainly reduce the velocity and acceleration.

The resulting velocity is nevertheless quite high. To establish the severity of the accelerations, and consequent velocities and displacements involved in the process, me may, assuming the accelerations are low, do quasi-static assessments of the resulting translation of the semi-submersible.

By utilizing the contact forces obtained in analysis 1, section 7.2.1, the resulting acceleration is computed by Newton's 2<sup>nd</sup> law. The resulting velocity and subsequent displacement is thus calculated by integrating the accelerations.

$$a_{\text{rig}}(t) = \frac{F_{\text{ship}}(t)}{m_{\text{rig}}} \quad (7.17)$$

$$v(t) = \int a_{\text{rig}}(t)dt \quad (7.18)$$

$$x(t) = \int v_{\text{rig}}(t)dt \quad (7.19)$$

By comparing the resulting curves for acceleration, velocity, and displacement with those of the ship, the relative importance of the motion of the rig can be gauged.

As the contact force steadily increases, so does the rig's response. During the initial second of the collision, the rig will have an acceleration of up 0.6 m/s<sup>2</sup>, a velocity of 0.4 m/s, and will have moved 0.2 m. This is an order of magnitude less than the motion of the ship, and can thus be neglected without introducing any significant error. It should also be noted that the opposite acting hydrodynamic damping force (proportional to the velocity squared), is not accounted for, and

will further reduce the acceleration, velocity, and displacement of the rig. The resulting motion of the semi submersible is thus believed to not play a significant part in determining the damage to the ship, but the effect could possibly be included in later simulations.

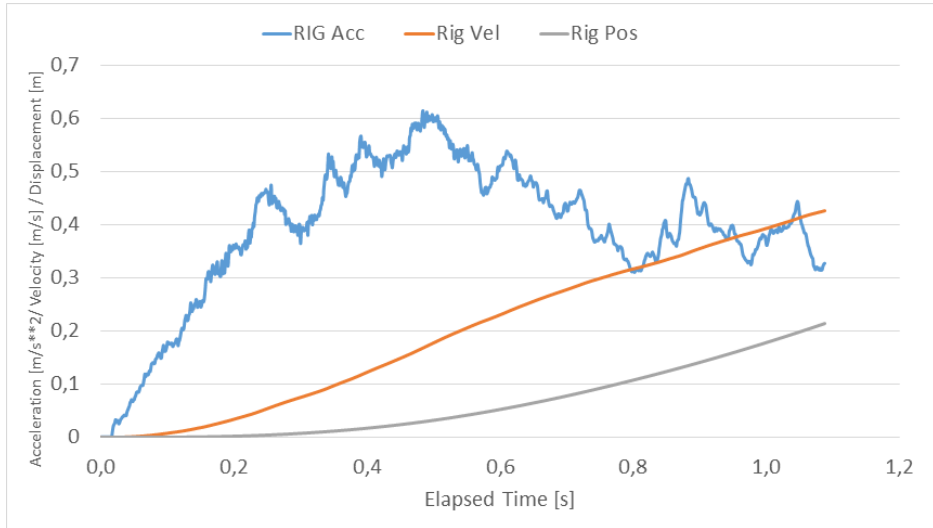


Figure 7.27: The calculated resulting acceleration, velocity, and displacement of the semi-submersible during the impact.

### 7.4.3 Living quarter

The living quarter is only partly modeled in detail, and this may prove to affect the validity of the final results. The fact that the applied material models lack a fracture criterion may create more robust structure than what is actually the case. This is particularly true for the horizontal impact scenario, where high strain and stress levels are observed.

The structure apart from the 1<sup>st</sup> deck is modeled as rigid. The assumption behind this is that the LQ is heavy enough to withstand the vertical force that it is subjected to. It also implies that the 2<sup>nd</sup> deck is stiff enough not to be deflected vertically during the impact. Due to the fact that the aluminium panels used to model the exterior bulkheads are relatively weak in bending, yet strong in membrane action, and that the beam lattice the LQ rests atop, the rigid boundary condition is believed to be good.

After having studied the vertical impact scenario, it is clear that the most severe damage occurs locally at some beam flanges and webs, and is not transferred further in any significant way. The maximum stresses and strain are well within the elastoplastic regime of aluminium, cf. figures B.1, B.2. The LQ is relatively lightweight, and thus may be subject to uplift if the vertical force is large enough. The mean vertical force is 6 MN (600 tons), while the mass of the LQ is just in excess of 1500 tons. From a purely quasi-static point of view, uplift should therefore not be possible. The rigid material boundary condition thus appears to be a good approximation to the real world problem.

The horizontal impact scenario, on the other hand, may experience a different outcome if a fracture criterion model was to be utilized. Screenshots of the stresses and plastic strains at different strain levels are found in appendix B. Relatively high stress-strain levels are found throughout the structure, related to the bending of flanges, which is not of importance. At some locations on the exterior bulkheads, strain levels high enough to warrant further investigation are identified. Several of these are no doubt related to local denting of the web and flange, which should not be considered critical. Strain levels in the bulkhead plate itself are in certain areas identified as very close to 10-15 %, which is near or at the ultimate strength at rupture,  $\varepsilon_t$ , cf. table 5.2. A crack would most likely propagate very quickly, possibly causing significantly increased damage to the LQ. The omission of the weld HAZ will further weaken the structure, making the appearance of a crack even more likely.

As the reserve strength of the tie-backs and vertical supports keeping the LQ in place is unknown, this could possibly compromise the integrity of the LQ. Leirivk Module Technology [2003] says that the LQ is demonstrated to stay in position with one tie-back removed while subject to one-year storm conditions and accelerations. These conditions are: horizontal acceleration  $0.8 \text{ m/s}^2$ , and vertical acceleration  $0.18 \text{ m/s}^2$ . By Newton's 2<sup>nd</sup> law, this yields a total force of 1.27 MN, well below the recorded contact forces in a collision. The implications of this is not certain, as the total capacity of the tie-backs are unknown. However, the findings are very interesting, and the implications should be investigated further. The full extent of a LQ impact could possibly be a topic for a master thesis in itself.

## 7.5 Comparison of results

### 7.5.1 Pressure-area relationships

Based on the contact forces and the reference contact area yielded by the LS-DYNA analysis, pressure-area relationships were established for the wheelhouse. Curves were made on background of the combined data gathered from the horizontal LQ and semi in survival draft condition, and from the ship vs rigid plate and ship vs deformable semi collision.

The contact areas and pressures are sampled at even intervals during the collision in order to collect data points. Power-law relationships were established by curve-fitting the results, visible in figures 7.28 and 7.29.

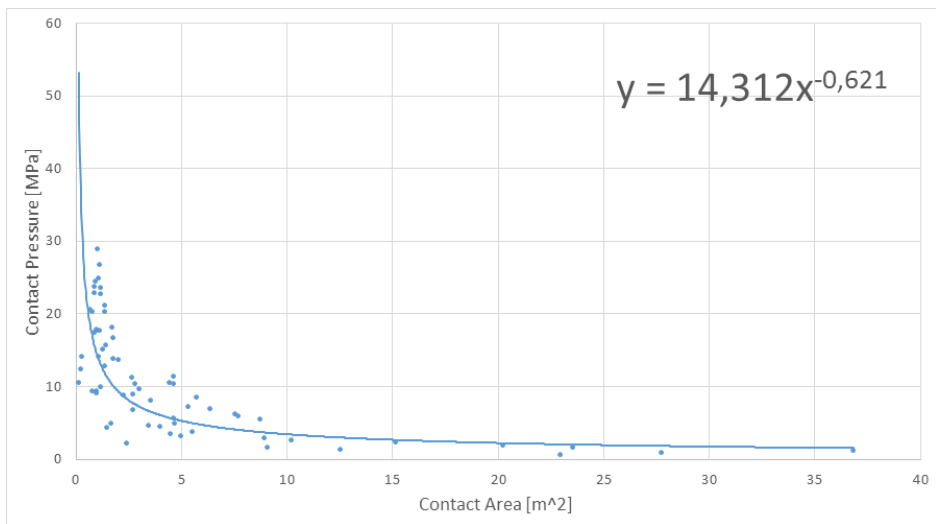


Figure 7.28: Pressure-area relationship based on low wheelhouse impact.

The following relationship was found to fit for the observed values in figure 7.28

$$p = 5.0381A^{-0.345} \quad (7.20)$$

For the low wheelhouse cases, the following equation was found to be a good fit to the data in figure 7.29 well:

$$p = 14.312A^{-0.621} \quad (7.21)$$



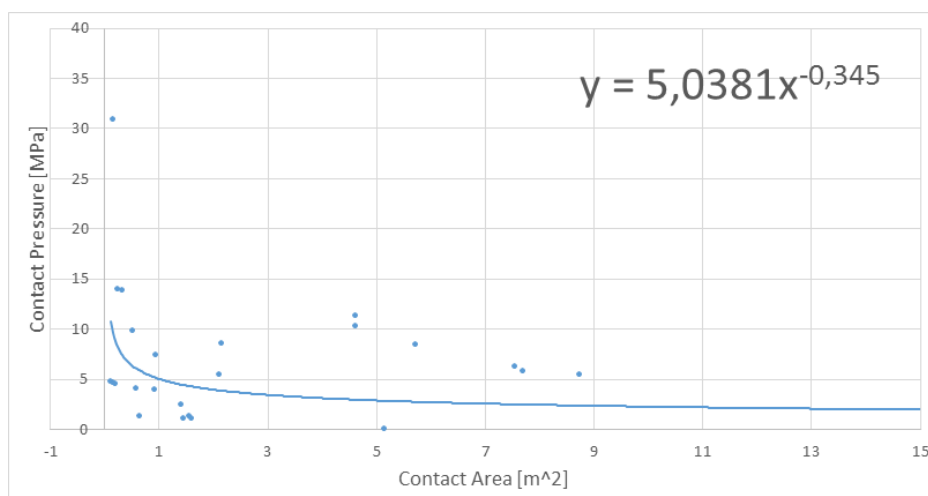


Figure 7.29: Pressure-area relationship based on high wheelhouse impact.

Where  $p$  is the contact pressure in MPa and  $A$  is the contact area of the surface in  $m^2$ . The relationships can be of practical use for design purposes.

## 7.5.2 Semi-submersible collisions

For the low superstructure impacts, the load histories are very similar (figure 7.30). Even though the collision takes place at the same vertical distance, the force level in the rigid plate collision reaches a plateau earlier than the deformable semi collision. The average force for the deformable semi collision is thus substantially higher. A reason for the increase in total force could be that due to the warping of the semi, a larger area is in contact with the ship, without actually reducing the contact pressure.

The increased contact force naturally creates a steeper incline of the strain energy curve, such that there is a slightly discernible difference between the two load cases (figure 7.31). A larger difference in friction- and hourglass energy is also noted for the deformable semi, believed to also be the result of the warping of the semi, creating a larger contact surface.

Storheim [2008] did analyses in LS-DYNA regarding the crushing of very large oil tanker bows. Tanker vessels are generally much more stiff than a corresponding wheelhouse structure, with scantlings easily twice what is applied to the model

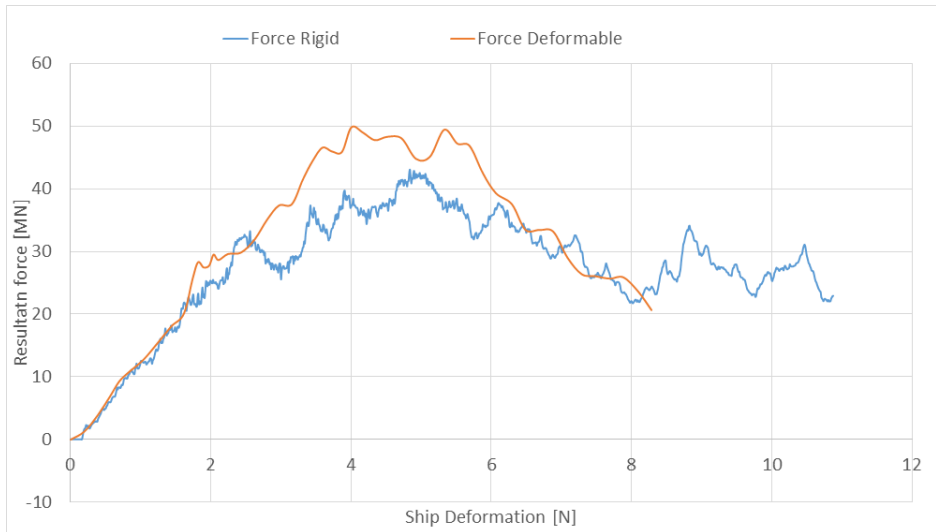


Figure 7.30: Comparison of the resultant contact force found in analysis 1 & 2.

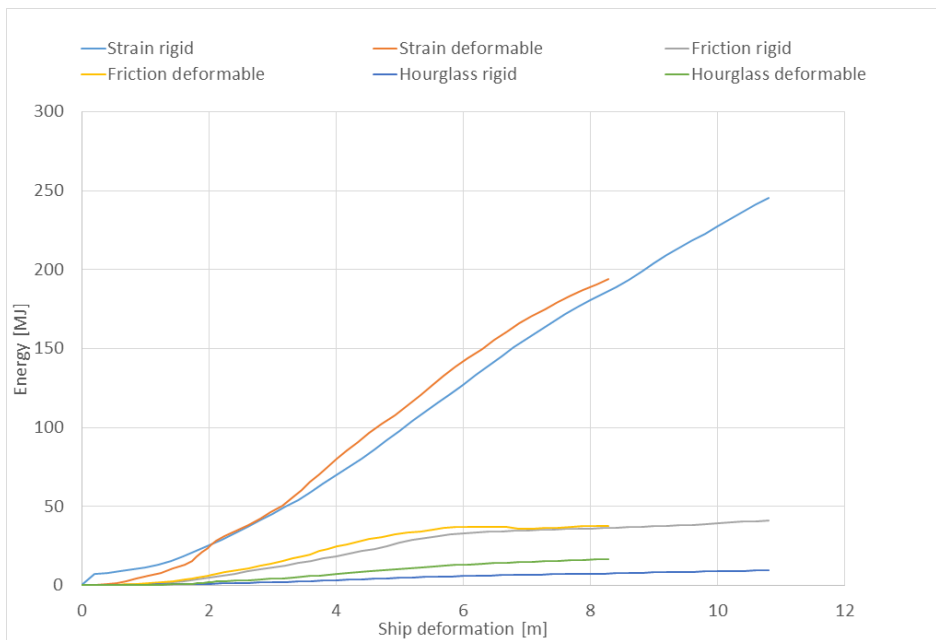


Figure 7.31: Comparison of the computed energies found in analysis 1 & 2.

presented in this project. In his thesis, Storheim presents force-deformation and energy-deformation curves that had maximum values of the order 100-200 MN and 500-1000 MJ, much greater than what is found in this thesis.

Pettersen [2008] did collision analyses with ice-stiffened supply vessel bows, and found resulting forces in the range 40-80 MN, as well as total energies up to 250 MJ for the total collision. It is natural to assume that both the force and energy levels in such collisions will be substantially higher than in a wheelhouse collision, as the structures are significantly stiffer.

The contact area in the semi-submersible collision is however quite large compared to that of a supply vessel bow, which might account for the relatively high contact force, despite not necessarily achieving equally high contact pressures. The results are nevertheless in the range of similar collision analyses, and can therefore be considered as reasonable.

### 7.5.3 Living quarter collision

Both the vertical and horizontal collision achieve similar peak force and deformation, even though the load carrying modes are dissimilar. The vertical collision has a large contact area while being a relatively weak mode, while the horizontal mode is stronger in crushing, yet has a smaller contact area.

The response histories of the two collisions vary, however. The horizontal collision is more similar to the semi-submersible collisions, where a near-linear load-deformations relationship is evident before the deck buckles, and the resistance plummets. The vertical force-deformation curve has a similar linear initialization, but reaches a plateau at  $\sim 6$  MN due to the formation of a plastic mechanism in the wheelhouse top deck and stiffeners. This mechanism acts as a hinge and limits the maximum force to the plastic capacity of the cross section.

The load history of the horizontal LQ impact also share quite a few characteristics with the collision in survival draft, even though the contact area is only half of what was used in analysis 4.

In figures 7.32 and 7.33, the results for analyses 4 & 6 are compared. The resultant contact forces are more or less identical in magnitude for the two load cases, aside from the load peaks attributed to buckling of the wheelhouse top deck, which is nearly double in magnitude. This shows that the damage level and crushing resistance is not particularly dependent of contact area in this section of the ship, as the structure in any case is so flexible that the deformation will not be contained to the impact area.

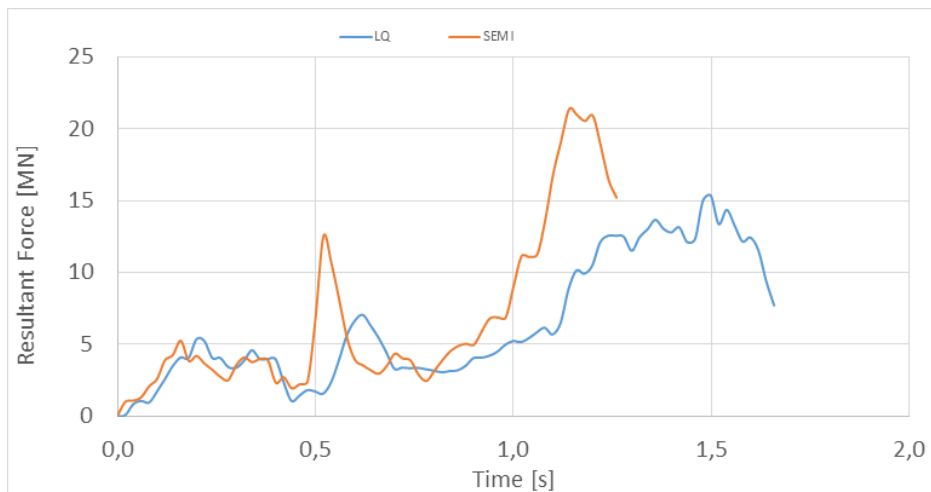


Figure 7.32: Comparison of the resultant force found in analysis 4 & 6.

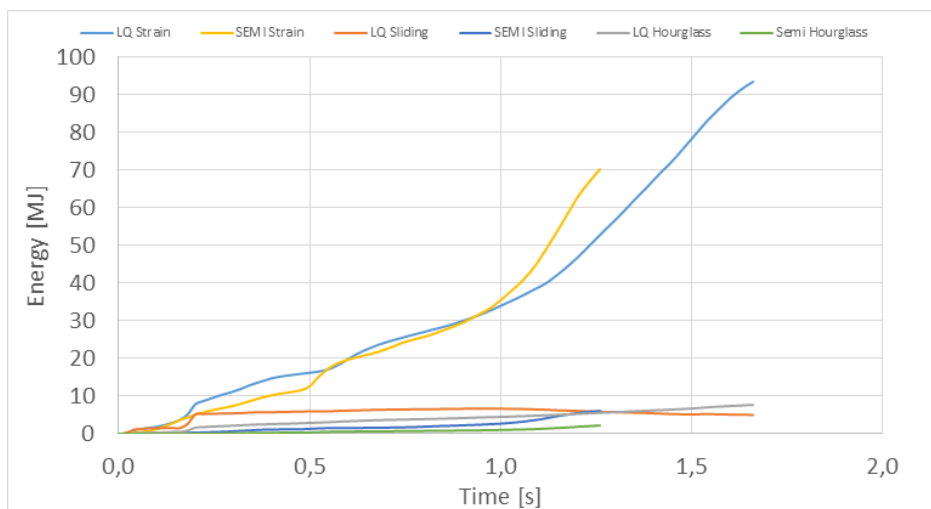


Figure 7.33: Comparison of the total computed energies found in analysis 4 & 6.

# Chapter 8

## Conclusion

Several analysis load cases have been run during the spring semester with a variety of settings and boundary conditions. The goal has been to investigate the crushing resistance of the wheelhouse and superstructure of a large service vessel subject to a collision with a large semi-submersible, and the living quarter of a jacket platform.

As not much data about wheelhouse collision is available to the author, it is hard to absolutely validate the results obtained from these analyses. It can be verified that the results are in the same order of magnitude as those reported by authors having conducted analyses of crushing of bows and ship sides, but other than that there has been little research done on the particular field.

The rules given in Norsk Standard [2012c] states that the design Accidental Limit State collision should be at 2 m/s, or approximately 4 knots, if no higher velocity has been determined based on risk analysis procedures. The vessel should not be any less than 5000 tons. This corresponds to a total collision energy of 10 MJ.

In the study of previous collisions in Chapter 2, it was uncovered that actual collision energies can be far in excess of that stated in the codes, ranging from 20-70 MJ. This shows that the design codes are actually not particularly conservative when it comes to ALS collision criteria. This should be kept in mind if risk evaluations require that collision analyses are made.

Results from this master thesis indicate that even though the superstructure is lightly stiffened, it *will* have significant crushing resistance if the collision is located near the forecastle deck, and thus involves a large part of the wheelhouse

in the deformations. The bridge itself however, does not show any significant strength due to the lack of stiffening, and will easily deform great amounts even at low velocities.

Collision Energy	10	50	100	[MJ]
Velocity	1.1	2.5	3.5	[m/s]
Rigid Plate	0.8	3.2	5.2	[m]
Deformable	1.3	2.4	4.7	[m]
Survival	4.0	11.2	-	[m]
Vertical	1.8	-	-	[m]
Horizontal	4.7	12.7	-	[m]

Table 8.1: Expected deformations vs. kinetic energies for various velocities.

Normal service speeds for service vessels is in the vicinity of 14 knots (7.2 m/s), meaning that a direct impact at this velocity would be completely devastating to the ship's bridge. An impact to the remaining superstructure would have dire consequences, particularly if the struck areas were to include crews' cabins or recreational areas. An impact to the ship's bridge could not necessarily just mean that the structure itself is damaged. Aside from crew fatalities, the manoeuvring consoles might be damaged beyond repair. In such a case, it would be highly difficult to manoeuvre the vessel away from the point of impact, possibly causing secondary damages to production risers, drilling equipment, or the platform itself.

Visible in the first three analyses is the fact that the ship superstructure will absorb the majority of the energy, whereas the semi-submersible is much more stiff, and will not deform in the same degree as the ship.

In analysis 2, the semi accounted for only 15% of the total absorbed strain energy (38 MJ), whereas in analysis 4 it was even less: only 5% of the total strain energy (3.4 MJ). In all the cases, only light to moderate damage is visible on the semi, while the ship is catastrophically damaged.

After having studied the obtained deformations, energies, and forces for the low semi collisions, it is clear that even though the recorded contact force is greater when the semi is regarded as deformable, the difference in absorbed strain energy for the ship is not great, cf. figure 7.31. Indeed, for the survival draft collision, the ship sees the semi as rigid for all practical purposes.

As such, it is a good and slightly conservative assumption to utilize strength design in the ship vs. semi-submersible collisions investigated herein.

For the horizontal living quarter impact, it is harder to draw a definitive conclusion. Even though the energy balance is heavily dominated by the ship's strain energy, the uncertain failure mode of the extruded aluminium panels is a factor that could affect the structural integrity LQ negatively. A more detailed material model should be utilized in order to determine the results accurately.

For the vertical living quarter collision, the resultant force quickly reaches a plateau as a plastic hinge appears in the wheelhouse top deck. Some local deformation is observed in the beam lattice supporting the LQ, thus little strain energy is absorbed. While no control analysis was conducted by crushing the ship vertically towards a rigid plate, the results suggest that strength design could be a good assumption for vertical impacts of small to moderate magnitude.

The following has been completed in this master thesis:

**Previous ship collisions** have been investigated in order to obtain realistic boundary conditions and reference collision energies. Several collision scenarios have been created based on these.

**Simple motion analysis- and statistics** have been calculated in order to estimate a likely vertical motion response for a ship in operating conditions.

**General design principles and collision mechanics** are briefly discussed. Some design rules are evaluated.

**Theory of NLFEA** is discussed. Various solution techniques are described in detail. Key details of LS-DYNA theory and functionality is touched upon. Theory behind material models used in the analyses is treated, as well as an overview of the finite element formulations used.

**A ship model** is created. The ship's superstructure is modeled in detail, while the hull included as a rigid shell. The superstructure is lightly stiffened, but proves tougher than anticipated when a large part of it is included in the collision. The ship's bridge has negligible strength.

**A semi-submersible rig model** is created. The rig is designed as an equivalent beam girder with scantlings comparable to a real-world ultra deep-water rig. The rig proved to be much tougher than the ship, and sustained only mild to moderate damage.

**A jacket living quarter model** is created. The model is based on the Kvitebjørn jacket, and is made of extruded aluminium profiles resting atop a heavy beam lattice. The LQ proved to be

**Reference models and their discretization** is treated in detail. This part deals with the assumptions upon which the models are created, and the

boundary conditions that are applied. Methods of applying symmetry conditions, ship restoring and ship inertia forces have been discussed.

**Five collision cases are analyzed.** Three collision deal with semi-submersible impacts, while two are living quarter collisions. Force-deformation-, and energy-deformation curves are created for the individual analyses. The similar load cases are compared in order to investigate the effect of changing boundary conditions. The implications of the chosen boundary conditions are investigated. Pressure-Area curves are created on background of the analyzed data.

One additional semi-submersible collision dealing with global response of the ship was not completed successfully.



# Chapter 9

## Further work

**Impact angle** It should be investigated how the ship heading will affect the resultant force and response of the ship.

**Sideways impact** A drift-off situation where the ship has transverse velocity towards an object should be investigated, e.g. a living quarter.

**Boundary conditions** Due to the duration of the impact, the motion of the semi-submersible could be a significant factor in assessing the damage. The semi-submersible should be modeled with representative inertia, damping, and restoring forces in order to account for the resulting motion caused by a collision. This could possibly be coupled with CFD analyses to account for the ship-water interaction.

**The global motion response of the ship** should be investigated, and the implications this has on the crushing resistance of the hull should be assessed. There is reason to believe that a pitch and heave component of motion may further increase the damage, as well as reduce the observed sliding energy.

**Living quarter model** It was discovered during the horizontal living quarter impact that the exterior bulkheads have significant stress and strain components. A fracture criterion should be applied in order to gauge the importance of a propagating crack.

**Living quarter supports** During the horizontal impact, the LQ is subject to large shear forces. It is unknown whether the horizontal tie-backs can withstand this force. The structural implications for such an impact should be investigated.

**Global mass, damping, and stiffness matrices** Global matrices able to describe the global response of the vessel should be included, not only in pitch and heave, but also other relevant degrees of freedom. This will enable the user to attain more accurate results if the impact angle is changed.

**Simplified methods** It is uncertain whether any of the simplified methods developed for bow/hull collisions are applicable in this setting. Various simplified methods could be compared to NLFEA results in order to ascertain their validity.

**Mesh improvements** of the ship superstructure should be made. The sheer size of the database demand relatively large computational resources. Also, the time step is very dependent on the mesh warping. As is, the model is prone to stop due to severe element distortion.

**Interaction with bow and column brace** Some semi-submersible rig design have transverse braces that run near the waterline, perpendicular to the pontoons. A ship passing atop such a brace may cut through it, or slide atop. If the latter is the case, an additional heave and pitch component may influence the load history.

# References

- Hagbart Alsos. *Ship Grounding - Analysis of Ductile Fracture, Bottom Damage and Hull Girder Response*. PhD thesis, Norwegian University of Science & Technology, 2008.
- Jørgen Amdahl and Anton Stornes. Energy dissipation in aluminium, high-speed vessel during grounding and collision. In *2nd Int. Conf. on Collision and Grounding of Ships, 'ICCGS-2001', Copenhagen, 2001*, 2001.
- M Baig and K Bathe. On direct time integration in large deformation dynamic analysis. *Massachusetts Institute of Technology*, 2005.
- Knut Aaberge Dahl. Analysis of accidental iceberg impacts with lng tank carriers. Master's thesis, NTNU, 2012.
- Det Norske Veritas. DNV-RP-C204 Design Against Accidental Loads, 2012.
- Odd M. Faltinsen. *Sea Loads on Ships and Offshore Structures*. Cambridge, 1990.
- Kurt Gieck and Reiner Gieck. *Engineering Formulas*. McGraw-Hill, 2006.
- John Hallquist. *LS-DYNA Theory Manual*. Dynamore, March 2006. URL <http://www.lstc.com/products/ls-dyna>.
- IHS. Ihs sea-web - [www.sea-web.com](http://www.sea-web.com), 2013.
- Erwin Kreyzig. *Advanced Engineering Mathematics*. Wiley, 2006.
- Arne Kvitrud. Collisions between platforms and ships in norway in the period 2001-2010. *OMAE*, Vol 2:637-641, 2011.
- Carl Martin Larsen. *Kompindium i TMR4180 Marin Dynamikk*. Institutt for Marin Teknikk, 2009.
- Leirivk Module Technology. STATOIL Kvitebjørn project - EPC living quarter. Technical report, Statoil, 2003.

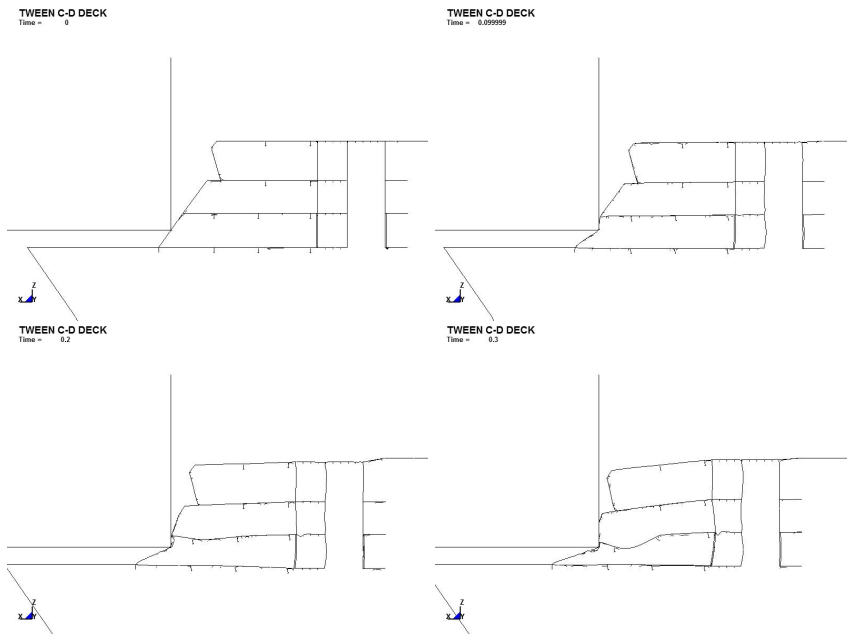
- Leirvik Module Technology. STATOIL Kvitebjørn project - EPC living quarter appendix a. Technical report, STATOIL, 2003.
- Federico Mazzolani. *Aluminium Alloy Structures*. Chapman and Hall, 1995.
- V.U. Minorsky. An analysis of ship collisions with reference to nuclear power plants. *Journal of Ship Research*, 3:1–4, 1959.
- Torgeir Moan. *Finite Element Modeling and Analysis of Marine Structures*. Institutt for Marin Teknikk, 2003.
- MSC Software Corporation. *MSC Patran User's Guide*. MSC Software Corporation, 2012.
- L. Munch-Soegaard and L. Pettersen. A study of the collision incident between West Venture and Far Symphony. Electronically, 2004. URL <http://www.ptil.no/getfile.php/z/%20Konvertert/Helse,%20milj%C3%B8%20og%20sikkerhet/Hms-Aktuelt/Dokumenter/westventurecollision.pdf>.
- Dag Myrhaug. *Stochastics Theory of Sea Loads*. Institutt for Marin Teknikk, 2005.
- Norsk Standard. NS-EN-10067 hot rolled bulb flats - dimensions and tolerances on shape, dimensions and mass, 2012a.
- Norsk Standard. Norsok N-003 Action and actions effects, 2012b.
- Norsk Standard. NORSOK N-004 design of steel structures, 2012c.
- Petroleumstilsynet. Granskningsrapport etter uønsket hendelse mellom Far Symphony og West Venture, 2004.
- Petroleumstilsynet. Granskningsrapport etter uønsket hendelse mellom Ocean Carrier og Ekofisk gangbro, 2005.
- Petroleumstilsynet. Investigation of Big Orange XVIIIs collision with Ekofisk 2/4-W 8.6.2009. Technical report, Petroleum Safety Authority Norway, 2009.
- T. Pettersen. Bow collision analysis of the Ulstein PX105 supply vessel. Master's thesis, Norwegian University of Science and Technology, 2008.
- Martin Storheim. Analysis of structural damage of tankers subjected to collision. Master's thesis, Norwegian University of Science and Technology, June 2008.
- Jan Børge Sætre. Analysis of a ship wheelhouse collision - project thesis, 2012.
- StruProg. *StruProg Theory Verification Manual*, 2012.

Y. Yamada and P. Pedersen. A benchmark study of procedures for analysis of axial crushing of bulbous bows. *Journal of Marine Structures*, 21:257–293, 2008.

# Appendix A

## Cutplanes

### A.1 Cutplanes analysis 1 - Ship vs rigid plate



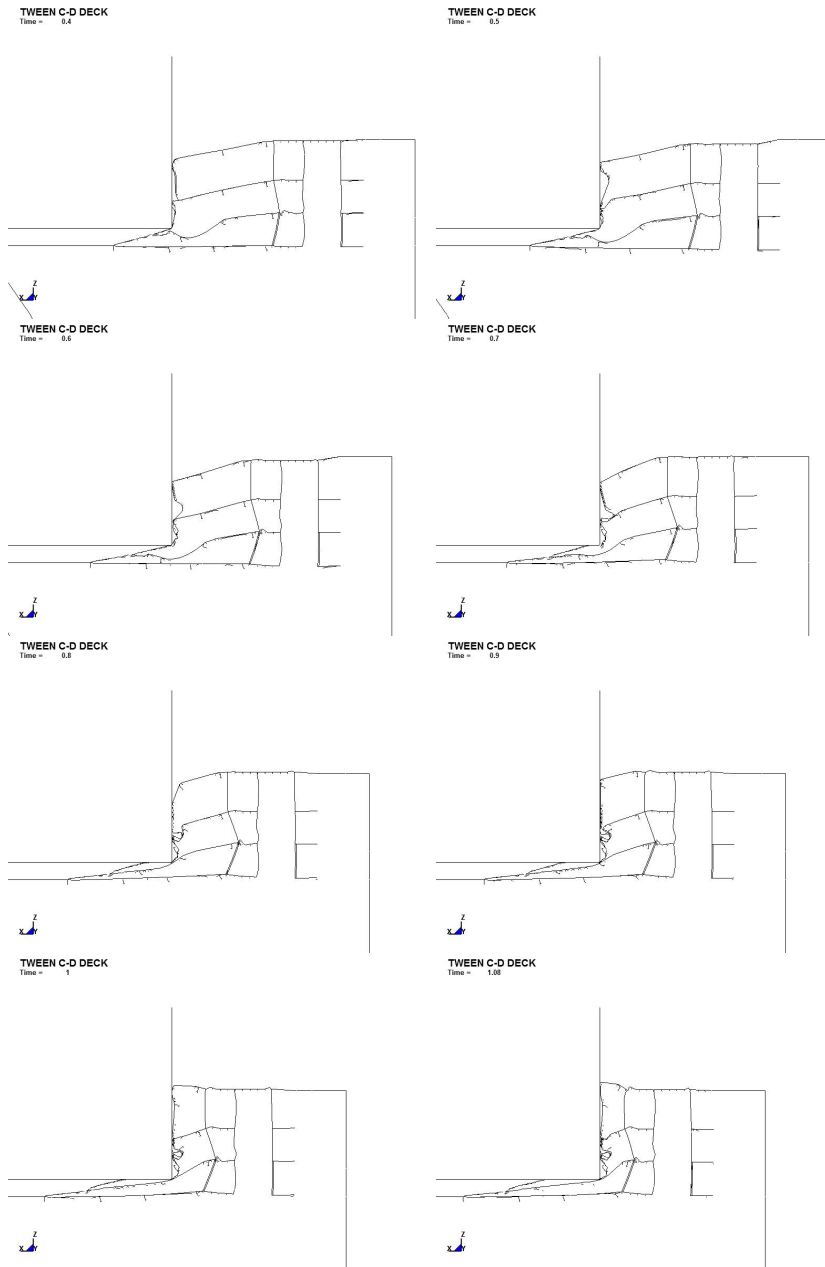
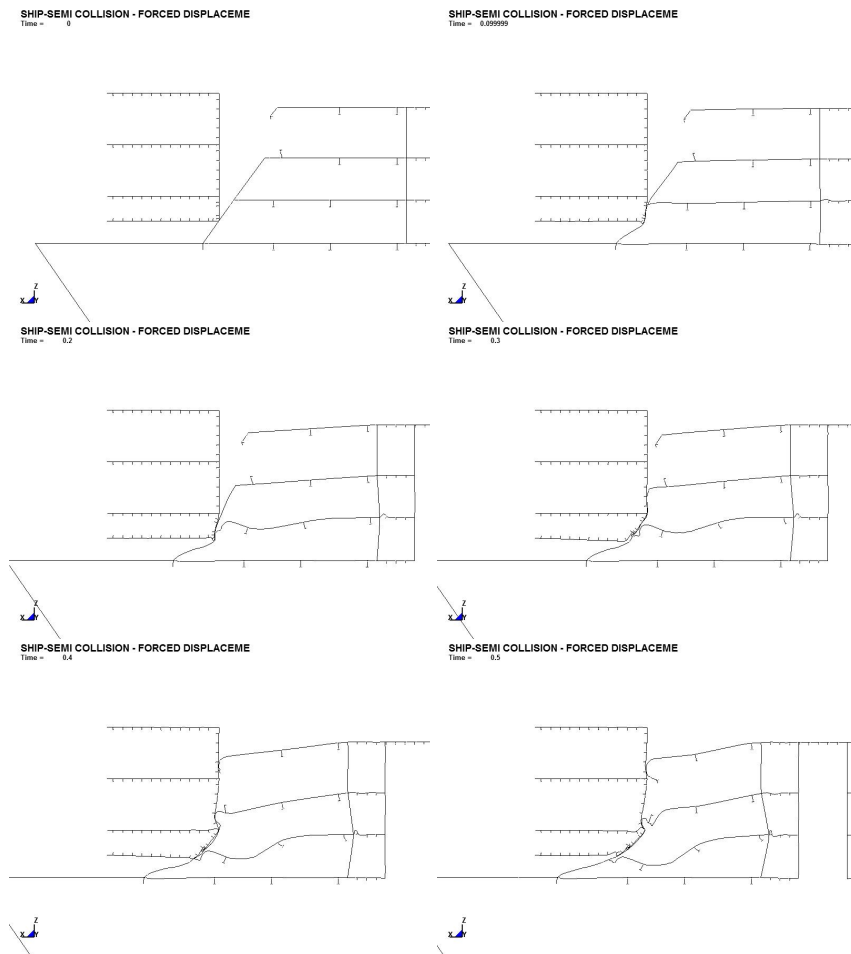


Figure A.1: Cutplanes for analysis 1 - Ship vs rigid plate.

## A.2 Cutplanes analysis 2 - Ship vs deformable semi, fixed





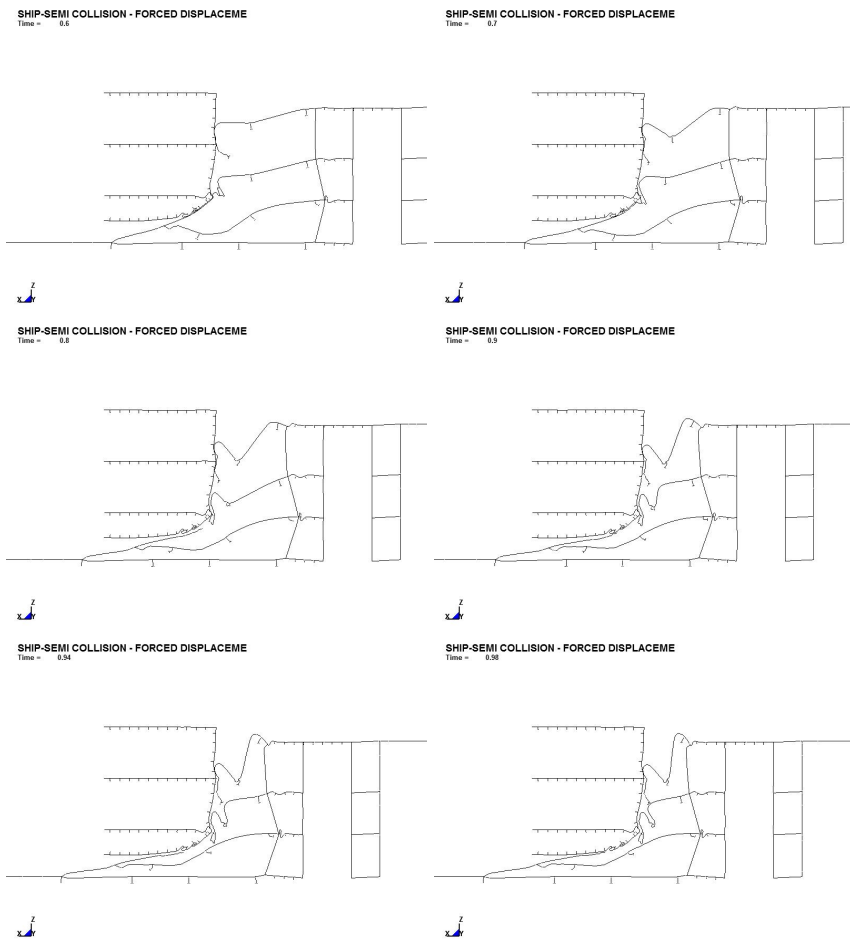
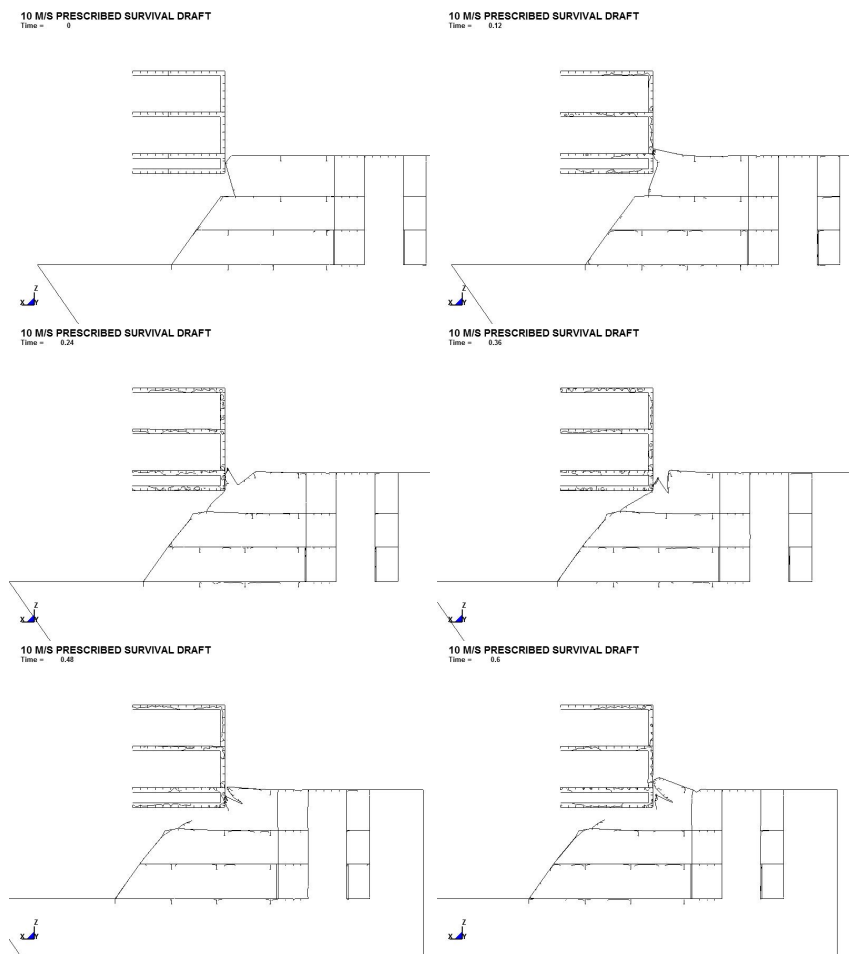


Figure A.2: Cutplanes for analysis 2 - Ship vs deformable semi.

## A.3 Cutplanes analysis 4 - Ship vs deformable semi, survival draft



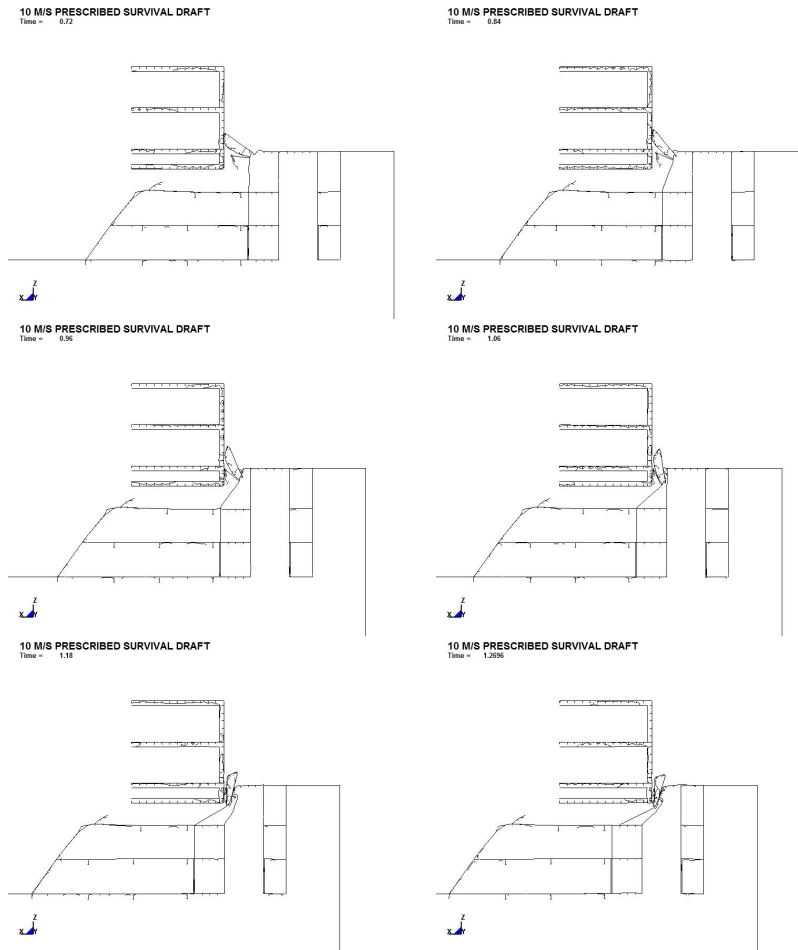
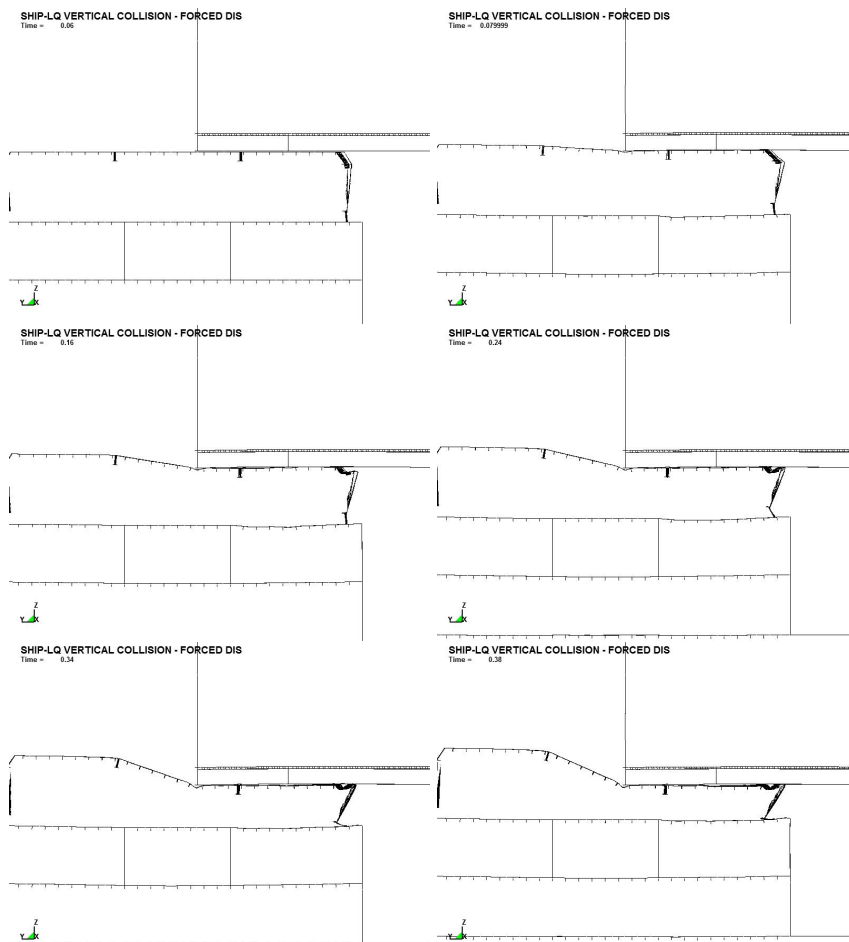


Figure A.3: Cutplanes for analysis 4 - Ship vs semi in survival draft.

## A.4 Cutplanes analysis 5 - Ship vs LQ, vertical



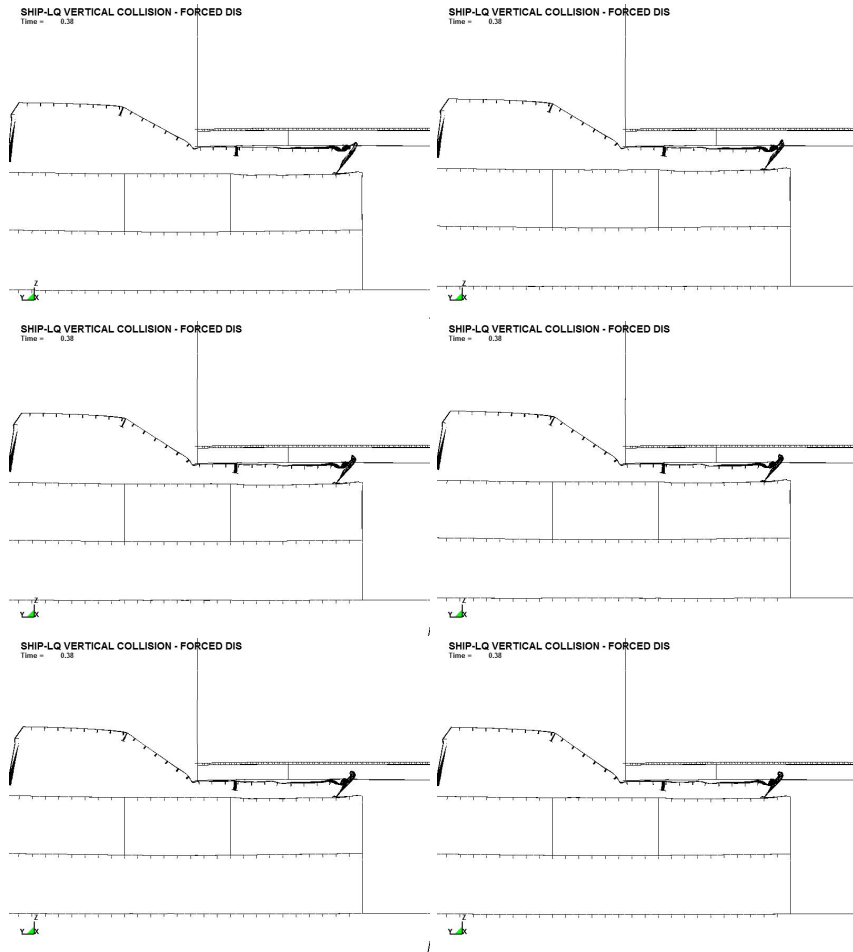
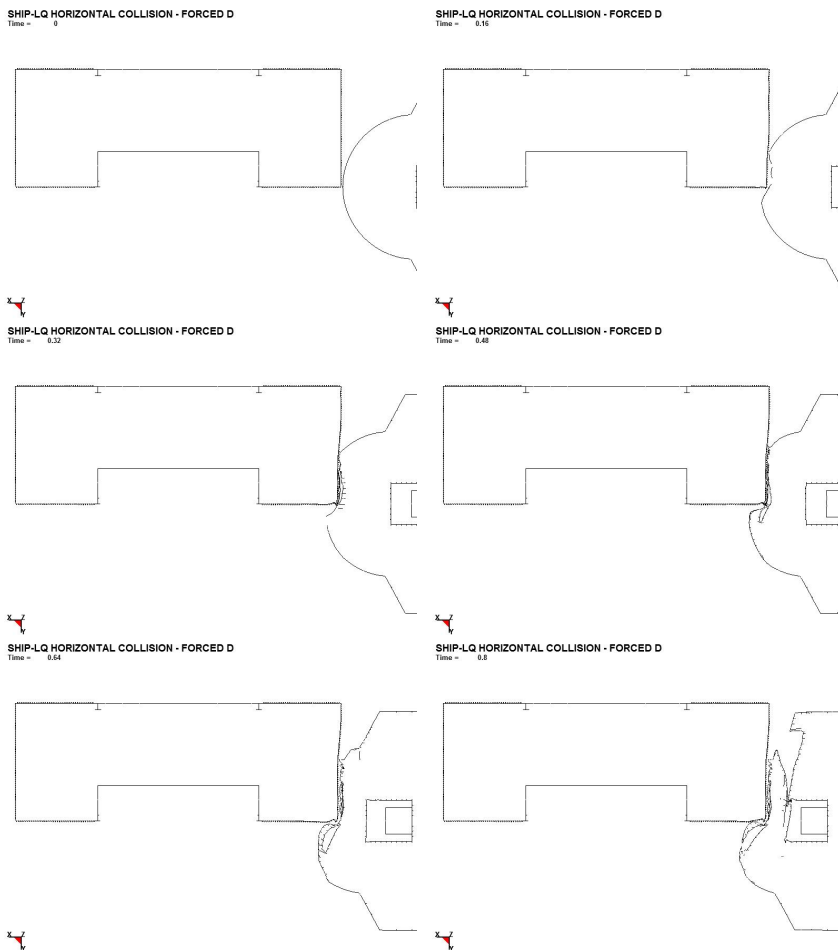


Figure A.4: Cutplanes for analysis 5 - Vertical LQ impact.

## A.5 Cutplanes analysis 6 - Ship vs LQ, horizontal



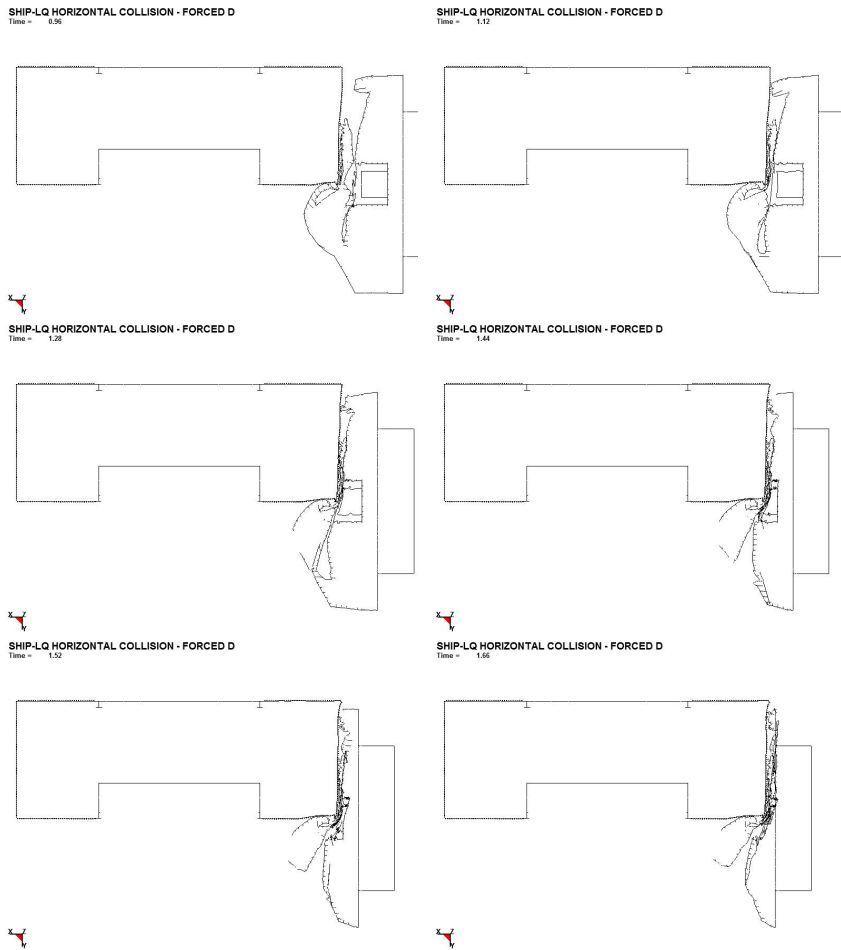


Figure A.5: Cutplanes for analysis 6 - Horizontal LQ impact.

# Appendix B

## Living Quarter $\sigma - \varepsilon$ contours.

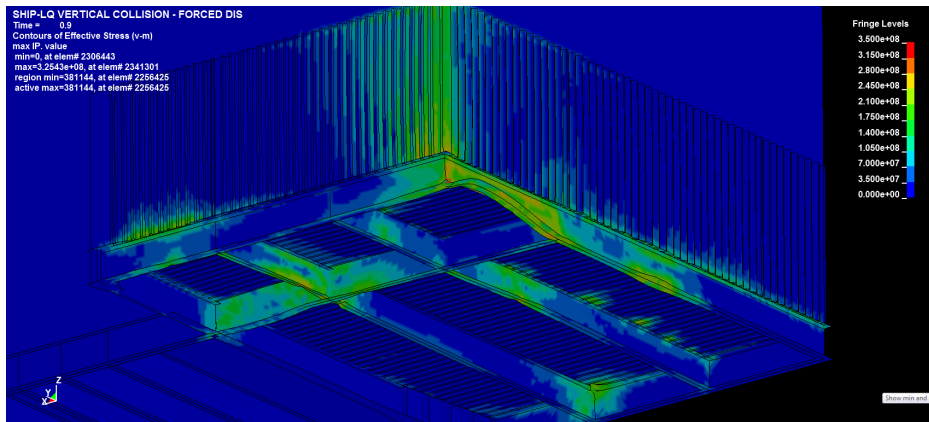


Figure B.1: Von Mises stress contours LQ, vertical collision.



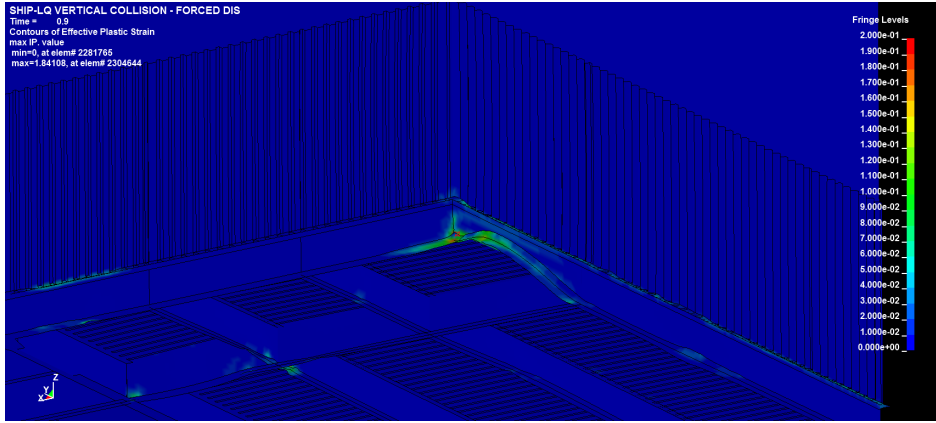


Figure B.2: Plastic strain contours LQ, vertical collision

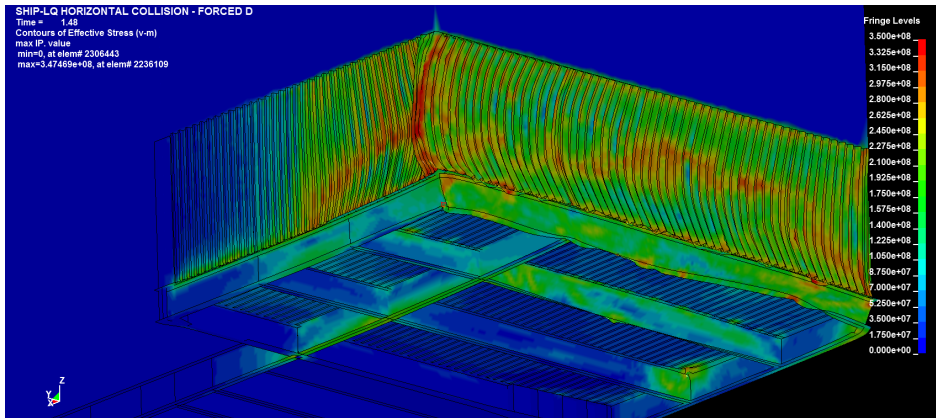


Figure B.3: Von Mises stress contours LQ, horizontal collision.

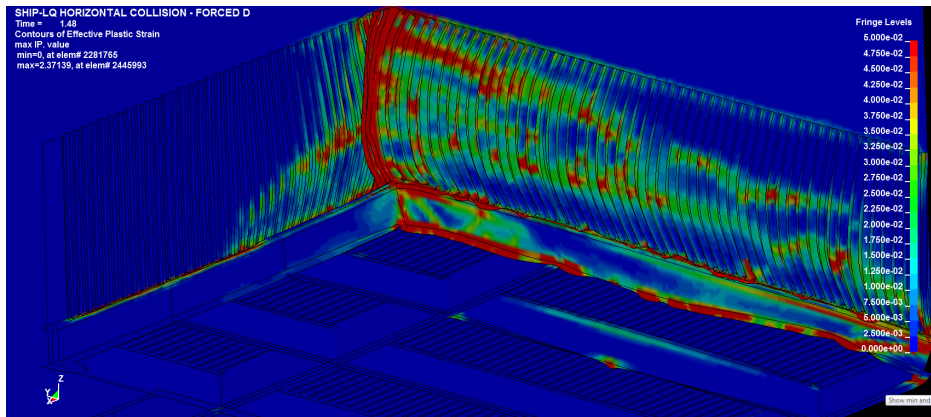


Figure B.4: Plastic strain contours LQ 5% level, horizontal collision

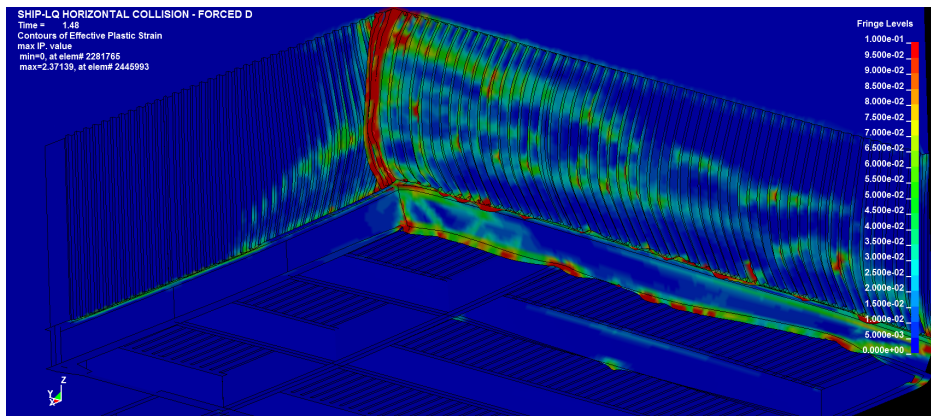


Figure B.5: Plastic strain contours LQ 10% level, horizontal collision

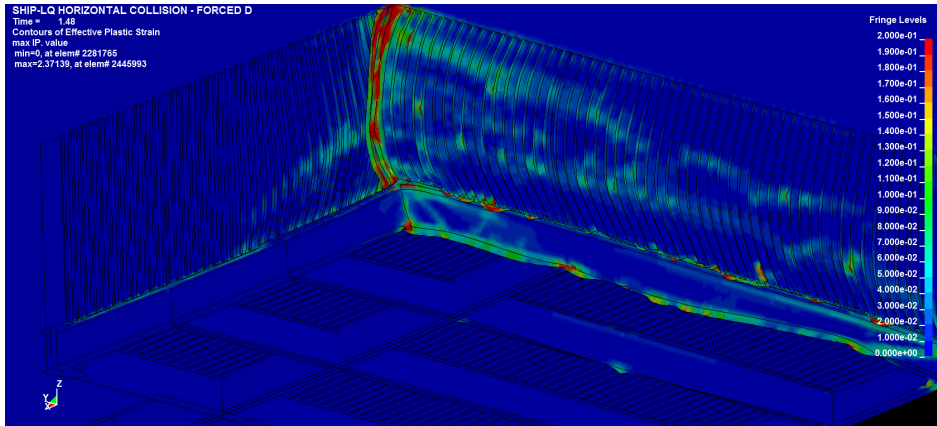


Figure B.6: Plastic strain contours LQ 20% level, horizontal collision

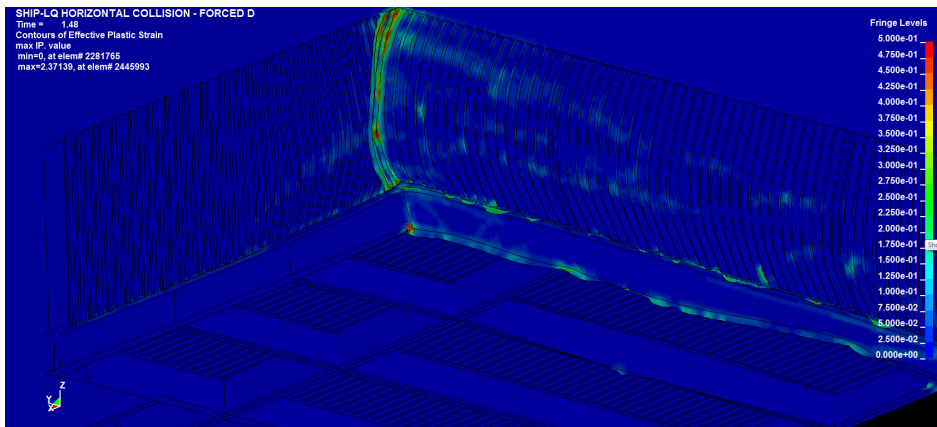


Figure B.7: Plastic strain contours LQ 50% level, horizontal collision

# Appendix C

## Motion characteristics for reference ship

### C.1 Response amplitude operators

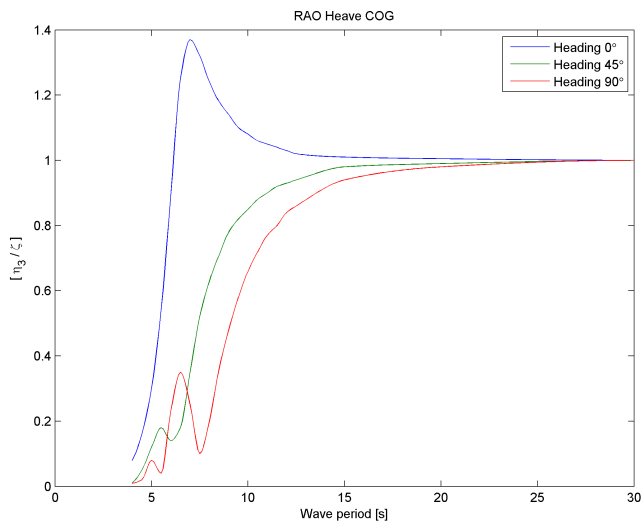


Figure C.1: RAO Heave center of gravity.

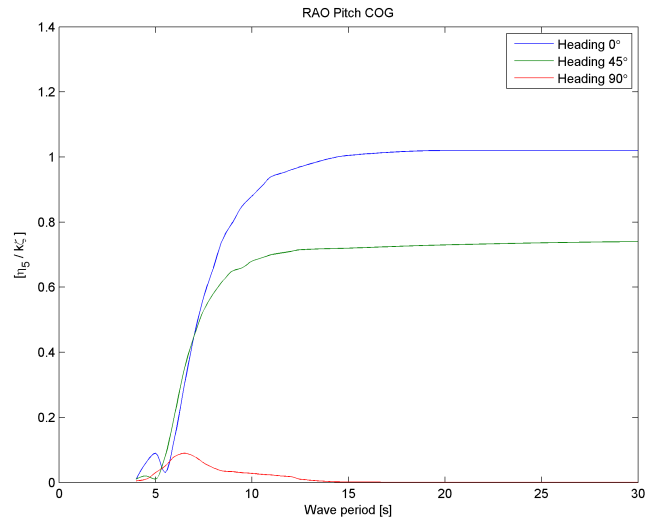


Figure C.2: RAO Pitch center of gravity.

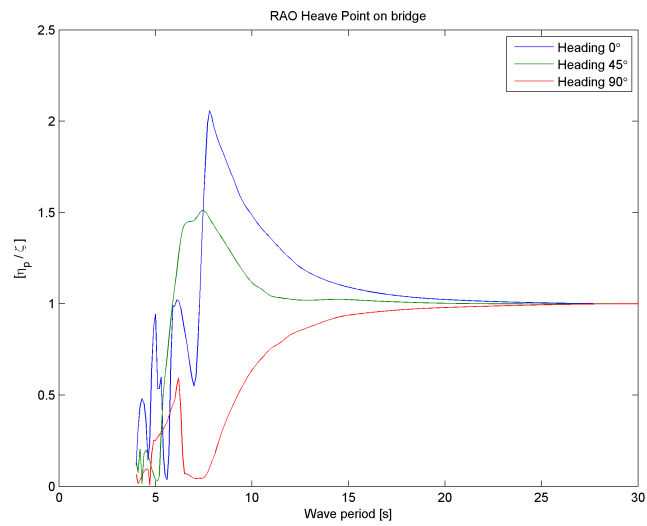


Figure C.3: Heave RAO at wheelhouse top.

## C.2 Phase angles

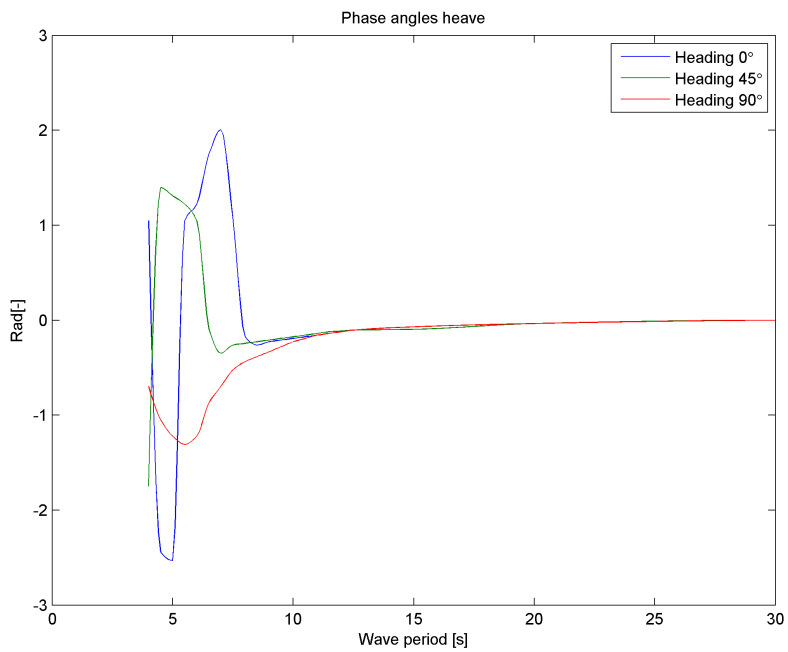


Figure C.4: Phase angles heave center of gravity.

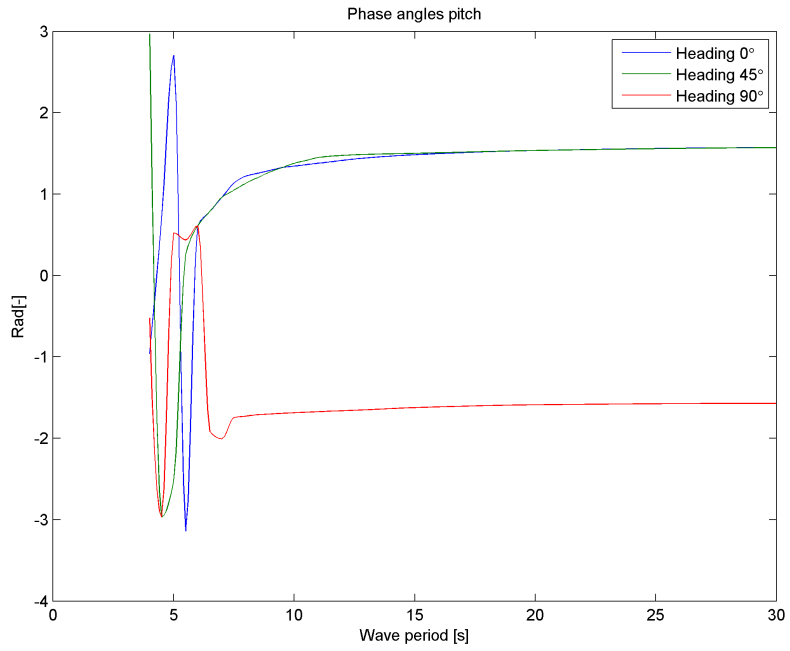


Figure C.5: Phase angles pitch center of gravity.